JOINT INSTITUTE FOR AERONAUTICS AND ACOUSTICS

STANFORD UNIVERSITY

AMES RESEARCH CENTER

JIAA TR - 3

PRESSURE FLUCTUATIONS ON THE SURFACE OF A CYLINDER IN UNIFORM FLOW

Alfred Ayoub and K. Karamcheti

STANFORD UNIVERSITY
Department of Aeronautics and Astronautics
Stanford, California 94305

June 1976

JIAA TR - 3

PRESSURE FLUCTUATIONS ON THE SURFACE OF A CYLINDER IN UNIFORM FLOW

ALFRED AYOUB AND K. KARAMCHETI

JUNE 1976

The work here presented has been supported by the National Aeronautics and Space Administration under Contracts NGR 05-020-676 and NSG 2007.

ACKNOWLEDGEMENTS

We are grateful for comments and interesting discussions to all the members of the Aeroacoustics Group at Stanford and in particular to Professors Milton Van Dyke and I-Dee Chang, who read the manuscript. Our special thanks are also due to Professor John Ffowcs Williams with whom we had the opportunity to discuss briefly some aspects of this research.

To Misses Patricia Ortiz and Phyllis Cain who helped in typing the first draft, and to Mrs. Kay Sprung who produced such an excellent final draft, we express our sincere thanks.

The permission by the Cambridge University Press and the American Society of Mechanical Engineers to reproduce some figures from earlier publications is gratefully acknowledged.

This research was carried out as part of the aeroacoustics program of the Joint Institute for Aeronautics and Acoustics, Department of Aeronautics and Astronautics, at Stanford University and was sponsored by NASA Ames Research Center under Contracts NASA NGR 05-020-676 and NASA NSG 2007. We are very thankful for this support. We are also thankful to Mr. David Hickey of NASA Ames for his continuous interest in this work.

One of us (A. Ayoub) is indebted to the Lebanese National Council for Scientific Research, for a fellowship during his graduate years at Stanford.

TABLE OF CONTENTS

Chapter 1

INTRODUCTION

When a solid object is placed in an otherwise uniform flow, vorticity develops in the vicinity of the solid boundary and in the wake as a result of the no-slip condition at the boundary. If the associated Reynolds number is high enough, fluctuations in the flow appear as a result of the instability of the shear flow thus established. Fluctuations can develop in the wake as well as in the boundary layer and around the separation points and may lead to turbulence at relatively high Reynolds numbers. These flow fluctuations in turn, whether turbulent or not, induce a fluctuating pressure field on the surface of the body. Similarly, if the main stream is turbulent or simply unsteady, it gives rise, after being distorted by the presence of the body, to pressure fluctuations on its surface. The pressure fluctuations in question are of the so-called pseudo-sound type, and are due primarily to the instantaneous response of the pressure forces to fluctuations in the inertia and viscous forces in the neighborhood of the body.

The knowledge of the details of the pressure fluctuations occurring on the surface of a solid boundary interacting with a complicated flow field is of considerable importance in many practical problems. The sound radiated by solid surfaces in the presence of unsteady flows (Curle 1955; Ffowcs Williams and Hanwkings 1969) is partly due to a distribution of dipoles whose strengt' depends upon the magnitude of the surface-pressure fluctuations. In many situations the contribution of these dipoles is the dominant one. In the recently recognized problem of airframe noise which is due simply to the motion of the aircraft

body in the atmpsphere, the dominant part of the sound radiated results from the interaction of the unsteady flow structure in the vicinity of the aircraft with the aircraft body itself. Many other problems in the area of aerodynamic sound can be associated with similar types of interaction. In addition to the sound radiated away from a solid boundary supporting a turbulent flow, one often is concerned with the sound transmitted through that boundary, an aircraft fuselage for instance, in which case knowledge of the details of the pressure fluctuations acting on the surface is essential. Finally, in the area of structural design, whether applied to aeronautical problems or more generally to problems involving the interaction of a structure with a fluid flow, it is very important to know the intensity and the scales of the surface-pressure fluctuations in order to determine the loads on the structure.

Practical problems of the type described above are usually very complicated and not amenable to direct analytical treatment. However, as is common in similar situations, one begins by decomposing the given problem into several simpler ones, in the hope that after these simpler problems have been solved, their combination in one way or another would reveal in an approximate manner the general behavior of the solution of the initial problem. Unfortunately in the type of situations we are concerned about, even after such a decomposition is made, and if the interesting features are to be preserved, one is still faced with complex phenomena such as separation and transition to turbulence, and to determine the details of the pressure fluctuations of interest via a complete solution of the problem is beyond the power of present day analytical techniques. In such circumstances one is compelled to seek a physical understanding of the phenomena involved in terms of cause

and effect in such a way as to identify each interacting component and to be able to formulate its role mathematically. It is very important to note however that such distinction between cause and effect is hardly unique when nonlinear processes are involved. For instance, in the case of interest here and which involves a solid body interacting with a complicated flow field, perhaps the only unambiguous way of describing the physics of the problem is by writing the general Navier-Stokes equations and the associated boundary conditions. The equations themselves are simply the expression of the balance of the inertia, perssure, and viscous forces while the boundary conditions describe the presence of the body and the nature of the incoming flow. In such a case the value of any causal theory would depend upon its usefulness in rendering the problem tractable mathematically. The Acoustic Theory of Airflows, now forgotten, of Shaw (1949) is one example where the theory failed to lead to an analytically tractable formulation. In that theory the vortex shedding behind an airfoil in a uniform flow was regarded as controlled by pressure fluctuations on the surface of the airfoil. If, on the other hand, we regard the pressure fluctuations occurring on the surface of the body as the result of the interaction of an already existing and known velocity field with the geometry of the body, the Navier-Stokes equations lead under certain conditions to a linear equation for the pressure of the Poisson type whose forcing term depends solely on the velocity field. The formal solution of such an equation is in the form of convolution product involving the forcing term ard an auxillary function which depends exclusively on the geometry of the body, depicting in this manner the separate roles of the different elements in the problem. Since it is rather the pressure field that we

are seeking here and since, in most cases, the velocity field is more accessible to measurement or experimental techniques, the above approach is the most promising one, and consequently will be followed in the present work.

Studies on the pressure fluctuations within a turbulent flow using the Poisson equation mentioned above began as early as 1948 with the work of Heisenberg, Obukhov, and Batchelor (1951). These early studies were concerned with the particular case of an unlimited field of homogeneous and isotropic turbulence and used extensively the results of the theory of Homogeneous Turbulence which was developing rapidly at that time. Kraichnan (1956a), in prepa ation of a subsequent work on the case of a turbulent boundary layer introduced a scale of anisotropy into the problem, and studied the effect of a mean shear by just superposing that shear on the initial field of homogeneous turbulence. In his second paper (Kraichnan, 1956b) he took into account the presence of an infinite plane boundary in an attempt to simulate the problem of the turbulent boundary layer. Although his work laid the foundation for subsequent works on the subject, his analysis was characterized by many artificial models which were only kinematically possible. Lilley and Hodgson (1960), and Lilley (1963) followed up on the subject using a different approach which took into account some of the physical properties of the flow known from velocity measurements in the turbulent boundary layer, but inevitably encumbered the analysis with many approximations and crude assumptions. Nevertheless, one interesting result emerged from their work which suggests that the wall pressure fluctuations are mainly due to contributions from sources located in the outer mixing region of the boundary layer where large eddies are swept in the

flow direction with relatively high speeds. Corcos (1964) elaborated further on this point in an interesting paper devoted to a discussion of the measurements of the statistical properties of the wall pressure and the associated difficulties.

The theoretical work on the wall pressure fluctuations beneath a turbulent boundary layer, some of which was briefly described above, was motivated by the great practical interest in that type of flows and the numerous experimental studies on the subject which appeared during the same period of time. But, due to the inherent difficulties of the structure of wall turbulence, the line of analytical approach based on the Poisson equation for the pressure was somewhat frustrated and as a result was abandoned for several years. Recently, however, Panton and Linebarger (1974) using that same equation attacked the problem with the help of the computer and obtained some interesting new results. In their work the flow direction wavenumber spectrum of the wall pressure was expressed as a five-fold multiple integral which was integrated numerically using the Monte Carlo method, in three different regions of the boundary layer, in order to assess the contribution of each region.

Except for the case of a turbulent boundary on an infinite plane surface, the pressure fluctuations occurring on the surface of bodies of arbitrary shape in the presence of an unsteady flow have not attracted the attention of theoretical workers.* On the other hand, examples where large-scale flow fluctuations not of the boundary layer type

*One exception is the work by Hunt (1973a) who considered the interaction of a bluff body with an incoming turbulent flow (Hunt, 1973b) on the basis of the theory of 'rapid distortion of turbulence' developed by Batchelor and Proudman.

occur in the vicinity of compact solid bodies, and consequently induc pressure fluctuations on their surfaces, are abundant and of considerable practical interest. The case of a cylindrical body interacting with its own wake may be the prominent example and constitutes the subject of the present work. Some aspects of this research have been presented previously by the authors at the Second and Third Interagency Symposiums on University Research in Transportation Noise (Karamcheti and Ayoub 1974; Ayoub and Karamcheti 1975).

In the next chapter the problem of determining the characteristics of the pressure fluctuations, induced on the surface of a cylinder by the fluctuating wake behind it is formulated. The flow in the wake is assumed incompressible and homogeneous in a direction along the span; the condition of incompressibility is discussed at the end of the chapter. A formal solution is then derived which relates the unsteady surface-pressure field to the velocity field in the wake. This allows certain general results to be derived, which are independent of the cylinder shape or the value of the Reynolds number. Although the next chapter is devoted primarily to the mathematical aspect of the problem, some discussion of the physical aspect of the flow in the wake is included, either to guide the mathematics or to interpret some new results. When this is done it is generally in connection with bluff cylinders.

In Chapter 3, the case of the circular cylinder is examined in detail, in light of the theory presented in Chapter 2.

CHAPTER 2

PROBLEM FORMULATION AND GENERAL ANALYSIS

2.1 Statement of the Problem

We consider an infinitely long cylinder of constant but arbitrary cross-section placed in a wind which, far upstream, is uniform of magnitude U_∞ and in a direction normal to the cylinder axis. A system of orthogonal coordinates $(0x_1, 0x_2, 0x_3)$ as shown in the figure, is set up. Let μ and ρ designate respectively the viscosity and density of the fluid which is assumed incompressible, and d a characteristic dimension of the cross-section. We assume that the value of the Reynolds number, which is defined by $Re = (\rho U_\infty d)/\mu$, is such that the perturbed flow is unsteady and three-dimensional, and also that the flow is homogeneous in the axial direction and of vanishing mean velocity component in that direction. The homogeneity in the axial direction implies that all mean values evaluated at a point in space are independent of the x_3-coordinate, while cross-correlations at two points (x_1, x_2, x_3) and (x_1', x_2', x_3') are functions of $(x_3 - x_3')$ and not of x_3 and x_3' separately. We further assume that all fluctuating quantities are stationary functions of time, and therefore all mean values will be taken with respect to time according to the formula:

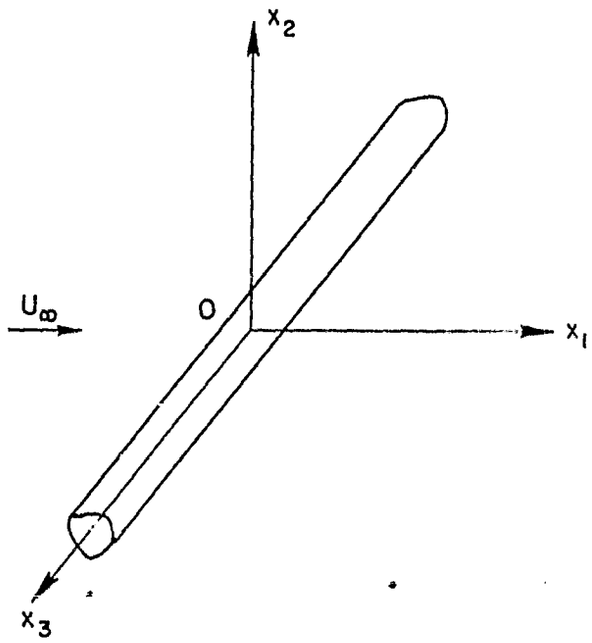

$$\overline{f(t)} = \lim_{T \to \infty} \frac{1}{2T} \int_{-T}^{+T} f(t)\, dt$$

where the bar over a quantity is used to designate the mean of that quantity. It is proposed to study the characteristics of the pressure fluctuations induced on the surface of the cylinder by the flow unsteadiness.

2.2 Governing Equations

The flow being incompressible the governing Navier-Stokes equations can be written in the form:

$$\left.\begin{aligned} &\frac{\partial v_i}{\partial t} + v_j \frac{\partial v_i}{\partial x_j} = -\frac{1}{\rho}\frac{\partial p}{\partial x_i} + \nu \frac{\partial^2 v_i}{\partial x_j \partial x_j} \quad ; \quad i = 1,2,3 \\ &\frac{\partial v_i}{\partial x_i} = 0 \ , \end{aligned}\right\} \qquad (2.1)$$

where v_1, v_2, v_3 are the three components of the velocity vector $\vec{v}$, p the pressure, t the time, ν the kinematic viscosity defined by $\nu = \frac{\mu}{\rho}$ and where the summation convection over repeated subscripts has been used. Equations (2.1) are to be supplemented by the no-slip condition at the solid boundary and appropriate conditions on the velocity and the pressure at infinity. By applying the operator $\frac{\partial}{\partial x_i}$ on the first equation of (2.1) and using the second, we obtain the following equation for the pressure:

$$\frac{\partial^2 p}{\partial x_i \partial x_i} = -\rho \frac{\partial^2 (v_i v_j)}{\partial x_i \partial x_j} \ . \qquad (2.2)$$

If we now express the flow field as composed of two parts, one a steady mean part and the other a time dependent fluctuating part in the following manner:

$$\left.\begin{aligned} v_i(\vec{x},t) &= \bar{v}_i(\vec{x}) + v_i'(\vec{x},t) \;\; ; \;\; i = 1,2,3 \\ p(\vec{x},t) &= \bar{p}(\vec{x}) + p'(\vec{x},t) \end{aligned}\right\} \qquad (2.3)$$

we obtain by substituting these expressions into (2.2), taking the time average, and substracting the resulting equation from (2.2) itself, the following equation:

$$\frac{\partial^2 p'}{\partial x_i \partial x_i} = -q \;, \qquad (2.4)$$

where

$$q(\vec{x},t) = \frac{\partial^2 q_{ij}}{\partial x_i \partial x_j} \qquad (2.5)$$

and

$$q_{ij}(\vec{x},t) = \rho(2\bar{v}_i v_j' + v_i' v_j' - \overline{v_i' v_j'}) \;. \qquad (2.6)$$

Again, if we substitute (2.3) into the first equation of (2.1), take the time average, and substract the resulting equation from the original one, we obtain:

$$\frac{1}{\rho}\frac{\partial p'}{\partial x_i} = -\frac{\partial v_i'}{\partial t} - \bar{v}_j \frac{\partial v_i'}{\partial x_j} - v_j' \frac{\partial \bar{v}_i}{\partial x_j} - v_j' \frac{\partial v_i'}{\partial x_j} + \overline{v_j' \frac{\partial v_i'}{\partial x_j}} + \nu \frac{\partial^2 v_i'}{\partial x_j \partial x_j} \;. \qquad (2.7)$$

On the surface S of the cylinder assumed rigid, the mean and fluctuating parts of the velocity vector vanish separately and we have using (2.7):

$$n_i \left.\frac{\partial p'}{\partial x_i}\right|_S = \mu\, n_i \left.\frac{\partial^2 v_i'}{\partial x_j \partial x_j}\right|_S \;, \qquad (2.8)$$

where $\vec{n}$ is the unit vector $(n_1, n_2, 0)$ along the inward normal to S. For large values of $|\vec{x}|$ in a plane $x_3 = \text{constant}$, the mean velocity approaches the constant value U_∞ while the velocity fluctuation components

decrease to zero like $1/(x_1^2+x_2^2)^{\frac{1}{4}}$ inside the wake,* and like $1/(x_1^2+x_2^2)^{5/4}$ outside it. The behavior outside the wake can be seen as follows. The flow far upstream being considered uniform, the unsteady part of the vorticity vector is generated in the neighborhood of the cylinder, and decays at large distances from it. The irrotational velocity fluctuations outside the wake can then be thought of as induced by a concentration of vorticity in the near-wake region. But we know that the velocity induced by a distribution of vorticity (in an incompressible flow), which decays satisfactorily in all directions in space, behaves like $1/|\vec{x}|^3$ at large distances (see Batchelor 1967 § 2.9). Therefore since the wake is assumed to extend to infinity in the $\pm x_3$-direction and is statistically homogeneous in that direction, the square of the velocity fluctuations outside the wake behaves like

$$\int_{-\infty}^{+\infty} \frac{dx_3}{|\vec{x}|^6}$$

from which the behavior stated above follows. Referring to (2.7) we can see that outside the wake $\partial p'/\partial x_i$ decays at least like $1/(x_1^2+x_2^2)^{5/4}$ and p' at least like $1/(x_1^2+x_2^2)^{3/4}$. Now inside the wake and at large distances downstream the flow has reached the equilibrium stage and the pressure p' can be assumed to have approximately the value it has outside, i.e., p' decays like $1/(x_1^2+x_2^2)^{3/4}$.

*Unsteady or turbulent wakes behind infinitely long cylinders remain so at arbitrarily large distances downstream. This is due to the fact that the Reynolds number based on the width W of the wake and a typical turbulent velocity u' is independent of the downstream coordinate x_1; $W \sim x_1^{\frac{1}{2}}$ and $u' \sim x_1^{-\frac{1}{2}}$ (see Landau and Lifshitz 1959 page 139).

The flow being considered homogeneous in the axial direction we perform a generalized Fourier decomposition in that direction according to the relations:

$$\left.\begin{aligned} p'(\vec{x},t) &= \frac{1}{2\pi}\int_{-\infty}^{+\infty} P(\vec{X},k,t)\, e^{ikx_3}\, dk \;,\quad P(\vec{X},k,t) = \int_{-\infty}^{+\infty} p'(\vec{x},t) e^{-ikx_3}\, dx_3 \;, \\ v_i'(\vec{x},t) &= \frac{1}{2\pi}\int_{-\infty}^{+\infty} V_i(\vec{X},k,t) e^{ikx_3}\, dk \;,\quad V_i(\vec{X},k,t) = \int_{-\infty}^{+\infty} v_i'(\vec{x},t) e^{-ikx_3} dx_3 \;; \\ & \qquad\qquad\qquad\qquad\qquad\qquad\qquad\qquad i = 1,2,3 \\ q(\vec{x},t) &= \frac{1}{2\pi}\int_{-\infty}^{+\infty} Q(\vec{X},k,t) e^{ikx_3}\, dk \;,\quad Q(\vec{X},k,t) = \int_{-\infty}^{+\infty} q(\vec{x},t) e^{-ikx_3} dx_3 \;, \end{aligned}\right\} \quad (2.9)$$

where $\vec{X} = (X_1, X_2)$ is the position vector in the plane normal to the cylinder, coinciding with the normal projection of $\vec{x}$ on that plane, k is a real variable representing the wavenumber in the x_3-direction, and P, V_i, Q are the complex Fourier amplitudes associated with k of the physical quantities p', v_i', q. In the transformed vaiables equation (2.4) becomes:

$$\frac{\partial^2 P}{\partial X_i \partial X_i} - k^2 P = -Q \;. \qquad (2.10)$$

Since $\vec{n} = (n_1, n_2, 0)$, Eq. (2.8) can be written explicitly as:

$$\left(n_1 \frac{\partial p'}{\partial x_1} + n_2 \frac{\partial p'}{\partial x_2}\right)\Big|_S = \mu\left(n_1 \frac{\partial^2 v_1'}{\partial x_j \partial x_j} + n_2 \frac{\partial^2 v_2'}{\partial x_j \partial x_j}\right)\Big|_S \;,$$

or since v_1', v_2' and consequently the derivative $\frac{\partial}{\partial x_3}$ of v_1' and v_2' vanish on S, as:

$$\left(n_1 \frac{\partial p'}{\partial x_1} + n_2 \frac{\partial p'}{\partial x_2}\right)\Big|_S = \mu\left[n_1\left(\frac{\partial^2 v_1'}{\partial x_1^2} + \frac{\partial^2 v_1'}{\partial x_2^2}\right) + n_2\left(\frac{\partial^2 v_2'}{\partial x_1^2} + \frac{\partial^2 v_2'}{\partial x_2^2}\right)\right]\Big|_S .$$

Upon taking the Fourier transform with respect to x_3, and noting that n_1 and n_2 are independent of x_3, we obtain:

$$\left(n_1 \frac{\partial P}{\partial X_1} + n_2 \frac{\partial P}{\partial X_2}\right)\Big|_S = \mu\left[n_1\left(\frac{\partial^2 V_1}{\partial X_1^2} + \frac{\partial^2 V_1}{\partial X_2^2}\right) + n_2\left(\frac{\partial^2 V_2}{\partial X_1^2} + \frac{\partial^2 V_2}{\partial X_2^2}\right)\right]\Big|_S ,$$

which can be written in a concise form as:

$$n_i \frac{\partial P}{\partial X_i}\Big|_S = \mu\left(n_i \frac{\partial^2 V_i}{\partial X_j \partial X_j}\right)\Big|_S . \qquad (2.11)$$

The condition on P at infinity is the same as that on p', i.e., both the real and imaginary parts of P vanish like $\frac{1}{|\vec{X}|^{3/2}}$ for sufficiently large values of $|\vec{X}|$. Consequently, $P(\vec{X},k,t)$ appears to be the solution of the two-dimensional boundary value problem defined by equation (2.10), the boundary condition (2.11) and the condition at infinity stated above. This problem is reproduced below for convenience:

$$\left.\begin{aligned} &\nabla^2 P - k^2 P = -Q \\ &\vec{n}.\nabla P\big|_C = \mu\, \vec{n}.\nabla^2\vec{V}\big|_C \\ &|P| \sim \frac{1}{|\vec{X}|^{3/2}} \quad \text{for} \quad |\vec{X}| \to \infty \end{aligned}\right\} \qquad (2.12)$$

where the operators ∇ and ∇^2 are respectively the gradient and Laplace operators in two dimensions, C the line intersection of S with the plane (X_1,X_2), and $\vec{V}$ the vector (V_1,V_2).

The differential equation in (2.12) is that which occurs in problems of steady diffusion with absorption proportional to the concentration.

Hence for a given value of k, P can be interpreted as the steady temperature distribution in a two-dimensional domain of thermal conductivity equal to 1, bounded internally be C and containing a source distribution of heat, of density $+Q$ (amount of heat generated per unit area per unit time). Across C heat flows at a prescribed rate and the medium absorbs heat in proportion to the local temperature at the constant positive rate k^2. P is therefore the solution of a well-posed boundary value problem and hence is uniquely determined,* if the boundary C satisfies certain conditions of regularity, by the data Q and the boundary values $\mu \vec{n}.\nabla^2\vec{V}$. Note that the boundary condition on $\vec{n}.\nabla P$ is not arbitrary in our problem but is compatible with the differential equation since they are both derived from the same Navier-Stokes equations. However, for the purpose of determining the pressure from a knowledge of the velocity field the value of $\vec{n}.\nabla P$ on C can be considered as prescribed. The interpretation of P in terms of a temperature distribution is useful in assessing the relative importance of the different spectral componerts of the pressure once some details on the distribution of Q and $\vec{n}.\nabla^2\vec{V}\big|_C$ for different values of k are known.

2.3 Formal Solution.

A formal integral representation of the solution of (2.12) can be derived using a Green's function $G(\vec{X}|\vec{Y};k)$ defined by the following

$$\left.\begin{aligned} &\nabla^2 G - k^2 G = -\delta(\vec{X}-\vec{Y}) \\ &\vec{n}.\nabla G\big|_C = 0 \\ &G \to 0 \quad \text{as} \quad |\vec{X}| \to \infty \end{aligned}\right\} \qquad (2.13)$$

*The fact that the coefficient of absorption is positive insures the uniqueness of the solution.

where the differentiations are with respect to $\vec{X}$, and $\vec{Y}=(Y_1,Y_2)$. It can be easily seen from the physical interpretation given in the preceding parapraph that (2.13) admits a unique solution. Multiplying the first equation of (2.12) by G and the first equation of (2.13) by P, subtracting the resulting two equations and integrating over the area Σ_R bounded by C and a large circle C_R of radius R centered at the origin we obtain:

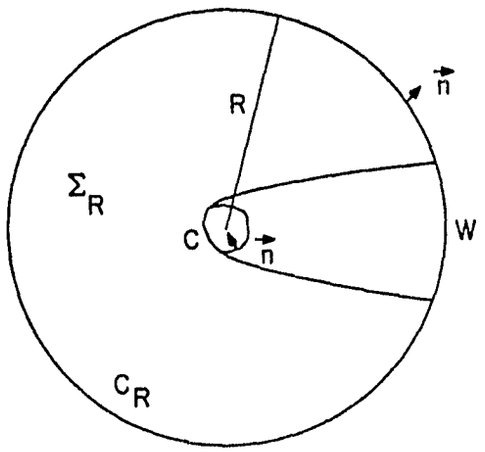

$$\iint_{\Sigma_R} (G\nabla^2 P - P\nabla^2 G)\,d\vec{X} = \iint_{\Sigma_R} P\delta(\vec{X}-\vec{Y})\,d\vec{X} - \iint_{\Sigma_R} GQ\,d\vec{X} \quad ,$$

where $d\vec{X}$ is an element of area. Using the Green's formula and integrating the term containing $\delta(\vec{X}-\vec{Y})$ we obtain:

$$P(\vec{Y},k,t) = \iint_{\Sigma_R} G\,Q\,d\vec{X} + \int_{C+C_R} (G\,\vec{n}.\nabla P - P\,\vec{n}.\nabla G)\,ds(\vec{X}) \quad , \qquad (2.14)$$

where $\vec{n}$ is the exterior normal to C and C_R, and $ds(\vec{X})$ is a line element of C and C_R. It is easily seen from the behavior of G and P at large distances that as R goes to infinity the integral over C_R vanishes. Furthermore, since $\vec{n}.\nabla G\big|_C = 0$, and $\vec{n}.\nabla P\big|_C = \mu\,\vec{n}.\nabla^2\vec{V}\big|_C$, relation (2.14) becomes:

$$P(\vec{Y},k,t) = \iint_{\Sigma} G(\vec{X}|\vec{Y};k)\, Q(\vec{X},k,t)d\vec{X} + \mu \int_{C} G(\vec{X}|\vec{Y};k)\vec{n}.\nabla^2\vec{V}(\vec{X},k,t)ds(\vec{X}) \quad , \quad (2.15)$$

where Σ is the region exterior to C extending to infinity.

Equation (2.15) expresses the fact that at a given time t and at any point in space or on the cylinder having the coordinates Y_1 and Y_2 in the x_1- and x_2-directions, the component of the pressure associated with the wavenumber k (in the axial direction) is determined uniquely by the corresponding Fourier components of the velocity fluctuations as distributed throughout the unsteady region in the (X_1,X_2) plane, and also by those pairs of components whose wavenumbers sums are equal to k . The contribution of the latter is due to the fact that q contains terms which are quadratic in the velocity fluctuations, and as can be easily seen the k-Fourier-component of the product $v_i'v_j'$, for instance, is nothing but:

$$\frac{1}{2\pi}\int_{-\infty}^{+\infty} V_i(\vec{X},k,t)V_j(\vec{X},k-k',t)dk' \quad .$$

The surface integral in (2.15) can be thought of as the contribution to the pressure fluctuations by the inertia forces and the integral over C as that of the viscous forces.* Some details of the structure of the forcing term Q will be given in a later section. In the following we turn to the discussion of some practical considerations concerning the

*In fact the effect of the viscous forces is also included in the integral over Σ because these forces are responsible for maintaining a particular form of the inertia forces. However, the above distinction is made only in consistence with the approach adopted and explained in the introduction.

Green's function G and the determination of the total forces acting on the cylinder.

2.4 The Green's Function - Total Lift and Drag for the Case of a Circular Cylinder.

Due to the linear character of the Poisson equation which governs the pressure p', we were able to perform a spectral decomposition in the axial direction, so that each spectral component of the pre sure can be studied separately as the solution of a well-posed boundary value problem in two dimensions. That such a decomposition is meaningful physically follows from the fact that the flow in general is homogeneous in the spanwise direction and is composed of two distinct parts: one is discrete and homogeneous (or periodic for certain values of the Reynolds number) in that direction; the other is random in nature and can be assumed homogeneous in the same direction, in view of the two-dimensionality of the obstacle and of the flow upstream. A detailed discussion of this and other features of the flow behind a typical two-dimensional body (the circular cylinder) will be given in the next chapter. However, in order to guide our discussion of the Green's function in this section, a few words on the origin and the relative importance of these two components of the flow are appropriate.

When a bluff cylinder is placed in a uniform flow at relatively high Reynolds numbers, two boundary layers form on the sides of the cylinder, separate from its surface and tend to interact with each other to form the wake behind it. In this process two different phenomena take place independently. The first is the transition in the individual separated shear layers, which leads to small scale fluctuations and eventually to turbulence. The second is the direct interaction of these two shear layers,

carrying vorticity of opposite signs, which results in the formation of the large scale vortices characteristic of wakes behind bluff bodies at almost all Reynolds numbers. The random fluctuations have scales of the order of the thickness of the shear layers emanating from the cylinder surface and contain only a fraction of the wake energy, while the discrete component has length scales in the axial direction ranging from 2 to 30 times a typical dimension of the cross-section and carries most of the energy in the wake. These two components which result from two independent phenomena in generally two different ranges of scales and frequencies preserve their separate identities for some distance downstream and do not interact with each other in the near-wake region (see for instance Roshko, 1954). With this in mind, it is clear that by studying the distribution of P on C for a given value of k, we evaluate the contribution to the pressure fluctuations on the cylinder, of a physically identifiable component of the flow.* The usefulness of the interpretation of P in terms of a temperature distribution is likewise easily seen from the above discussion, for the wavenumber k is of the order of an inverse length scale in the spanwise direction, and k^2 is the rate of absorption in the analogue problem.

In the form (2.15) the solution of the problem requires, among other things, a knowledge of the Green's function G which satisfies (2.13). The usual method of finding G consists of writing it as follows:

$$G(\vec{X}|\vec{Y};k) = G_0(\vec{X}|\vec{Y};k) + G_1(\vec{X}|\vec{Y};k) \quad , \tag{2.16}$$

*Here we are implicitly assuming that the contribution from the quadratic terms in the forcing function can be neglected. We will do the same in some of the discussions of §2.6 and §2.7. The role of these quadratic terms is discussed in Appendix A.

where $G_0(\vec{X}|\vec{Y};k)$ is the free-space Green's function satisfying the first equation of (2.13) and the boundary condition at infinity, and G_1 is a solution of the corresponding homogeneous equation, which is regular everywhere outside C and such that the sum G_0+G_1 satisfies the second boundary condition in (2.13). G_0 is given by (see Stakgold, 1968):

$$G_0(\vec{X}|\vec{Y};k) = \frac{1}{2\pi}K_0[|k(\vec{X}-\vec{Y})|] \quad , \tag{2.17}$$

where K_0 is the zero-order modified Bessel function of the second kind. This function is tabulated (Abramowitz and Stegun, 1964), and has the following asymptotic behavior for large and small values of the argument:

$$\left.\begin{aligned} K_0(\alpha) &\sim \sqrt{\frac{\pi}{2\alpha}}\, e^{-\alpha} \quad \text{for} \quad \alpha \to \infty \quad , \\ K_0(\alpha) &\sim -\log\alpha \qquad \text{for} \quad \alpha \to 0 \end{aligned}\right\} \tag{2.18}$$

As for G_1, it satisfies the following problem:

$$\left.\begin{aligned} &\nabla^2 G_1 - k^2 G_1 = 0 \\ &\vec{n}.\nabla G_1\Big|_C = -\frac{1}{2\pi}\vec{n}.\nabla K_0[|k(\vec{X}-\vec{Y})|]\Big|_C \\ &G_1 \to 0 \quad \text{as} \quad |\vec{X}| \to \infty \end{aligned}\right\} \tag{2.19}$$

For certain particular shapes of the boundary C, (2.19) can be solved by the method of separation of variables. The solution obtained is usually in the form of an infinite series of cylinder functions. When C is a circle centered at the origin, separation in the polar coordinates r and θ yields an infinite sum of terms involving the circular functions $e^{in\theta}$ and the modified Bessel functions of the second kind $K_n(|k\vec{X}|)$,

whose asymptotic behavior for large values of the argument is similar to that of K_0 . Approximate solutions can then be found in some circumstances depending on the value of k . Another way of approaching the problem is by using the free-space Green's function alone in (2.14), and instead of (2.15) the resulting relation becomes:

$$P(\vec{Y},k,t) = \iint_S G_0(\vec{X}|\vec{Y};k)\, Q(\vec{X},k,t)d\vec{X} + \mu \int_C G_0(\vec{X}|\vec{Y};k)\vec{n}.\nabla^2\vec{V}(\vec{X},k,t)ds(\vec{X})$$

$$- \int_C P(\vec{X},k,t)\vec{n}.\nabla G_0(\vec{X}|\vec{Y};k)ds(\vec{X}) \quad , \tag{2.20}$$

where G_0 is given by (2.17). If Q and $\vec{n}.\nabla^2\vec{V}$ are sssumed known this equation is an inhomogeneous integral equation of the second kind in the curvilinear domain C , to which in principle several approximate and numerical techniques can be applied to yield a solution for P on the surface of the cylinder.*

The methods of solution comtemplated above are all approximate and have as a goal the determination of P , for a given value of k , as a function of position on the boundary C . Although it is usually desirable to have such a solution it is often sufficient in practice, to obtain expressions for certain parameters, related in a global way to the detailed solution P . Among such parameters perhaps the most important ones, in the case of a bluff cylinder, are the total lift and drag forces acting on the cylinder. Using (2.20) we derive below such expressions for the case of a circular cross-section.

*If such a course is to be followed (2.20) requires some modification unless the dependence on time is simple, nevertheless in its present form Eq. (2.20) is useful as we will see below.

Let r, θ designate the polar coordinates of $\vec{X}$ and ρ, φ those of $\vec{Y}$, $d/2$ being the radius of C. We multiply (2.20) by $-\sin\varphi \frac{d}{2} d\varphi$, after setting $\rho = d/2$, and integrate from $\varphi = 0$ to $\varphi = 2\pi$, to obtain:

$$L(k,t) \int_0^{2\pi} -P(\vec{Y},k,t) \sin\varphi \frac{d}{2} d\varphi$$

$$= -\frac{d}{2}\int_0^{2\pi} \sin\varphi \{ \iint_{\Sigma} G_0(\vec{X}|\vec{Y},k)\, Q(\vec{X},k,t) d\vec{X} \} d\varphi$$

$$-(\frac{d}{2})^2 \mu \int_0^{2\pi} \sin\varphi \{ \int_0^{2\pi} G_0(\vec{X}|\vec{Y};k) \vec{n}.\nabla^2\vec{V}(\vec{X},k,t) d\theta \} d\varphi$$

$$+(\frac{d}{2})^2 \int_0^{2\pi} \sin\varphi \{ \int_0^{2\pi} P(\vec{X},k,t) \vec{n}.\nabla G_0(\vec{X}|\vec{Y};k) d\theta \} d\varphi, \quad (2.21)$$

where $L(k,t)$ designates the fluctuating lift per unit span associated with the wavenumber k*, and evaluated at time t. We now set:

$$\left.\begin{aligned} Q_s(k,t) &= -\frac{d}{2}\int_0^{2\pi} \sin\varphi \{ \iint_{\Sigma} G_0 Q\, d\vec{X} \} d\varphi \\ S_s(k,t) &= -\mu (\frac{d}{2})^2 \int_0^{2\pi} \sin\varphi \{ \int_0^{2\pi} G_0 \vec{n}.\nabla^2\vec{V} d\theta \} d\varphi \end{aligned}\right\} \quad (2.22)$$

and noticing that $\vec{n}.\nabla G_0(\vec{X}|\vec{Y};k) = -\frac{\partial G_0}{\partial r}(\vec{X}|\vec{Y};k)\Big|_{r=d/2}$ we obtain, after interchanging the integration in the last term of (2.21):

*The spanwise correlation length of the fluctuating surface-pressure at a particular frequency is found experimentally to be a function of the azimuthal angle φ in general. The spectral decomposition in the x_3-direction has therefore the advantage of removing the ambiguity associated with the choice of a characteristic spanwise length scale of the fluctuating lift (or drag) at a given frequency.

$$L(k,t) = Q_s(k,t) + S_s(k,t) - \left(\frac{d}{2}\right)^2 \int_0^{2\pi} P(\vec{X},k,t)\left\{\frac{\partial}{\partial r}\int_0^{2\pi} G_0(\vec{X}|\vec{Y};k)\sin\gamma\, d\ell \Big|_{r=d/2}\right\} d\theta \quad . \tag{2.23}$$

The integral inside the brackets in the last term of (2.23), which we denote by I, is evaluated at constant r and for $\vec{Y}$ on the circle C. Now since $G_0(\vec{X}|\vec{Y};k)$ is a function of $|\vec{X}-\vec{Y}|$ only, when $\vec{Y}$ is on the circle, it becomes a function $\tilde{G}_0(\varphi-\theta,r;k)$ of r and $(\varphi-\theta)$ only. Therefore the integral in question can be written as:

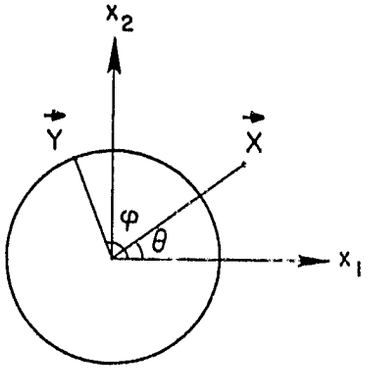

$$I = \int_0^{2\pi} \tilde{G}_0(\varphi-\theta,r;k)\sin\varphi\, d\varphi \quad ,$$

or, after making the change of variable $\nu = \varphi-\theta$, as:

$$I = \int_{-\theta}^{2\pi-\theta} \tilde{G}_0(\nu,r;k)\sin(\nu+\theta)d\nu$$

$$= \int_{-\theta}^{0} \tilde{G}_0(\nu,r;k)\sin(\nu+\theta)d\nu + \int_0^{2\pi} \tilde{G}_0(\nu,r;k)\sin(\nu+\theta)d\nu$$

$$= \int_{2\pi}^{2\pi-\theta} \tilde{G}_0(\nu,r;k)\sin(\nu+\theta)d\nu \quad .$$

Since $\tilde{G}_0(\nu+2\pi,r;k) = \tilde{G}_0(\nu,r;k)$ the first and third terms in the above expression can be easily seen to cancel, and we have:

$$1 = \cos\theta \int_0^{2\pi} G_0(\gamma,r;k)\sin\gamma\,d\gamma + \sin\theta \int_0^{2\pi} \tilde{G}_0(\gamma,r;k)\cos\gamma\,d\gamma \quad .$$

Hence, (2.23) becomes:

$$L(k,t) = Q_s(k,t)+S_s(k,t)-(\tfrac{d}{2})^2\Big[\Big\{\frac{\partial}{\partial r}\int_0^{2\pi} \tilde{G}_0(\gamma,r;k)\sin\gamma\,d\gamma\Big\}_{r=\frac{d}{2}} \int_0^{2\pi} P(\vec{X},k,t)\cos\theta\,d\theta$$

$$+\Big\{\frac{\partial}{\partial r}\int_0^{2\pi} \tilde{G}_0(\gamma,r;k)\cos\gamma\,d\gamma\Big\}_{r=d/2} \int_0^{2\pi} P(\vec{X},k,t)\sin\theta\,d\theta\Big] \quad .$$

If we define $D(k,t)$ to be the fluctuating drag per unit span associated with the wavenumber k, we have:

$$D(k,t) \quad -\int_0^{2\pi} P(\vec{X},k,t)\cos\theta\,\frac{d}{2}\,d\theta \quad ; \quad \vec{X} \text{ on } C$$

and finally:

$$L(k,t) = Q_s(k,t)+S_s(k,t)+\frac{d}{2}\Big\{\frac{\partial}{\partial r}\int_0^{2\pi} \tilde{G}_0(\gamma,r;k)\sin\gamma\,d\gamma\Big\}_{r=\frac{d}{2}} D(k,t)$$

$$+\frac{d}{2}\Big\{\frac{\partial}{\partial r}\int_0^{2\pi} \tilde{G}_0(\gamma,r;k)\cos\gamma\,d\gamma\Big\}_{r=\frac{d}{2}} L(k,t) \quad . \qquad (2.24)$$

Similarly if we multiply (2.20) by $-\cos\varphi\,\frac{d}{2}\,d\varphi$, and integrate from $\varphi = 0$ to $\varphi = 2\pi$ we obtain following the same procedure:

$$D(k,t) = Q_C(k,t)+S_C(k,t)+\frac{d}{2}\Big\{\frac{\partial}{\partial r}\int_0^{2\pi} \tilde{G}_0(\gamma,r;k)\cos\gamma\,d\gamma\Big\}_{r=\frac{d}{2}} D(k,t)$$

$$-\frac{d}{2}\Big\{\frac{\partial}{\partial r}\int_0^{2\pi} \tilde{G}_0(\gamma,r;k)\sin\gamma\,d\gamma\Big\}_{r=\frac{d}{2}} L(k,t) \quad . \qquad (2.25)$$

where Q_C and S_C are defined as in (2.22) by replacing $\sin\gamma$ by $\cos\gamma$. Eqs. (2.24) and (2.25) are two independent algebraic equations in L and D, and hence yield the following expressions for the lift and drag forces L(k,t) and D(k,t):

$$L(k,t) = \frac{\{Q_S(k,t)+S_S(k,t)\}\{1-\tilde{G}_{0C}(k)\}+\{Q_C(k,t)+S_C(k,t)\}\tilde{G}_{0S}(k)}{\{1-\tilde{G}_{0C}(k)\}^2+\tilde{G}_{0S}(k)^2} , \tag{2.26}$$

$$D(k,t) = \frac{\{Q_C(k,t)+S_C(k,t)\}\{1-\tilde{G}_{0C}(k)\}-\{Q_S(k,t)+S_S(k,t)\}\tilde{G}_{0S}(k)}{\{1-\tilde{G}_{0C}(k)\}^2+\tilde{G}_{0S}(k)^2} . \tag{2.27}$$

where

$$\tilde{G}_{0C}(k) = \frac{d}{2}\left\{\frac{\partial}{\partial r}\int_0^{2\pi}\tilde{G}_0(\nu,r;k)\cos\nu\,d\nu\right\}_{r=d/2} ,$$

$$\tilde{G}_{0S}(k) = \frac{d}{2}\left\{\frac{\partial}{\partial r}\int_0^{2\pi}\tilde{G}_0(\nu,r;k)\sin\nu\,d\nu\right\}_{r=d/2} .$$

An important feature of the formal solution (2.15) and the expressions (2.26) and (2.27) is that the integrals over Σ involved converge very rapidly. These integrals which in principle should be integrated over the entire region where Q is different from zero, can be integrated in a practical problem over a limited region around the point $\vec{Y}$, due to the asymptotic behavior of G and G_0 for large values of $|\vec{X}-\vec{Y}|$. If P is to be evaluated on C the domain of integration is generally confined to the near-wake and is smaller the larger the value of k for which the pressure is to be evaluated (see, for instance, equation (2.17) and the asymptotic behavior given in (2.18)). From an experimental point of view, this constitutes a considerable advantage because the amount of velocity measurements needed would be very limited.

Before leaving this section we note that in practical applications our analysis so far can be applied only to situations where the length of the cylinder is many times the diameter of the cross-section and more important, many times the largest length scale in the spanwise direction (in which case the assumption of homogeneity in the x_3-direction is valid). This is usually the case at high Reynolds numbers.

2.5 The Two-Dimensional Case.

For relatively low values of the Reynolds number (Re less than 90 in the case of the circular cylinder for instance), the large vortices in the wake have a correlation length in the spanwise direction many times the diameter of the cross-section and within a correlation length these vortices have straight axis parallel to the cylinder. In addition the random component of the velocity fluctuations is practically absent. In such circumstances the flow can be assumed two-dimensional and equation (2.4) can be integrated using the two-dimensional Green's function $G(\vec{X}|\vec{Y})$ associated with the Laplace equation.* The boundary condition at large distances outside the wake can be derived as in § 2.2 using (2.7) and the behavior of the velocity fluctuations there. The latter is given (upon integrating the three-dimensional behavior along the x_3-direction, in view of the two-dimensional assumption) by:

*Note that the two-dimensional Green's function $G(\vec{X}|\vec{Y})$ has a singular behavior for large values of $|\vec{X}-\vec{Y}|$. In other words for very small values of the wavenumber k, corresponding to very large values of the spanwise length scale $2\pi/k$, $G(\vec{X}|Y;k)$ approaches $G(\vec{X}|\vec{Y})$ only in a finite domain around the point $\vec{Y}$; this can be seen from the second relation in (2.18) and by solving (2.19) to the first order in k^2. This singular behavior however does not introduce any difficulty in the following because in (2.30) the first integral can be integrated by parts and the second is negligibly small as we will see in the next chapter.

$$\int_{-\infty}^{+\infty} \frac{dx_3}{|\vec{x}|^3} \quad ,$$

or

$$\frac{1}{x_1^2+x_2^2} \quad ,$$

and therefore p' decays like $1/(x_1^2+x_2^2)^{\frac{1}{2}}$ for large values of $|\vec{X}|$ outside and inside the wake. Hence p' is the solution of the following problem:

$$\left.\begin{aligned} &\nabla^2 p' = -q \\ &\vec{n}.\nabla p'\big|_C = \mu\, \vec{n}.\nabla^2\vec{v}'\big|_C \\ &p' \sim \frac{1}{|\vec{X}|} \quad \text{as} \quad |\vec{X}| \to \infty \quad . \end{aligned}\right\} \qquad (2.28)$$

The two-dimensional Green's function $G(\vec{X}|\vec{Y})$ is the solution of:

$$\left.\begin{aligned} &\nabla^2 G = -\delta(\vec{X}-\vec{Y}) \\ &\vec{n}.\nabla G\big|_C = 0 \\ &|\nabla G| \to 0 \quad \text{as} \quad |\vec{X}| \to \infty \quad . \end{aligned}\right\} \qquad (2.29)$$

$G(\vec{X}|\vec{Y})$ as defined by (2.29) is nothing but the velocity potential of the flow created by a negative unit source at the point $\vec{Y}$ in presence of the solid boundary C. The function G can therefore be constructed for a variety of shapes of the boundary C, using the method of images and the techniques of conformal mappings, as it will be shown in the next chapter.

It is to be noted that the solution of (2.29) is determined up to an arbitrary harmonic function, regular everywhere outside C, bounded at

infinity and satisfying the second condition of (2.29). However, it can be easily verified that when such an arbitrary function is added to G the resulting expression for p' is not altered. Combining (2.28) and (2.29) as in § 2.3 and noting that the integral:

$$\int_{C_R} (G\vec{n}.\nabla p' - p'\vec{n}.\nabla G)ds(\vec{X})$$

over a large circle C_R of radius R and centered at the origin, vanishes as R goes to infinity, we obtain:

$$p'(\vec{Y},t) = \iint_{\Sigma} G(\vec{X}|\vec{Y})\, q(\vec{X},t)d\vec{X} + \mu \int_{C} G(\vec{X}|\vec{Y})\vec{n}.\nabla^2\vec{v}\,(\vec{X},t)ds(\vec{X}) \quad . \quad (2.30)$$

The Green's function in two dimensions behaves like $\log|\vec{X}|$ for large values of $|\vec{X}|$. Therefore in order to improve the convergence of the integral over Σ in (2.30), we perform a double integration by parts, by using (2.5) and (2.6), in the following manner:

$$Gq = G\frac{\partial^2 q_{ij}}{\partial X_i \partial X_j}$$

$$= \frac{\partial^2 G}{\partial X_i \partial X_j} q_{ij} + \frac{\partial}{\partial X_i}\left(G\frac{\partial q_{ij}}{\partial X_j}\right) - \frac{\partial}{\partial X_j}\left(\frac{\partial G}{\partial X_i} q_{ij}\right) \quad .$$

Hence:

$$\iint_{\Sigma} Gq\, d\vec{X} = \iint_{\Sigma} \frac{\partial^2 G}{\partial X_i \partial X_j} q_{ij}\, d\vec{X} + \int_{C+C_R} G\frac{\partial q_{ij}}{\partial X_j} n_i\, ds(\vec{X}) - \int_{C+C_R} \frac{\partial G}{\partial X_i} q_{ij} n_j ds(\vec{X}).$$

Now:

$$\frac{\partial q_{ij}}{\partial X_j} = \rho\left(2\frac{\partial \bar{v}_i}{\partial X_j} v_j' + \frac{\partial v_i'}{\partial X_j} v_j' - \overline{\frac{\partial v_i'}{\partial X_j} v_j'}\right) .$$

Therefore both q_{ij} and $\frac{\partial q_{ij}}{\partial X_j}$ vanish on C . On C_R-W , q_{ij} is of the order of $1/R^2$ and $\partial q_{ij}/\partial X_j$ is of the order of $1/R^3$, consequently the integrals over C_R-W vanish as R goes to infinity. On W , the wake width, which is of the order of $R^{\frac{1}{2}}$, q_{ij} is of the order of $1/R^{\frac{1}{2}}$ and $\partial q_{ij}/\partial X_j$ is of the order of $1/R^{3/2}$ and therefore the integrals over W also vanish. We have finally:

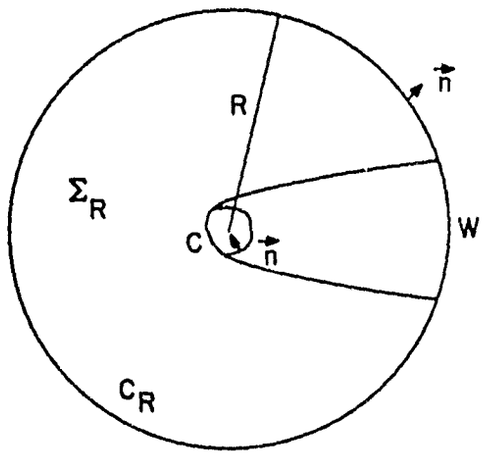

$$p'(\vec{Y},t) = \iint_{\Sigma} \frac{\partial^2 G(\vec{X}|\vec{Y})}{\partial X_i \partial X_j} q_{ij}(\vec{X},t)\, d\vec{X} + \mu \int_C G(\vec{X}|\vec{Y})\vec{n}.\nabla^2\vec{v}'(\vec{X},t)\, ds(\vec{X}) \quad .(2.31)$$

2.6 Structure of the Source Term Q - Some Practical Considerations.

In many practical problems an interesting and important question arises as to how the magnitude of the pressure fluctuations on the cylinder surface, or the magnitude of the lift and drag forces varies with Reynolds number. A quantitative answer to such a question would require quantitatively detailed information about the changes which occur in the flow when the Reynolds number is varied. However, at this stage of our knowledge of the complicated flow field behind bluff bodies, a qualitative analysis is useful in pointing out the major factors which come into play in determining the pressure fluctuations on the cylinder. To this end we take in this section a closer look at the source term Q in the three-dimensional case (corresponding to high Reynolds numbers) and compare with the two-dimensional one. Also, we concentrate on the discrete compo-

nent of the flow and the corresponding surface-pressure which is dominant at almost all Reynolds numbers and is of considerable interest in application.

First, we note that the continuity equation (the second in (2.1)) can be shown to be satisfied separately by the mean and the fluctuating parts of the velocity vector. Therefore, we have:

$$\frac{\partial \bar{v}_1}{\partial x_1} + \frac{\partial \bar{v}_2}{\partial x_2} = 0 \quad , \tag{2.32}$$

and

$$\frac{\partial v_1'}{\partial x_1} + \frac{\partial v_2'}{\partial x_2} + \frac{\partial v_3'}{\partial x_3} = 0 \quad . \tag{2.33}$$

Also if we denote by $\bar{\omega}_i$ and ω_i' , $i = i,2,3$ the mean and fluctuating components of the vorticity vector $\vec{\omega}$, we have:

$$\left.\begin{aligned} \omega_1' &= \frac{\partial v_3'}{\partial x_2} - \frac{\partial v_2'}{\partial x_3} \\ \omega_2' &= \frac{\partial v_1'}{\partial x_3} - \frac{\partial v_3'}{\partial x_1} \\ \omega_3' &= \frac{\partial v_2'}{\partial x_1} - \frac{\partial v_1'}{\partial x_2} \end{aligned}\right\} \tag{2.34}$$

Upon taking the Fourier transform of both sides of each relation in (2.34) and defining Ω_i $(i = 1,2,3)$ as:

$$\Omega_i(\vec{X},k,t) = \int_{-\infty}^{+\infty} \omega_i'(\vec{X},t) e^{-ikx_3} dx_3 \quad ; \quad i = 1,2,3 \quad . \tag{2.35}$$

we obtain:

$$\left.\begin{aligned} \Omega_1 &= \frac{\partial V_3}{\partial X_2} - ikV_2 \\ \Omega_2 &= ik V_1 - \frac{\partial V_3}{\partial X_1} \\ \Omega_3 &= \frac{\partial V_2}{\partial X_1} - \frac{\partial V_1}{\partial X_2} \end{aligned}\right\} \qquad (2.36)$$

Now:

$$\begin{aligned} q &= \frac{\partial^2 q_{ij}}{\partial x_i \partial x_j} \\ &= \frac{\partial^2 q_{11}}{\partial x_1^2} + \frac{\partial^2 q_{12}}{\partial x_1 \partial x_2} + \frac{\partial^2 q_{13}}{\partial x_1 \partial x_3} \\ &\quad + \frac{\partial^2 q_{21}}{\partial x_2 \partial x_1} + \frac{\partial^2 q_{22}}{\partial x_2^2} + \frac{\partial^2 q_{23}}{\partial x_2 \partial x_3} \\ &\quad + \frac{\partial^2 q_{31}}{\partial x_3 \partial x_1} + \frac{\partial^2 q_{32}}{\partial x_3 \partial x_2} + \frac{\partial^2 q_{33}}{\partial x_3^2} \end{aligned}$$

By referring to (2.6) and noting that $\overline{v}_3 = 0$, we have:

$$\begin{aligned} q &= \frac{\partial^2 q_{11}}{\partial x_1^2} + \frac{\partial^2 q_{12}}{\partial x_1 \partial x_2} \\ &\quad + \frac{\partial^2 q_{21}}{\partial x_2 \partial x_1} + \frac{\partial^2 q_{22}}{\partial x_2^2} \\ &\quad + \frac{\partial^2}{\partial x_1 \partial x_3} 2\rho(\overline{v}_1 v_3' + v_1' v_3' - \overline{v_1' v_3'}) \\ &\quad + \frac{\partial^2}{\partial x_2 \partial x_3} 2\rho(\overline{v}_2 v_3' + v_2' v_3' - \overline{v_2' v_3'}) \end{aligned}$$

$$+ \frac{\partial^2}{\partial x_3^2} \rho (v_3'^2 - \overline{v_3'^2}) \quad .$$

Let us designate by $F[\alpha]$ the Fourier transform with respect to x_3 of any quantity α. We have by applying the Fourier transform to q and noting, in view of the assumption of homogeneity in the x_3-direction, that $\overline{v_1'v_3'}$, $\overline{v_2'v_3'}$, and $\overline{v_3'^2}$ are independent of x_3:

$$Q = \frac{\partial^2 Q_{11}}{\partial X_1^2} + \frac{\partial^2 Q_{12}}{\partial X_1 \partial X_2}$$

$$+ \frac{\partial^2 Q_{21}}{\partial X_2 \partial X_1} + \frac{\partial^2 Q_{22}}{\partial X_2^2}$$

$$+ ik \frac{\partial}{\partial X_1} 2\rho(\overline{v}_1 V_3 + F[v_1'v_3'])$$

$$+ \frac{\partial}{\partial X_2} 2\rho(\overline{v}_2 V_3 + F[v_2'v_3'])$$

$$- k^2 \rho F[v_3'^2] \quad ,$$

where

$$Q_{ij} = \int_{-\infty}^{+\infty} q_{ij}(\vec{x},t) e^{-ikx_3} dx_3 \quad ; \quad i,j = i,2 \qquad (2.37)$$

or, using (2.32):

$$Q = \frac{\partial^2 Q_{ij}}{\partial X_i \partial X_j} + 2ik\rho(\overline{v_1} \frac{\partial V_3}{\partial X_1} + \overline{v_2} \frac{\partial V_3}{\partial X_2} + F[\frac{\partial}{\partial X_1}(v_1'v_3') + \frac{\partial}{\partial X_2}(v_2'v_3')]) - k^2 \rho F[v_3'^2] \quad .$$

The second term on the right-hand side can be written as:

$$2ik\rho(\overline{v_1}\frac{\partial V_3}{\partial X_1}+\overline{v_2}\frac{\partial V_3}{\partial X_2}+F[v_3'(\frac{\partial v_1'}{\partial X_1}+\frac{\partial v_2'}{\partial X_2})+v_1'\frac{\partial v_3'}{\partial X_1}+v_2'\frac{\partial v_3'}{\partial X_2}])\quad ,$$

or, using (2.33), (2.34), and (2.36) as:

$$2ik\rho\{\overline{v_1}(ikV_1-\Omega_2)+\overline{v_2}(ikV_2+\Omega_1)+$$

$$F[-v_3'\frac{\partial v_3'}{\partial x_3}+v_1'(\frac{\partial v_1'}{\partial x_3}-\omega_2')+v_2'(\frac{\partial v_2'}{\partial x_3}-\omega_1')]\}\quad ,$$

and finally as:

$$2ik\rho\{ik(\overline{v_1}V_1+\overline{v_2}V_2)+(\overline{v_2}\Omega_1-\overline{v_1}\Omega_2)-\tfrac{1}{2}ikF[v_3'^2]$$

$$+\tfrac{1}{2}ikF[v_1'^2+v_2'^2]+F[v_2'\omega_1'-v_1'\omega_2']\}\quad .$$

Consequently Q is given by:

$$Q=\frac{\partial^2 Q_{ij}}{\partial X_i\partial X_j}+2ik\rho(\overline{v_2}\Omega_1-\overline{v_1}\Omega_2)+2ik\rho F[v_2'\omega_1'-v_1'\omega_2']$$

$$-2k^2\rho(\overline{v_1}V_1+\overline{v_2}V_2)-k^2\rho F[v_1'^2+v_2'^2]\quad . \tag{2.38}$$

We emphasise that the first term on the right-hand side of (2.38) is the sume of four terms only and Q_{ij} is given by:

$$Q_{ij}=\rho(2\overline{v_i}V_j+F[v_i'v_j'-\overline{v_iv_j}])\quad ;\quad i,j=1,2 \tag{2.39}$$

In order to appreciate the expression of Q in the form (2.38), another feature of the discrete component of the fluctuating wake is worth elaborating upon. We have said in a previous section that this component results from the interaction of the two shear layers emanating from the surface of the cylinder, and has a finite length scale in the spanwise direction whose value varies with Reynolds number. While the interaction of

the two shear layers is a two-dimensional phenomenon, it is obvious that the finite spanwise length scale is the result of some three-dimensional effect. This effect which can be expected to be due to the presence of three-dimensional disturbances in the flow, takes place in each of the two shear layers separately. The evidence for this is provided by the experiment of Humphreys (1960) in the particular case of a circular cylinder at Reynolds numbers close to the critical value. Humphreys observed a periodic cellular structure along the length of the cylinder which was not altered by the introduction of a splitter plate in the wake, the effect of which is normally to prevent the interaction of the two shear layers (more discussion of this point is given in the next chapter). As for the nature of the effect of the three-dimensional disturbances on the individual shear layers, one might think that it is restricted to the generation of the small scale fluctuations which lead to the random component. However, since potentially amplifiable disturbances with wavevectors in all directions are usually present, the ones with wavevectors making a large angle with the direction of the mean flow have wavelengths large compared with the thickness of the shear layers. This is due to the fact that in the direction of such wavevectors the velocity jump across the layer is relatively small and correspondingly the wavelengths of the most amplified disturbances are likely to be large. Furthermore, when such disturbances grow to the extent of being able to change the direction of the flow streamlines from that of the main flow, which is in the plane normal to the cylinder, secondary flows in the form of flow-wise vorticity are generated* which strengthen the spanwise non-uniformity and

*Flow-wise vorticity is generated whenever a shear flow is turned in a plane normal to the velocity gradient.

create in a remarkable and puzzling manner a stable situation whose energy is continuously supplied by the mean shear flow. This flow-wise vorticity which is absent in the two-dimensional case constitutes, in addition to the finite character of the axial correlation length, the main distinguishing features of the flow at high Reynolds numbers. To see how this is reflected in the source function Q we consider the integral over Σ in the solution (2.15) namely:

$$\iint_{\Sigma} G(\vec{X}|\vec{Y};k)\, Q(\vec{X},t)\, d\vec{X} \quad .$$

Referring to (2.38) and integrating by parts the first term as in the two-dimensional case we obtain:

$$\iint_{\Sigma} \frac{\partial^2 G(\vec{X}|\vec{Y};k)}{\partial X_i \partial X_j}\, Q_{ij}(\vec{X},t)\, d\vec{X}$$

$$+ 2i\rho k \iint_{\Sigma} G(\vec{X}|\vec{Y};k)\, \{(\overline{v}_2\Omega_1 - \overline{v}_1\Omega_2) + F[v_2'\omega_1' - v_1'\omega_2']\}\, d\vec{X}$$

$$- \rho k^2 \iint_{\Sigma} G(\vec{X}|\vec{Y};k)\{2(\overline{v}_1 V_1 + \overline{v}_2 V_2) + F[v_1'^2 + v_2'^2]\}\, d\vec{X} \quad . \quad (2.40)$$

The first integral in (2.40) is the same as the one in (2.31) except that in (2.40) only the component with wavenumber k of q_{ij} is taken, and correspondingly $G(\vec{X}|\vec{Y};k)$ instead of $G(\vec{X}|\vec{Y})$ is used (note $G(\vec{X}|\vec{Y})$ is nothing but $G(\vec{X}|\vec{Y};0)$). Hence varying the Reynolds number means, for the discrete component, varying the value of k, higher values of k being in general associated with higher values of Re. Therefore, this term which can be thought of as a quasi-two-dimensional term reflects only

the effect of the finite spanwise correlation length of the large vortices at high Reynolds number. The second integral in (2.40) represents the contribution of the fluctuating flow-wise vorticity to the pressure fluctuations. In fact, the mean flow being steady the first term in that integral reflects the departure of this flow-wise vorticity from its mean position, since $(\bar{v}_2\bar{\omega}_1 - \bar{v}_1\bar{\omega}_2)$ vanishes when the vorticity vector in the plane (X_1,X_2) coincides with the mean velocity vector. The second term is a nonlinear effect resulting from the non-alignment of the two-dimensional components of the velocity and vorticity fluctuations vectors. The third integral is an additional term involving only the components of the velocity fluctuations in the plane (X_1,X_2) .

In conclusion we note that the solution of the problem as given in (2.15) or in the form (2.26) and (2.27) is a function of time. In practical problems one is interested in averaged quantities like correlations, intensities, and frequency spectra. Therefore, we define in general the two-point space-time correlation of the surface-pressure associated with the wavenumber k as:

$$R_{pp}(\vec{Y},\vec{Y},k,\tau) = \overline{P(\vec{Y},k,t)\, P^*(\vec{Y}',k,t+\tau)} \tag{2.41}$$

where the star indicates that the complex conjugate should be taken. Similarly for the lift and drag forces we define:

$$\left.\begin{aligned} R_{LL}(k,\tau) &= \overline{L(k,t)\, L^*(k,t+\tau)} \\ R_{DD}(k,\tau) &= \overline{D(k,t)\, D^*(k,t+\tau)} \end{aligned}\right\} \tag{2.42}$$

When the formal expressions of P , L and D are used in (2.41) and

(2.42), we obtain sums of double integrals over terms involving the factor $G(\vec{X}|\vec{Y};k)G(\vec{X}'|\vec{Y}';k)$ or $G_0(\vec{X}|\vec{Y};k)G_0(\vec{X}'|\vec{Y}';k)$, and averaged products of the form:

$$R_{AB}(\vec{X},\vec{X}',k,\tau) = \overline{A(\vec{X},k,t)B^*(\vec{X}',k,t+\tau)}$$

where A and B are the Fourier transforms of some physical quantities $a(\vec{x},t)$ and $b(\vec{x}',t+\tau)$. In accordance with the definition of Fourier transforms of quantities stationary with respect to the variable of transformation we have:

$$R_{AB}(\vec{X},\vec{X}',k,\tau) = \int_{-\ell/2}^{\ell/2}\int_{-\ell/2}^{\ell/2} \overline{a(\vec{x},t)b(\vec{x}',t+\tau)}\, e^{-ik(x_3-x_3')}\, dx_3 dx_3'$$

where ℓ is very large but finite (for instance the length of the cylinder), or:

$$R_{AB} = \int_{-\ell/2}^{\ell/2}\int_{-\ell/2}^{\ell/2} R_{ab}(\vec{X},\vec{X}',x_3-x_3',\tau)\, e^{-ik(x_3-x_3')}\, dx_3 dx_3'$$

$$= \ell \int_{-\ell/2}^{\ell/2} R_{ab}(\vec{X},\vec{X}',\xi,\tau)\, e^{-ik\xi}\, d\xi \quad .$$

Consequently, the spectrum densities per unit length of the cylinder R_{PP}/ℓ, R_{LL}/ℓ, and R_{DD}/ℓ are given as sums of double integrals over terms involving quantities of the form $F[R_{ab}]$. Therefore, from an experimental point of view the quantities to be measured, in order to determine the pressure characteristics, are the various cross-correlation functions $R_{ab}(\vec{X},\vec{X}',\xi,\tau)$.

2.7 Limitations of the Incompressible Flow.

The general analysis given in the previous sections is based on the incompressible form of the Navier-Stokes equations. In a steady flow it is well known that variations in the density of the fluid can be neglected if the Mach number is very small. However, for a time-dependent flow this condition is not sufficient, for no matter how slight the compressibility of the fluid is, compression waves make their appearance in the medium and affect a change in the incompressible flow condition. Nevertheless, it can be shown that within a length scale of the motion, and if that length scale is much smaller than the wavelength of these compression waves, the dynamics of the flow can be described as if the fluid were incompressible. More specifically if λ and τ are respectively a length and a time scale of the velocity fluctuations the condition for local incompressibility is:

$$\lambda \ll a_\infty \tau \quad , \tag{2.43}$$

where a_∞ is a typical speed of sound in the medium (see Landau and Lifshitz 1959, §10 or Batchelor 1967, §3.6). Since the Navier-Stokes equations are simply the expression of the dynamics of the flow within a small neighborhood of a given point the above condition (together with that of small Mach number) is sufficient for the validity of equations (2.1). However when these equations are combined together (to yield equation (2.4) and later (2.10)) an equation of the elliptic type is obtained which says that the pressure fluctuations at a point are not determined only by the local velocity field, but by the velocity field (both mean and fluctuating parts) throughout the entire unsteady region of the flow, the effect of each point, whether close or remote, being propagated with

an infinite speed. For this to be valid it remains to be shown that the major contribution to the pressure fluctuations as given by the solution of that elliptic equation (i.e., equations (2.15) and (2.31)) comes from points within a distance of the order of the length scale λ .

In the wake behind a cylinder several length and time scales are present in general. However since we have considered each length scale $\frac{2\pi}{k}$ in the axial direction separately, we can check the condition (2.43) for each separate value of k . When k corresponds to the discrete component of the wake the time scale can be taken as the inverse of the shedding frequency f of the vortices and the length scale in the plane (X_1, X_2) as the longitudinal spacing a of these vortices. Both a and f depend on the shape of the cylinder and for a given cylinder on the value of the Reynolds number. However for the sake of illustration we consider briefly the case of a circular cylinder. Then (2.43) can be written as:

$$a \ll a_\infty \frac{1}{f} \quad ,$$

or as:

$$\frac{1}{a_\infty} \ll \frac{1}{af}$$

and finally as:

$$\frac{U_\infty}{a_\infty} \ll \frac{d/a}{St} \quad ,$$

where St is the Strouhal number defined by $St = \frac{fd}{U_\infty}$. The lateral spacing of the vortices is generally of the order of the diameter d and therefore the ratio d/a is approximately equal to 0.28 (the Kármán ratio). On the other hand St is always between the values 0.12 and 0.21 (Roshko

1954). Consequently the above condition is the same as that of small Mach number. As for the relative importance of the contributions to the pressure fluctuations (on the surface of the cylinder for instance) from different regions of the flow field, it can be shown that, due to the rapid convergence of the integrals involved, the major one comes from points within a distance of the order of the longitudinal spacing of the vortices. In fact is is shown in the next chapter that this is true even for the least convergent case, namely the two-dimensional one.

When the random component is considered, for each value of k there exist several length and time scales in the (X_1, X_2) plane. Nevertheless a length scale of the velocity fluctuations in low Mach number turbulence is much smaller than the wavelength of the sound having the frequency of those fluctuations. Therefore (2.43) can be assumed to be satiffied for all the scales present. On the other hand for a given value of k the rate of convergence of the integrals in the solution is fixed since the Green's function $G(\vec{X}|\vec{Y};k)$ is fixed. Hence for each k there exist frequencies which are high enough for their wavelengths to be comparable with or smaller than the size of the region over which these integrals converge satisfactorily. For such frequencies the incompressible model breaks down and the compressibility of the medium must be taken into account.

CHAPTER 3

THE CIRCULAR CYLINDER IN UNIFORM CROSS FLOW

3.1 Introduction.

We shall now concern ourselves with the case of a circular cylinder in uniform cross flow. Our present state of knowledge of the nature of the unsteady forces acting on the surface of a circular cylinder in uniform cross flow is due primarily to a number of experimental investigations which were conducted and reported in the literature during the last twenty years. These investigations consisted in the first place of measuring directly the forces in question, either locally as pressure distributions or on a short segment of the cylinder as total lift and drag forces. In some instances direct measurements were made of the moment acting on the cylinder, from which values of the average forces were deduced. The objective behind these various measurements was to provide valuable data necessary for the design of cylindrical structures subject to cross winds, and also to provide information needed in the evaluation of the acoustic intensity radiated as aeolian tones. Concurrently, but quite independently, considerable effort was directed toward achieving a better understanding of the unsteady wake structure behind the cylinder. This effort was a continuation of an earlier interest in the subject which began after the discovery of the asymmetric arrangement of the vortices in the wake by Ahlborn and Bénard, and the subsequent work on the stability of such arrangement by von Kármán. Except in few cases, these two aspects of the problem, namely the wake structure on one hand and the unsteady loading on the cylinder on the other, continued to be treated separately and no attempt was ever made to study their interdependence. This is perhaps not

surprising because the study of the development of the vortices in the wake, their stability, their convection, and subsequent decay downstream was considered of a fundamental interest, while the determination of the unsteady loading on the cylinder was motivated by purely practical problems. In fact, the part of the wake which is intimately connected to that loading, namely the near-wake region, where the vortices are first formed and which is sometimes called the 'formation region' was seldom investigated in detail by the students of the first aspect. The few papers which considered the relationship between the structure of the near-wake and the unsteady forces were motivated by the inconsistency of the available data on these forces: measurements made under slightly different conditions yielded results with substantial discrepancies. Such discrepancies were suspected to be due, in addition to differences in the modes of measurements and the imperfections of the measuring devices, to differences in the free-stream turbulence level and the details of the experimental setup, and an attempt was made to explain the effect of these differences on the unsteady forces through their effect on the properties of the near-wake region. Although this attempt was only partially successful, being limited to qualitiative arguments, it led to substantial insight into the mechanics of the 'formation region.' Numerical solutions of the complete Navier-Stokes equations were equally attempted, but these cannot be expected to shed any light on controversial issues of the type in question since they depend on the manner in which the flow is perturbed and are based on purely two-dimensional models.

We present the theory of the preceding chapter as an alternative approach to the problem which clarifies the relationship between the flow

structure in the near-wake and the unsteady loading on the cylinder and puts it on a more firm and rigorous basis. This will enable us to reconsider some previously published incorrect results and will lead us to the discussion of some interesting features of the flow in the wake. In the next section a description of the flow field in the near-wake is given, together with a review of the available data on the unsteady loading and the available work relating the two aspects of the problem. This is followed by a detailed study of a representative case of the low Reynolds number regime. Finally, the high Reynolds number case is discussed in the last section.

3.2 Description of the Flow Field - Review of Previous Work.

The entire range of Reynolds number Re (based on the cylinder diameter), insofar as the nature of the fluctuating wake is concerned, can be broadly classified into three ranges (Roshko 1954). The first range extends from a value of Re between 30 and 40 to some value between 150 and 200 and is characterized by a stable and regular vortex street extending far downstream. The fluctuating energy of the flow is concentrated into discrete frequencies and decays downstream by the mere action of viscosity; no turbulence occurs in the flow. The second range which extends from Re between 150 and 200 to Re between 300 and 400 is a transition range characterized by irregular bursts in the velocity signal from a hot-wire placed in the flow indicating a laminar-turbulence transition and making the determination of the frequency of the dominant component rather difficult. The third range called the irregular range extends from Re between 300 and 400 to a value near 10^7 the highest

value of Reynolds number investigated up to date. In this range turbulent fluctuations accompany the periodic fluctuations; however the frequency of the latter is easily detected over most of the range. There is transfer of energy from the discrete components to the random ones as the fluctuations are convected downstream, and the wake decays by the combined action of viscous and turbulent stresses. It can be noted right away that the reason for which the limits between the various ranges are not well defined lies in the sensitivity of the flow to the experimental environment. For instance, the value of Re which marks the first appearance of fluctuations in the wake depends mainly on the ratio of the tunnel width to the cylinder diameter, being higher for smaller values of this ratio. On the other hand varying the level of turbulence in the free-stream can vary the limits between the first and second ranges and between the second and third ranges. We now consider in detail each of the three ranges separately.

The Stable Range.

For values of Re below 30 or 40 (and above a value near 6) the flow in the wake is steady and consists of two standing oppositely rotating eddies at the back of the cylinder and a laminar trail immediately downstream as shown in the figure. The vorticity generated in the boundary layer on the forward face of the cylinder goes in part into the standing eddies and in part into the trail forming the laminar wake (see Batchelor 1967, § 4.12). Föppl (see Goldstein

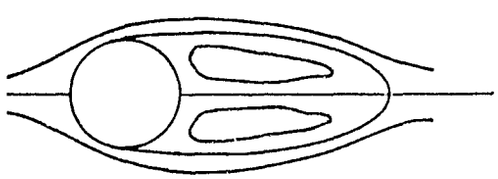

1938) showed, using an idealized model of two potential flow vortices that the symmetrical arrangement of the two eddies is unstable for asymmetric disturbances. It is an experimental fact (Kovasznay 1949, Taneda 1956) that when a value of Re between 30 or 40 is reached the laminar wake shows signs of instability before the standing eddies do. Regular sinusoidal fluctuations antisymmetric in the longitudinal velocity develop and are convected downstream in the form of a vortex street. As Re is increased, these fluctuations move closer to the cylinder and at a value of about 45 they begin to affect the tip of the standing eddies which begin to oscillate laterally assuming an asymmetric position. Below a value of Re between 90 and 110 (Tritton 1959, 1971) the standing eddies, although oscillating, remain attached and fluid does not leave them; above that value fluid moves continually out into the street, and Tritton speaks of two different modes of vortex shedding, a 'low-speed mode' which has its origin in the instability of the laminar wake and a 'high-speed mode' in which shedding starts in the immediate vicinity of the cylinder. Tritton (1959) discovered these two modes when studying the variation of the Strouhal number with Reynolds number, he observed a discontinuity in the St vs. Re curve at Re equal to 90, separating two different laws of variation of St with Re , and also irregularities in the street when Re was close to that value. Later Gaster (1969, 1971) found that such discontinuity or irregularities could arise from slight nonuniformities in the cylinder or in the free-stream in a direction along the span. Berger (see Wille, 1966) found another mode, the 'basic mode,' for Re above 120 similar to the 'low-speed mode' of Tritton. Tritton (1971) argued that the 'basic mode' of Berger could possibly occur throughout the whole

stable range instead of his two modes depending on the level of disturbances in the free-stream. These different findings were for some time the subject of a controversy which does not seem to have been settled yet (see the review by Berger and Wille, . .2).

The basic mechanism involved in the development of the laminar vortex street is two-dimensional; however three-dimensionalities in the wake in the form of slantwise shedding or waviness in the vortex filaments have been observed in this range of Reynolds number. These observations vary from one experiment to another especially as far as the degree of inclination of the vortices to the cylinder axis and the existence of waviness are concerned, which emphasizes once more the sensitivity of the flow to the experimental conditions and the level of disturbances in the free-stream. Gerrard (1966a) and Berger and Wille (1972) summarized the observations of various experimenters, and the picture which emerges indicates that for values of Re not exceeding 60 the flow is stable for small three-dimensional disturbances or slight non-uniformities in the cylinder or in the flow upstream and is truly two-dimensional. This is supported by experiments in both water tanks and wind tunnels (Kovasznay, 1949; Taneda, 1952; and Phillips, 1956). Gerrard (1966a) further concludes, on the basis of his own experiment and his analysis of the occurence of three-dimensionality that for values of Re below that of Tritton's transition "the wake is intrinsically stable and would exhibit a stable two-dimensional character if the flow and model arrangement were two-dimensional." This suggests that for such values of Re the attached eddies behind the cylinder provide at least in the near-wake region a stabilizing factor against three-dimensional disturbances. On the other hand,

for values of Re above that of the transition the shear layers which spring freely from the sides of the cylinder are more vulnerable to such disturbances and slantwise shedding or waviness in the vortex filaments occur inevitably as it is observed by most experimenters.

Results on the fluctuating loads in this first range of Reynolds number are scarce, in particular, the ones from direct measurements. The only available data are due to Tanida et al. (1973), and their Figure 3(b) is reproduced here for reference. In this figure $|\widetilde{C}_L|$ is the

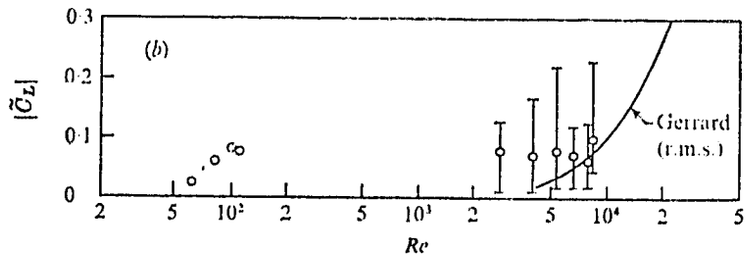

amplitude of the fluctuating lift coefficient defined by:

$$L = \frac{1}{2}\rho U_\infty^2 d \widetilde{C}_L \quad ,$$

where L is the lift per unit length. Tanida et al. made their measurements in an oil tank (for the low values of Re) on a 100 mm long central segment of a cylinder 352 mm long and 30 mm in diameter. The main feature of their results is the low level of lift fluctuations at low Reynolds numbers. Phillips (1956) using the data of Kovasznay (1949) at

Re equal to 56 , calculated the amplitude of the fluctuating lift and drag and obtained the rather high value of $|\tilde{C}_L| = 0.76$ for the lift. Jordan and Fromm (1972) solved numerically the complete time-dependent incompressible Navier-Stokes equations in two dimensions and obtained at Re equal to 100 the value $|\tilde{C}_L| = 0.27$. These variations in the results will be discussed at length later in this chapter.

The Transition Range.

When Re reaches a value between 150 and 200 , the flow in the near-wake, though still laminar, contains low-frequency irregularities which become more violent downstream and eventually render the far-wake turbulent (Bloor 1964). These low-frequency irregularities are believed to be due to three-dimensionalities in the flow. However, small bursts of turbulence do not make their appearance before a value of Re of 300 is reached (Bloor 1964). These occur at random in time and in a direction parallel to the cylinder axis making the vortex filaments in the street partly laminar, partly turbulent until a value of Re equal to 400 is reached. It has been argued by Roshko (1954) and Roshko and Fiszdon (1967) and observed by Bloor (1964) that these turbulent bursts occur right before the end of the formation region which is defined by Bloor as the beginning of the (turbulent) vortex street and by Roshko and Fiszdon as being located near the closure point or the tip of the two standing eddies of the corresponding mean flow.* As a result of the low-frequency irregularities associated with large scale three-dimensionalities and the intermittent turbulent bursts, the flow in the near-wake in this transi-

*Imai (1964) has shown that up to a value of Reynolds number of at least 6000 the mean flow pattern is similar to that at low Re where two standing eddies exist right behind the cylinder.

tion range is obviously three-dimensional. No information is available on the nature of the unsteady loading on the cylinder in this range except the numerical results of Jordan and Fromm (1972) at $Re = 400$. They obtained the value 0.75 for the amplitude of the lift coefficient.

The Irregular Range.

When a value of Re of about 400 is exceeded the turbulent bursts start to occur more systematically before the end of the formation region so all vortices in the street are turbulent on formation (Bloor 1964). The low-frequency irregularities continue to exist in the formation region and farther downstream with substantial reduction in intensity in the region in between. This state of affairs continues until a value of Re of about 1.3×10^3 is reached when sinusoidal waves of the Tollmien-Schlichting type begin to precede the turbulent bursts (Bloor 1964). These, called by Bloor, "transition waves " have a definite frequency f_t which is greater than the fundamental shedding frequency and varies (for a constant cylinder diameter) as $U_\infty^{3/2}$. The ratio of f_t to the fundamental frequency is proportional to $Re^{\frac{1}{2}}$ at high Reynolds number and it is equal to 2.5 at $Re = 1.3 \times 10^3$ and to 8 at $Re = 5 \times 10^3$. Below 1.3×10^3 the transition waves are not detected and as suggested by Roshko and Fiszdon (1967) it is possible that, since their frequency is very close to the shedding frequency in this range, there is a coupling between the two modes, in particular when Re is close to 400. Above 1.3×10^3 the low-frequency irregularities continue to exist in the formation region but disappear in the wake downstream. As Re is increased from 1.3×10^3 to 8×10^3 (Bloor 1964) the transition points in the separated shear layers move upstream rendering the downstream part of these shear layers more and more turbulent. Beyond $Re = 8 \times 10^3$ the transition waves are no longer visible

inside the wake, the laminar portion of the separated shear layers being rapidly followed by turbulence (Bloor 1964). Transition to turbulence continues to move upstream along the shear layers as Re is increased until it becomes very close to the separation points on the surface of the cylinder. When a value of Re of about 2×10^5, the so-called critical value, is reached and while the separation is still laminar, transition is followed by reattachment which in turn is followed by turbulent separation on the back of the cylinder. The wake is narrower, there is a sudden fall in the drag coefficient and a loss of periodicity in the wake. This continues until the transcritical regime is reached ($Re > 3.5\times10^6$) in which transition to turbulence precedes separation (Roshko 1961) and where a definte vortex shedding occurs as at subcritical Reynolds numbers. The critical or supercritical regime ($2\times10^5 < Re < 3.5\times10^6$) is characterized by a great sensitivity to surface roughness and free-stream turbulence, one manifestation of which is the loss of regular vortex shedding caused by gross non-uniformity along the length of the cylinder. Using highly polished cylinders Bearman (1969) conducted interesting experiments in the range $10^5 < Re < 7.5\times10^5$ and found that by carefully and frequently cleaning the cylinder during the experiment regular vortex shedding could continue up to a Reynolds number of 5.5×10^5.

There is less disagreement among the various experimenters about the existence and nature of three-dimensionalities in the irregular range than in the stable or transition range. As noted by Gerrard (1966a), "this is perhaps because the chaotic nature of the three-dimensional structure allows less precise description of the phenomena." Most workers describe

the three-dimensionality in terms of a spanwise correlation length, i.e., the distance in the axial direction over which the fluctuations of some property of the flow are well correlated. By correlating velocity fluctuations Roshko (1954) finds a value of 3 diameters at $Re = 500$. Prendergast (1958) correlated surface-pressure fluctuations but his correlation functions did not tend to zero for large separations. El Baroudi (1960) repeated the same experiment but instead correlated velocity fluctuations near the shoulder of the cylinder and found a correlation length which increases slowly with Reynolds number in the range $10^4 < Re < 4.5 \times 10^4$, being about 3 diameters at $Re = 10^4$ and about 6 diameters at $Re = 4.5 \times 10^4$. Phillips (1956) gives a value of 3 diameters at $Re = 5 \times 10^3$. Mattingly (1962) observed a spanwise periodicity on the surface of the cylinder in the range $10^4 < Re < 10^5$ with a wavelength of a few diameters. Using threads attached to the cylinder Humphreys (1960) observed a periodic cellular pattern with a wavelength of about 1.5 diameters at the critical Reynolds number. Gerrard (1966a) describes the nature of three-dimensionality in the irregular range as a combination of randomness associated with the small-scale turbulent structure and a "more gentle variation of the low Reynolds number type" probably associated with the low-frequency irregularities.

The bulk of the experimental data available concerning the unsteady loading on the cylinder corresponds to values of Re in the irregular range, and more specifically to values of Re greater than 2×10^3. Yet from these data it is not possible to draw any firm conclusion about the "true" level of the loading or its real behavior when the Reynolds number is varied across the range. This is perhaps best illustrated in Figure 15

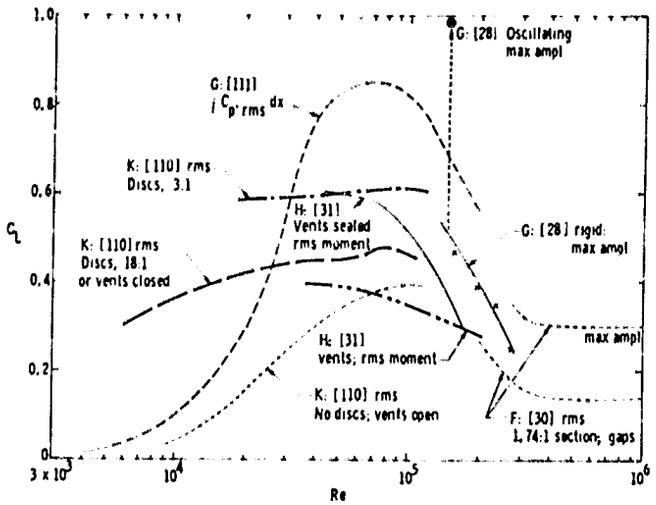

FIG. 15. OSCILLATORY LIFT COEFFICIENT.

of Morkovin's (1964) review which is reproduced here and in which the root mean square value or the maximum amplitude of the unsteady lift coefficient is shown. In this figure the results of Gerrard (1961), Keefe (1961), Humphreys (1960), Goldman (1958), and Fung (1960) are summarized and indicated symbolically by G[111] , K[110] , H[31], G[28], and F[30] respectively. Gerrard measured the r.m.s. value of the local pressure fluctuations at the shedding frequency and assuming a constant phase on each half (upper and lower) of the cylinder surface integrated to obtain the lift. Keefe measured the forces on a central segment of 1 diameter in length and examined the effects of fastening to the cylinder ends two circular discs (in order

to reduce the interference of the wall boundary layers) of diameter five times that of the cylinder and separated by a distance of 3 or 18 cylinder diameters and also the effect of sealing the clearance holes at both cylinder ends. Humphreys' results are based on measurements of the moment on a cantilevered cylinder; he also studied the effect of changing the end conditions. Fung measured the fluctuating forces on a short segment of 1.74 diameters at supercritical Reynolds numbers and noted the effect of the gaps between the force transducer and the rest of the cylinder, but did not recognize the effect of the length of his transducer being larger than the correlation length at these high Reynolds numbers. To these various data sets, others can be added but only to complicate further the general picture, the reason being, as we have stated earlier, the sensitivity of pressure or forces measurements to the details of the experimental setup, the imperfections of the measuring devices and the level of disturbances in the free-stream. Results not mentioned above include those of Macovsky (1958), McGregor (1957) who measured local pressure fluctuations, Jones et al (1969) at supercritical and transcritical Reynolds numbers, and also at these high Reynolds numbers those of Schmidt (1965, 1966). These latter (i.e., the high Re data, in particular those at supercritical Re) show in addition a strong dependence on the state of cleanliness of the cylinder which is a consequence of the extreme sensitivity of the flow to local surface roughness.

Among the various factors which can have a major impact on the measured values of the unsteady forces the free-stream turbulence is the only one which received some attention by the workers in the field. Gerrard (1965) puzzled by the large discrepancies between his results (of 1961) and those of Keefe (1961) and others, and by the low level of lift fluctua-

tions he observed at $Re = 4\times10^3$, investigated the effect of increasing the turbulence in his wind tunnel. Instead of measuring again the pressure fluctuations he measured the velocity fluctuations near the shoulder of the cylinder and found an increase (when the wind tunnel turbulence was increased) in the intensity of these velocity fluctuations similar to the discrepancy between his results and those of Keefe, indicating that this discrepancy is perhaps due to differences in the level of disturbances in the free-stream. He also recognized the role of characteristic length played by the length of the formation region but stopped short of considering the effect of an increase in free-stream turbulence to be equivalent to an effective increase in Re because the shedding frequency remained unchanged. Later he (Gerrard 1966b) discovered a second characteristic length, the length to which the shear layers diffuse at the end of the formation region and as a consequence achieved a substantial insight into the mechanics of the formation of vortices in the wake. On the basis of the two characteristic lengths Gerrard could explain why the Strouhal number remained constant over a wide range of Reynolds numbers and why the shedding frequency was insensitive to changes in the free-stream turbulence level. However, on the basis of the same arguments Gerrard could not explain the great change he observed (but Keefe did not) in the level of fluctuating lift when Re was varied from 4×10^3 to 7×10^4. This led him to suggest that possibly at the lower Reynolds number and in the absence of free-stream turbulence the two separated shear layers develop independently of each other creating a symmetrical formation region, the periodic wake downstream being formed in a manner similar to that at Reynolds numbers below 90 . The idea of a symmetrical formation region was, in fact, inspired by the results of his potential flow model (Gerrard

1967a) in which the shear layers separating from the sides of the cylinder were modelled by a distribution of elementary vortices moving under the action of the flow past the body and the velocity field of the vortices. This model however, when forced to generate a fluctuating lift in agreement with Gerrard's data at low Re , gave a formation region much larger than the value measured by Bloor (1964). Some comments on the model in question will be given at the end of the present chapter as part of our general discussion.

Finally, mention should be made of the few data points obtained by Tanida et al. (1973) in the range $2\times10^3 < Re < 10^4$ (using the same test cylinder as at low Re but with water as the medium) which are shown in the figure already introduced in connection with the low Reynolds number range, and also the value 0.95 for the amplitude of the lift coefficient found in the computations of Jordan and Fromm (1972) at $Re = 10^3$.

3.3 A Representative Case of the Low-Speed Mode of Vortex Shedding.

In this section we consider in detail the problem of determining analytically the unsteady pressure distribution on the surface of the cylinder when the Reynolds number Re is equal to 56 . At this Reynolds number Kovasznay (1949) investigated in some detail the velocity field in the wake and his data will be used to generate the essential terms needed for the application of the theory of the preceding chapter. Also at this Re the wake structure and the nature of the relationship between the near-wake and the surface-pressure are typical of the whole range below $Re = 90$, namely the vortex street develops as a result of the instability of the laminar wake and is stable and laminar. The velocity fluctuations are negligibly small near the cylinder and reach a maximum intensity some

distance downstream (Kovasznay 1949). The flow is two-dimensional and therefore the results of § 2.5 are applicable. In addition, in this range of Re we can make the assumption:

$$\vec{n}.\nabla p'\Big|_C = \mu\,\vec{n}.\nabla^2\vec{v}'\Big|_C = 0 \quad .$$

This is based on the following argument: since the vortex street develops some distance downstream of the cylinder, the unsteady part $\vec{\omega}'$ of the vorticity vector vanishes in the neighborhood of the cylinder, the small velocity fluctuations there being irrotational and induced by the vortical street further downstream; nevertheless at the boundary C and as a result of the no-slip condition additional unsteady vorticity might be generated locally, in other words, while the velocity fluctuations themselves are vanishingly small there their gradient can be large; this latter possibility however can be eliminated on the assumption that the frequency of the oscillatory motion in the wake is high, i.e., the "relaxation time" associated with the viscous flow is of the same order as, or even greater than, the time scale of the oscillations, and therefore the viscous effects do not have the time to respond to the full no-slip condition.* From this it follows that $\vec{\omega}'$ vanishes at and near the boundary C , and since

$$\nabla^2\vec{v}' = -\mathrm{Curl}\,\vec{\omega}'$$

*This is similar to the argument sometimes invoked in connection with the Kutta condition at the trailing edge of a thin airfoil shedding vortices at high frequencies. Previous experience has shown that relaxation of the Kutta condition in such circumstances yields results in better agreement with observations (see for instance Davis 1974). The question remains however whether the above condition is satisfied for values of Re above 90. It is interesting to note that in all the previous studies made on the case of a turbulent boundary layer the condition $\vec{n}.\nabla p' = 0$ at the solid boundary has been adopted.

the above condition can be considered satisfied. The resulting expression for the pressure p' is:

$$p'(\vec{Y},t) = \iint_{\Sigma} \frac{\partial^2 G(\vec{X}|\vec{Y})}{\partial X_i \partial X_j} q_{ij}(\vec{X},t)\, d\vec{X} \quad . \tag{3.1}$$

3.3.1 The Green's Function $G(\vec{X},\vec{Y})$.

As previously noted, the two-dimensional Green's function $G(\vec{X},\vec{Y})$ is nothing but the velocity potential of a negative unit source at $\vec{Y}$ in the presence of the boundary C which in the present case is a circle of diameter d . G is therefore the sum of the potential of that source in absence of C , plus that of a similar source at the inverse point $\vec{Y}'$ of $\vec{Y}$ with respect to C , and plus the potential of a source of opposite sign at the origin. In other words, G can be written as:

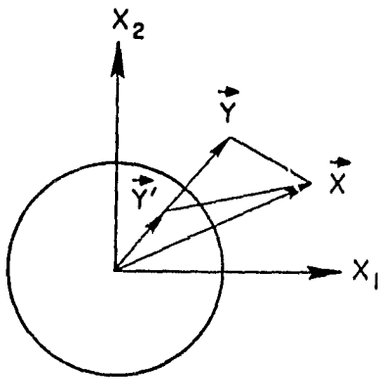

$$G(\vec{X}|\vec{Y}) = -\frac{1}{2\pi}\log|\vec{X}-\vec{Y}| - \frac{1}{2\pi}\log|\vec{X}-\vec{Y}'| + \frac{1}{2\pi}\log|\vec{X}| \quad ,$$

or as:

$$G(\vec{X}|\vec{Y}) = -\frac{1}{2\pi}\log\{(X_1-Y_1)^2+(X_2-Y_2)^2\}^{\frac{1}{2}} - \frac{1}{2\pi}\log\{(X_1-Y_1')^2+(X_2-Y_2')^2\}^{\frac{1}{2}}$$

$$+\frac{1}{2\pi}\log\{X_1^2+X_2^2\}^{\frac{1}{2}} \quad ,$$

where

$$Y_1' = \frac{(d/2)^2 Y_1}{Y_1^2+Y_2^2} \quad , \quad Y_2' = \frac{(d/2)^2 Y_2}{Y_1^2+Y_2^2} \quad .$$

Since in (3.1) the derivatives of G appear rather than G itself, we differentiate with respect to X_1 and X_2 to obtain the following expressions:

$$\frac{\partial^2 G}{\partial X_1^2} = -\frac{1}{2\pi}\left\{\frac{(X_2-Y_2)^2-(X_1-Y_1)^2}{[(X_1-Y_1)^2+(X_2-Y_2)^2]^2} + \frac{(X_2-Y_2')^2-(X_1-Y_1')^2}{[(X_1-Y_1')^2+(X_2-Y_2')^2]^2} - \frac{X_2^2-X_1^2}{(X_1^2+X_2^2)^2}\right\}$$

$$\frac{\partial^2 G}{\partial X_1 \partial X_2} = \frac{1}{2\pi}\left\{\frac{2(X_1-Y_1)(X_2-Y_2)}{[(X_1-Y_1)^2+(X_2-Y_2)^2]^2} + \frac{2(X_1-Y_1')(X_2-Y_2')}{[(X_1-Y_1')^2+(X_2-Y_2')^2]^2} - \frac{2X_1X_2}{(X_1^2+X_2^2)^2}\right\} ,$$

and since G is a harmonic function of X_1 and X_2 we have:

$$\frac{\partial^2 G}{\partial X_2^2} = -\frac{\partial^2 G}{\partial X_1^2} \quad \text{for} \quad X_1 \neq Y_1 \quad , \quad X_2 \neq Y_2 \quad .$$

When we evaluate the surface-pressure fluctuations as given by (3.1), $\vec{Y}$ goes onto the circle C and Y_1', Y_2' become respectively Y_1 and Y_2; the above expressions reduce to:

$$\frac{\partial^2 G}{\partial X_1^2} = -\frac{1}{\pi}\left\{\frac{(X_2-Y_2)^2-(X_1-Y_1)^2}{[(X_1-Y_1)^2+(X_2-Y_2)^2]^2} - \frac{1}{2}\frac{X_2^2-X_1^2}{(X_1^2+X_2^2)^2}\right\} \quad , \quad \vec{Y} \text{ on } C \quad (3.2)$$

$$\frac{\partial^2 G}{\partial X_1 \partial X_2} = \frac{1}{\pi}\left\{\frac{2(X_1-Y_1)(X_2-Y_2)}{[(X_1-Y_1)^2+(X_2-Y_2)^2]^2} - \frac{1}{2}\frac{2X_1X_2}{(X_1^2+X_2^2)^2}\right\} \quad , \quad \vec{Y} \text{ on } C \quad (3.3)$$

3.3.2 The Velocity Field in the Wake.

Both the mean and the fluctuating parts of the velocity field in the wake at $Re = 56$ were investigated by Kovasznay using the hot-wire technique. Measurements of the total mean velocity distribution and that of the r.m.s. value of the velocity fluctuations were made at several down-

stream stations. In addition, it was observed that the fluctuating velocity had two components with two different frequencies, one is the shedding frequency f, the other is the double frequency $2f$, and the phases of these two components as functions of X_1 were determined. At the middle of the wake only the double frequency component was present, but this decreased rapidly with distance from the wake centerline and disappeared almost completely before the point of maximum fluctuations was reached.

In order to determine the various q_{ij} terms in (3.1) the two components $\overline{v_1}$ and $\overline{v_2}$ of the mean velocity vector are needed. However, by examining the mean streamline pattern plotted in Kovasznay's work and a similar plot made during the present work it was judged that the $\overline{v_2}$ component is everywhere a small fraction (perhaps 10% or less) of the total mean value except in a central narrow region of width $1.5d$ bounded downstream by $X_1 = 5d$; in that region the total mean velocity is a small fraction of the free-stream velocity U_∞; consequently it will be assumed here that everywhere $\overline{v_2}$ is an order of magnitude smaller than U_∞. As for $\overline{v_1}$ it is to a good approximation equal to the measured value $\overline{v} = (\overline{v_1}^2+\overline{v_2}^2)^{\frac{1}{2}}$ except in the narrow region mentioned above. This region contains the two standing eddies in which there is a reverse flow (see Taneda's 1956 picture at $Re = 57.7$). Kovasznay measured $\overline{v}$ at $X_1 = 2d, 3.5d, 5d, 8d, \ldots$ At $X_1 = 2d$ and $3.5d$ the measured values on the wake centerline which are exactly those of $\overline{v_1}$, were taken here as negative and an interpolation (numerical, using spline functions) was made between these values and values off the centerline which were judged to be a good approximation of $\overline{v_1}$. In this manner the distribution of $\overline{v_1}$ in the region of the standing eddies where $\overline{v_2}$ can be larger than $\overline{v_1}$ and in particular where $\overline{v_1}$ changes sign was determined. Again it is believed

that $\overline{v_1}$ as determined by the data and the above procedure is accurate up to 10% .

In addition to the mean velocity components the determination of q_{ij} requires a knowledge of the fluctuating velocity components v_1' and v_2' . Since the hot-wire is more sensitive to the fluctuating velocity component in the direction of the mean flow and since the direction of the latter is, to a good approximation, in the X_1-direction everywhere except in the neighborhood of the standing eddies, the r.m.s. values as measured by Kovasznay can be taken as those of v_1' except in that region; there a similar procedure to the one used above was adopted. As suggested by Kovasznay, we can write:

$$v_1' = \varphi_1(X_1,X_2)\cos 2\pi[\theta_1(X_1)-ft]+\varphi_2(X_1,X_2)\cos 4\pi[\theta_2(X_1)-ft] , \tag{3.4}$$

where φ_1 and φ_2 are respectively the amplitudes of the fundamental component and its first harmonic and θ_1 and θ_2 their phases.* In addition, φ_1 is an odd function of X_2 and φ_2 is an even function of X_2 which can be assumed to vanish parabolically in the transversal direction, i.e.,

$$\varphi_2(X_1,X_2) = \varphi_2(X_1,0)\left[1-\frac{X_2^2}{X_{20}^2}\right] , \tag{3.5}$$

where X_{20} is the value of X_2 for which the total fluctuations are a maximum. Using (3.4) and (3.5) and noting that:

*In fact, Kovasznay had a + sign inside the brackets in the expression corresponding to (3.4), but since the vortices are convected in the positive X_1-direction and θ_1 and θ_2 are increasing functions of X_1 a - sign is more appropriate.

$$\overline{v_1'^2} = \frac{1}{2}(\varphi_1^2 + \varphi_2^2) \quad ,$$

φ_1 and φ_2 can be calculated from the measured r.m.s. values. These latter are vanishingly small for $X_1 < 2d$, peak at about $X_1 = 7d$ and slightly off the wake centerline, and are everywhere an order of magnitude smaller than the mean velocity. As for v_2', which was not measured by Kovasznay it will be determined here using the continuity equation. First we note that like v_1', v_2' has two components with two different frequencies. One is f, the other is $2f$. It can be easily seen that the continuity equation must be satisfied separately by each frequency component; in other words, if we denote by v_{11}' and v_{12}' the components of v_1' with frequencies f and $2f$ respectively, and by v_{21}' and v_{22}' those of v_2', we have:

$$\frac{\partial v_{11}'}{\partial X_1} + \frac{\partial v_{21}'}{\partial X_2} = 0$$

and

$$\frac{\partial v_{12}'}{\partial X_1} + \frac{\partial v_{22}'}{\partial X_2} = 0 \quad .$$

v_{21}' and v_{22}' vanish at $X_2 = \pm\infty$, in addition v_{22}' vanishes at $X_2 = 0$. This can be seen by examining the velocity field of an idealized vortex street where it is found that v_2' on the wake axis is of pure fundamental frequency. This is also observed experimentally in the wake of cylindrical bodies shedding vortices (see for instance Campbell 1957). Consequently, integrating the above equations yields:

$$v_{21}' = -\int_{-\infty}^{X_2} \frac{\partial}{\partial X_1} v_{11}'(X_1, \xi_2, t)\, d\xi_2$$

and

$$v'_{22} = -\int_0^{X_2} \frac{\partial}{\partial X_1} v'_{11}(X_1, \xi_2, t)\, d\xi_2 \quad ,$$

therefore:

$$v'_2 = -\int_{-\infty}^{X_2} \frac{\partial}{\partial X_1} v'_{11}(X_1, \xi_2, t)\, d\xi_2 - \int_0^{X_2} \frac{\partial}{\partial X_1} v'_{12}(X_1, \xi_2, t)\, d\xi_2 \quad ,$$

or

$$v'_2 = -\frac{\partial w}{\partial X_1} \quad , \tag{3.6}$$

where

$$w = \int_{-\infty}^{X_2} v'_{11}(X_1, \xi_2, t)\, d\xi_2 + \int_0^{X_2} v'_{12}(X_1, \xi_2, t)\, d\xi_2$$

or

$$w(X_1, X_2, t) = \psi_1(X_1, X_2) \cos 2\pi[\theta_1(X_1) - ft] + \psi_2(X_1, X_2) \cos 4\pi[\theta_2(X_1) - ft] \quad , \tag{3.7}$$

where

$$\left.\begin{aligned} \psi_1(X_1, X_2) &= \int_{-\infty}^{X_2} \varphi_1(X_1, \xi_2)\, d\xi_2 \\ \psi_2(X_1, X_2) &= \int_0^{X_2} \varphi_2(X_1, \xi_2)\, d\xi_2 \end{aligned}\right\} \tag{3.8}$$

In order to evaluate ψ_1 inside the wake, values of φ_1 outside the wake are needed. The available data from which φ_1 was calculated cover the wake region up to 5 or 6 diameters from the centerline, at these borderlines the r.m.s. values of the fluctuations are very small and so is φ_1. However, in order to account for the remaining part of the integral, i.e., the part beyond $X_2 = 5$ or $6d$, φ_1 was assumed to decay like

$1/X_2^2$ in the $\pm X_2$-direction (see § 2.5).

3.3.3 The Fluctuating Surface-Pressure Field - Lift and Drag Fluctuations.

The fluctuating surface-pressure field is given by (3.1) where $\vec{Y}$ is taken on the circle C . By expanding (3.1) we obtain:

$$p'(\vec{Y},t) = \iint_\Sigma \frac{\partial^2 G}{\partial X_1^2} q_{11} dX_1 dX_2 + \iint_\Sigma \frac{\partial^2 G}{\partial X_1 \partial X_2} q_{12} dX_1 dX_2$$

$$+ \iint_\Sigma \frac{\partial^2 G}{\partial X_2 \partial X_1} q_{21} dX_1 dX_2 + \iint_\Sigma \frac{\partial^2 G}{\partial X_2^2} q_{22} dX_1 dX_2 \quad .$$

We also have:

$$q_{ij}(\vec{X},t) = \rho(2\overline{v_i} v_j' + v_i' v_j' - \overline{v_i' v_j'}) \quad .$$

Therefore:

$$p'(\vec{Y},t) = 2\rho \iint_\Sigma \frac{\partial^2 G}{\partial X_1^2} \overline{v_1} v_1' dX_1 dX_2 + 2\rho \iint_\Sigma \frac{\partial^2 G}{\partial X_1 \partial X_2} \overline{v_1} v_2' dX_1 dX_2$$

$$+ 2\rho \iint_\Sigma \frac{\partial^2 G}{\partial X_1 \partial X_2} \overline{v_2} v_1' dX_1 dX_2 - 2\rho \iint_\Sigma \frac{\partial^2 G}{\partial X_1^2} \overline{v_2} v_2' dX_1 dX_2$$

$$+ \rho \iint_\Sigma \frac{\partial^2 G}{\partial X_1^2} (v_1'^2 - \overline{v_1'^2}) dX_1 dX_2 + 2\rho \iint_\Sigma \frac{\partial^2 G}{\partial X_1 \partial X_2} (v_1' v_2' - \overline{v_1' v_2'}) dX_1 dX_2$$

$$- \rho \iint_\Sigma \frac{\partial^2 G}{\partial X_1^2} (v_2'^2 - \overline{v_2'^2}) dX_1 dX_2 \quad . \qquad (3.9)$$

In evaluating p' only the first two terms in (3.9) will be retained, these are thought to contain the major contributions to the real value of p' . The contribution from the third and fourth terms which contain the

mean velocity component $\overline{v_2}$ can be expected not to exceed 10% of the contribution from the first two, and is perhaps of the same order of magnitude as the error involved in evaluating the first two integrals with $\overline{v_1}$ as determined in the last section. The contribution from the remaining terms, which are quadratic in the velocity fluctuations, is discussed in the Appendix. With the understanding that we are computing only an approximate value we write:

$$p'(\vec{Y},t) = 2\rho \iint_{\Sigma} \frac{\partial^2 G}{\partial X_1^2} \overline{v_1}\, v_1'\, dX_1\, dX_2 + 2\rho \iint_{\Sigma} \frac{\partial^2 G}{\partial X_1 \partial X_2} \overline{v_1}\, v_2'\, dX_1\, dX_2 \quad , (3.10)$$

or

$$p'(\vec{Y},t) = 2\rho \iint_{\Sigma} \frac{\partial^2 G}{\partial X_1^2} \overline{v_1}\, v_1'\, dX_1\, dX_2 - 2\rho \iint_{\Sigma} \frac{\partial^2 G}{\partial X_1 \partial X_2} \overline{v_1}\, \frac{\partial w}{\partial X_1}\, dX_1\, dX_2$$

$$= 2\rho \iint_{\Sigma} \frac{\partial^2 G}{\partial X_1^2} \overline{v_1}\, v_1'\, dX_1\, dX_2 - 2\rho \iint_{\Sigma} \frac{\partial}{\partial X_1} \left(\frac{\partial^2 G}{\partial X_1 \partial X_2} \overline{v_1} w\right) dX_1\, dX_2$$

$$+ 2\rho \iint_{\Sigma} \frac{\partial^3 G}{\partial X_1^2 \partial X_2} \overline{v_1}\, w\, dX_1\, dX_2 + 2\rho \iint_{\Sigma} \frac{\partial^2 G}{\partial X_1 \partial X_2} \frac{\partial \overline{v_1}}{\partial X_1}\, w\, dX_1\, dX_2 \quad .$$

The second integral in the above expression can be integrated partially with respect to X_1 between some value X_{10} of X_1 such that $\frac{1}{2}d < X_{10} < 2d$ and $X_1 = +\infty$. At X_{10} φ_1 and φ_2 are vanishingly small and since $\overline{v_1}$ and $\frac{\partial^2 G}{\partial X_1 \partial X_2}$ are finite there, the product $\frac{\partial^2 G}{\partial X_1 \partial X_2} \overline{v_1}\, w \Big|_{X_{10}}$ is negligible. Furthermore, as $X_1 \to +\infty$ $\overline{v_1}$ and w remain finite, however, $\frac{\partial^2 G}{\partial X_1 \partial X_2}$ decays like $\frac{1}{X_1^3}$ (see equation (3.3)) and the product vanishes again. Therefore the integral in question vanishes and we have:

$$p'(\vec{Y},t) = 2\rho \iint_{\Sigma} \frac{\partial^2 G}{\partial X_1^2} \overline{v_1}\, v_1'\, dX_1\, dX_2 + 2\rho \iint_{\Sigma} \frac{\partial^3 G}{\partial X_1^2 \partial X_2} \overline{v_1}\, w\, dX_1\, dX_2$$

$$+ 2\rho \iint_{\Sigma} \frac{\partial^2 G}{\partial X_1 \partial X_2} \frac{\partial \overline{v_1}}{\partial X_1}\, w\, dX_1\, dX_2 \quad . \tag{3.11}$$

The above step, i.e. the partial integration with respect to X_1 is vital for maintaining a good accuracy of the numerical computations. The data which will be used to evaluate the physical functions in the above integrals cover only the part of the wake between $X_1 = 2d$ and $X_1 = 40d$. Although ψ_1 and ψ_2 are small for $X_1 < 2d$, their derivatives with respect to X_1 there cannot be accounted for numerically with a good accuracy. In addition, the form assumed for φ_2 and the numerical representation of φ_1 are approximate; therefore while their integrated values ψ_1 and ψ_2 are still a good approximation, the derivatives of the latter, i.e., $\partial\psi_1/\partial X_1$ and $\partial\psi_2/\partial X_1$ (taken numerically) are not.* Finally, while in (3.11) only one numerical differentiation is required, in (3.10) four are necessary to evaluate v_2'.

We now define the following functions:

$$\left.\begin{aligned} \alpha(X_1,X_2) &= \frac{X_2^2 - X_1^2}{(X_1^2+X_2^2)^2} \\ \beta(X_1,X_2) &= \frac{2X_2(3X_1^2 - X_2^2)}{(X_1^2+X_2^2)^3} \\ \gamma(X_1,X_2) &= \frac{2X_1X_2}{(X_1^2+X_2^2)^2} \end{aligned}\right\} \tag{3.12}$$

*Numerical integration is always a smoothing process, unlike numerical differentiation which reduces the accuracy.

It follows from (3.2) and (3.3) that when $\vec{Y}$ lies on C :

$$\frac{\partial^2 G}{\partial X_1^2} = -\frac{1}{\pi}\{\alpha(X_1-Y_1, X_2-Y_2) - \tfrac{1}{2}\alpha(X_1, X_2)\} \tag{3.13}$$

$$\frac{\partial^2 G}{\partial X_1 \partial X_2} = \frac{1}{\pi}\{\gamma(X_1-Y_1, X_2-Y_2) - \tfrac{1}{2}\gamma(X_1, X_2)\} \tag{3.14}$$

and also after one additional differentiation with respect to X_1 :

$$\frac{\partial^3 G}{\partial X_1^2 \partial X_2} = -\frac{1}{\pi}\{\beta(X_1-Y_1, X_2-Y_2) - \tfrac{1}{2}\beta(X_1, X_2)\} \quad . \tag{3.15}$$

We note that α is an even function of X_2 and β and γ are odd functions of X_2 . In addition, $\overline{v_1}$ and $\partial\overline{v_1}/\partial X_1$ are even functions of X_2 , φ_1 and ψ_2 are odd functions of X_2 , and finally φ_2 and ψ_1 are even functions of X_2 . Using the equations (3.4), (3.7), (3.13), (3.14), and (3.15), relation (3.11) can be written in the form:

$$p'(\vec{Y},t) = -\frac{2\rho}{\pi}\iint_{\Sigma}\{\alpha(X_1-Y_1, X_2-Y_2) - \tfrac{1}{2}\alpha(X_1, X_2)\}\overline{v_1}\{\varphi_1 \cos 2\pi(\theta_1 - ft) +$$

$$+ \varphi_2 \cos 4\pi(\theta_2 - ft)\}\, dX_1\, dX_2$$

$$-\frac{2\rho}{\pi}\iint_{\Sigma}\{\beta(X_1-Y_1, X_2-Y_2) - \tfrac{1}{2}\beta(X_1, X_2)\}\overline{v_1}\{\psi_1 \cos 2\pi(\theta_1 - ft) +$$

$$+ \psi_2 \cos 4\pi(\theta_2 - ft)\}\, dX_1\, dX_2$$

$$+ \frac{2\rho}{\pi} \iint \{\nu(X_1 - Y_1, X_2 - Y_2) - \frac{1}{2}\nu(X_1, X_2)\} \frac{\partial \overline{v_1}}{\partial X_1} \{\psi_1 \cos 2\pi(\theta_1 - ft) +$$

$$+ \psi_2 \cos 4\pi(\theta_2 - ft)\} dX_1\, dX_2$$

It is easily seen that after expanding the above expression, the integrals which contain the product $\alpha \overline{v_1} \varphi_1$, $\beta \overline{v_1} \psi_1$ and $\nu \frac{\partial \overline{v_1}}{\partial X_1} \psi_1$ vanish and what remains can be written in the form:

$$p'(\vec{Y}, t) = - \frac{2\rho}{\pi} \iint_{X_2 \geq 0} \alpha_1 \overline{v_1} \varphi_1 \cos 2\pi(\theta_1 - ft)\, dX_1\, dX_2$$

$$- \frac{2\rho}{\pi} \iint_{X_2 \geq 0} \alpha_2 \overline{v_1} \varphi_2 \cos 4\pi(\theta_2 - ft)\, dX_1\, dX_2$$

$$+ \frac{2\rho}{\pi} \iint_{X_2 \geq 0} \alpha \overline{v_1} \varphi_2 \cos 4\pi(\theta_2 - ft)\, dX_1\, dX_2$$

$$- \frac{2\rho}{\pi} \iint_{X_2 \geq 0} \beta_1 \overline{v_1} \psi_1 \cos 2\pi(\theta_1 - ft)\, dX_1\, dX_2$$

$$- \frac{2\rho}{\pi} \iint_{X_2 \geq 0} \beta_2 \overline{v_1} \psi_2 \cos 4\pi(\theta_2 - ft)\, dX_1\, dX_2$$

$$+ \frac{2\rho}{\pi} \iint_{X_2 \geq 0} \beta \overline{v_1} \psi_2 \cos 4\pi(\theta_2 - ft)\, dX_1\, dX_2$$

$$+ \frac{2\rho}{\pi} \iint_{X_2 \geq 0} \gamma_1 \frac{\partial \overline{v_1}}{\partial X_1} \psi_1 \cos 2\pi(\theta_1 - ft)\, dX_1\, dX_2$$

$$+\frac{2\rho}{\pi}\iint_{X_2\geq 0}\gamma_2\frac{\partial\overline{v_1}}{\partial X_1}\psi_2\cos 4\pi(\theta_2-ft)\,dX_1\,dX_2$$

$$-\frac{2\rho}{\pi}\iint_{X_2\geq 0}\gamma\frac{\partial\overline{v_1}}{\partial X_1}\psi_2\cos 4\pi(\theta_2-ft)\,dX_1\,dX_2\quad,$$

where:

$$\left.\begin{aligned}\alpha_1(\vec{X};\vec{Y}) &= \alpha(X_1-Y_1,X_2-Y_2)-\alpha(X_1-Y_1,X_2+Y_2)\\ \alpha_2(\vec{X};\vec{Y}) &= \alpha(X_1-Y_1,X_2-Y_2)+\alpha(X_1-Y_1,X_2+Y_2)\end{aligned}\right\}\qquad(3.16)$$

$$\left.\begin{aligned}\beta_1(\vec{X};\vec{Y}) &= \beta(X_1-Y_1,X_2-Y_2)-\beta(X_1-Y_1,X_2+Y_2)\\ \beta_2(\vec{X};\vec{Y}) &= \beta(X_1-Y_1,X_2-Y_2)+\beta(X_1-Y_1,X_2+Y_2)\end{aligned}\right\}\qquad(3.17)$$

$$\left.\begin{aligned}\gamma_1(\vec{X};\vec{Y}) &= \gamma(X_1-Y_1,X_2-Y_2)-\gamma(X_1-Y_1,X_2+Y_2)\\ \gamma_2(\vec{X};\vec{Y}) &= \gamma(X_1-Y_1,X_2-Y_2)+\gamma(X_1-Y_1,X_2+Y_2)\end{aligned}\right\}\qquad(3.18)$$

Finally, if we denote by ω the angular frequency $2\pi f$ and we introduce the non-dimensional quantitites $\overline{v_1}/U_\infty$, φ_1/U_∞, φ_2/U_∞, $\psi_1/U_\infty d$, $\psi_2/U_\infty d$, $\frac{\partial(\overline{v_1}/U_\infty)}{\partial(X_1/d)}$, $\frac{X_1}{d}$, and $\frac{X_2}{d}$ we obtain:

$$\frac{p'(\vec{Y},t)}{\rho U_\infty^2}=-\frac{2}{\pi}\cos\omega t\iint_{X_2\geq 0}d^2\left(\alpha_1\frac{\overline{v_1}}{U_\infty}\frac{\varphi_1}{U_\infty}+d\beta_1\frac{\overline{v_1}}{U_\infty}\frac{\psi_1}{U_\infty d}-\gamma_1\frac{\partial(\overline{v_1}/U_\infty)}{\partial(X_1/d)}\frac{\psi_1}{U_\infty d}\right)\cos 2\pi\theta_1\,d\left(\frac{X_1}{d}\right)d\left(\frac{X_2}{d}\right)$$

$$-\frac{2}{\pi}\sin\omega t\iint_{X_2\geq 0}d^2\left(\alpha_1\frac{\overline{v_1}}{U_\infty}\frac{\varphi_1}{U_\infty}+d\beta_1\frac{\overline{v_1}}{U_\infty}\frac{\psi_1}{U_\infty d}-\gamma_1\frac{\partial(\overline{v_1}/U_\infty)}{\partial(X_1/d)}\frac{\psi_1}{U_\infty d}\right)\sin 2\pi\theta_1\,d\left(\frac{X_1}{d}\right)d\left(\frac{X_2}{d}\right)$$

$$
-\frac{2}{\pi}\cos 2\omega t \iint_{X_2\geq 0} d^2\left(\alpha_2 \frac{\overline{v_1}}{U_\infty}\frac{\varphi_2}{U_\infty} + d\beta_2 \frac{\overline{v_1}}{U_\infty}\frac{\psi_2}{U_\infty d} - \gamma_2 \frac{\partial(\overline{v_1}/U_\infty)}{\partial(X_1/d)}\frac{\psi_2}{U_\infty d}\right)\cos 4\pi\theta_2 d\left(\frac{X_1}{d}\right) d\left(\frac{X_2}{d}\right)
$$

$$
-\frac{2}{\pi}\sin 2\omega t \iint_{X_2\geq 0} d^2\left(\alpha_2 \frac{\overline{v_1}}{U_\infty}\frac{\varphi_2}{U_\infty} + d\beta_2 \frac{\overline{v_1}}{U_\infty}\frac{\psi_2}{U_\infty d} - \nu_2 \frac{\partial(\overline{v_1}/U_\infty)}{\partial(X_1/d)}\frac{\psi_2}{U_\infty d}\right)\sin 4\pi\theta_2 d\left(\frac{X_1}{d}\right) d\left(\frac{X_2}{d}\right)
$$

$$
+\frac{2}{\pi}\cos 2\omega t \iint_{X_2\geq 0} d^2\left(\alpha \frac{\overline{v_1}}{U_\infty}\frac{\varphi_2}{U_\infty} + d\beta \frac{\overline{v_1}}{U_\infty}\frac{\psi_2}{U_\infty d} - \gamma \frac{\partial(\overline{v_1}/U_\infty)}{\partial(X_1/d)}\frac{\psi_2}{U_\infty d}\right)\cos 4\pi\theta_2 d\left(\frac{X_1}{d}\right) d\left(\frac{X_2}{d}\right)
$$

$$
+\frac{2}{\pi}\sin 2\omega t \iint_{X_2\geq 0} d^2\left(\alpha \frac{\overline{v_1}}{U_\infty}\frac{\varphi_2}{U_\infty} + d\beta \frac{\overline{v_1}}{U_\infty}\frac{\psi_2}{U_\infty d} - \gamma \frac{\partial(\overline{v_1}/U_\infty)}{\partial(X_1/d)}\frac{\psi_2}{U_\infty d}\right)\sin 4\pi\theta_2 d\left(\frac{X_1}{d}\right) d\left(\frac{X_2}{d}\right) . \tag{3.19}
$$

Note that:

$$
d^2\alpha_1(\vec{X};\vec{Y}) = \alpha_1(\vec{X}/d;\vec{Y}/d)
$$

$$
d^3\beta_1(\vec{X};\vec{Y}) = \beta_1(\vec{X}/d;\vec{Y}/d)
$$

$$
d^2\gamma_1(\vec{X};\vec{Y}) = \nu_1(\vec{X}/d;\vec{Y}/d)
$$

and that similar identities hold for α_2 , β_2 , γ_2 and α , β , γ .

As is clear from (3.10) the surface-pressure fluctuations contain two components with two different frequencies, one is the fundamental or shedding frequency and is represented by the first two terms in (3.19); the other is the double frequency and is represented by the remaining four terms. In addition, we note that α_1 , β_1 , and γ_1 are odd functions of Y_2 while α_2 , β_2 , and γ_2 are even functions of Y_2 . This implies that the fundamental frequency component is antisymmetric with respect to

to the direction of the free-stream, while the double frequency component is symmetric with respect to that direction. In terms of the lift and drag fluctuations this means that the lift fluctuates with the shedding frequency and the drag fluctuates with twice that frequency!

The data of Kovasznay were used to determine the integrands in (3.19) as was indicated in the last section. These data were first smoothed and interpolations were made using spline functions; the results of the interpolations were checked and proved to be excellent. Then the various functions θ_1 , θ_2 , $\overline{v_1}/U_\infty$, $\frac{\partial(\overline{v_1}/U_\infty)}{\partial(X_1/d)}$, $\frac{\varphi_1}{U_\infty}$, $\frac{\varphi_2}{U_\infty}$, $\frac{\psi_1}{U_\infty}$, $\frac{\psi_2}{U_\infty}$ were determined in the domain $2 \le X_1/d \le 20$, $0 \le X_2/d \le 5$ using Simpson's rule of integration for the last two, and the aforementioned interpolating functions (which are twice continuously differentiable) for $\frac{\partial(\overline{v_1}/U_\infty)}{\partial(X_1/d)}$. Finally the coefficient of $\cos \omega t$, $\sin \omega t$, $\cos 2\omega t$ and $\sin 2\omega t$ (i.e. the integrals) in (3.19) were evaluated at 19 different points (separated by a uniform angular distance of 10^o) on the upper side of the circle C . The integration was done over the domain $2 \le \frac{X_1}{d} \le 20$, $0 \le \frac{X_2}{d} \le 5$, using Simpson's rule and a mesh size of $0.5\ d$. This domain covers in the X_1-direction two wavelengths of the vortex street, and the major part of the unsteady region in the X_2-direction. In the next section it will be shown that the major contribution to the complete integrals comes from this limited domain.

For convenience and in order to determine the phase variations of the surface-pressure fluctuations we write (3.19) in the following form:

$$\frac{p'}{\rho U_\infty^2} = P_1 \cos 2\pi(\delta_1 - ft) + P_2 \cos 4\pi(\delta_2 - ft) \qquad (3.20)$$

where P_1 , P_2 , δ_1 , δ_2 are functions of the angular position on the circle C . In addition, P_1 has an antisymmetric distribution with respect

to the X_1-axis, and P_2 , δ_1 , and δ_2 have symmetric distributions with respect to that axis. These functions were determined and are plotted in Figures 1 and 2. In Figure 2 the phases are plotted in such a way (by a translation of the phase ordinate, different in each case) that they are zero at the back stagnation point. It follows from the form of the phase distributions that as the vortices are shed in the downstream direction the pressure pattern at each frequency travels along the surface of the cylinder in the upstream direction. Note also that the intensity of the shedding frequency component is maximum at about 120° from the front stagnation point while that of the double frequency component is maximum on the back of the cylinder. These results will be discussed in a later section.

The results of the integration in (3.19) can be used to determine the magnitude of the lift and drag fluctuations on the cylinders. If $L(t)$ and $D(t)$ designate respectively the lift and the fluctuating part of the drag per unit span we have:

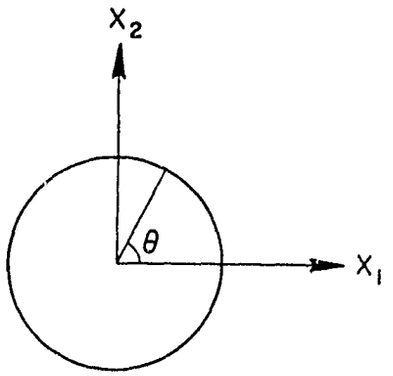

$$L(t) = -\frac{d}{2}\int_0^{2\pi} p' \sin\theta \, d\theta$$

$$D(t) = -\frac{d}{2}\int_0^{2\pi} p' \cos\theta \, d\theta$$

where in the first integral only the antisymmetric part of p' has a net contribution while in the second only the symmetric one does.

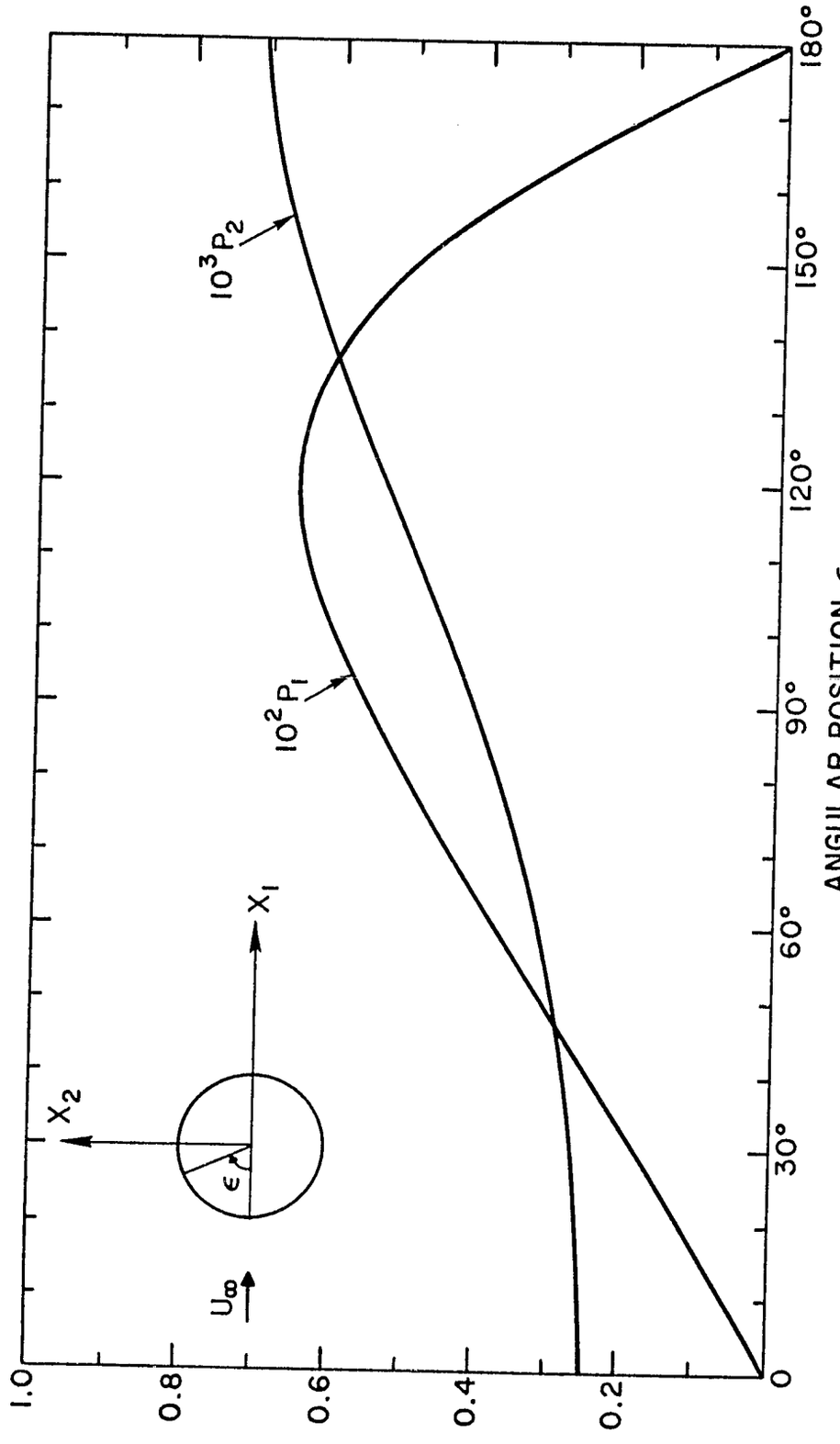
1.0
0.8
0.6
0.4
0.2
0
30°
60°
90°
120°
150°
180°
ANGULAR POSITION ϵ
$10^3 P_2$
$10^2 P_1$
X_1
X_2
U_∞
ϵ

Figure 1.

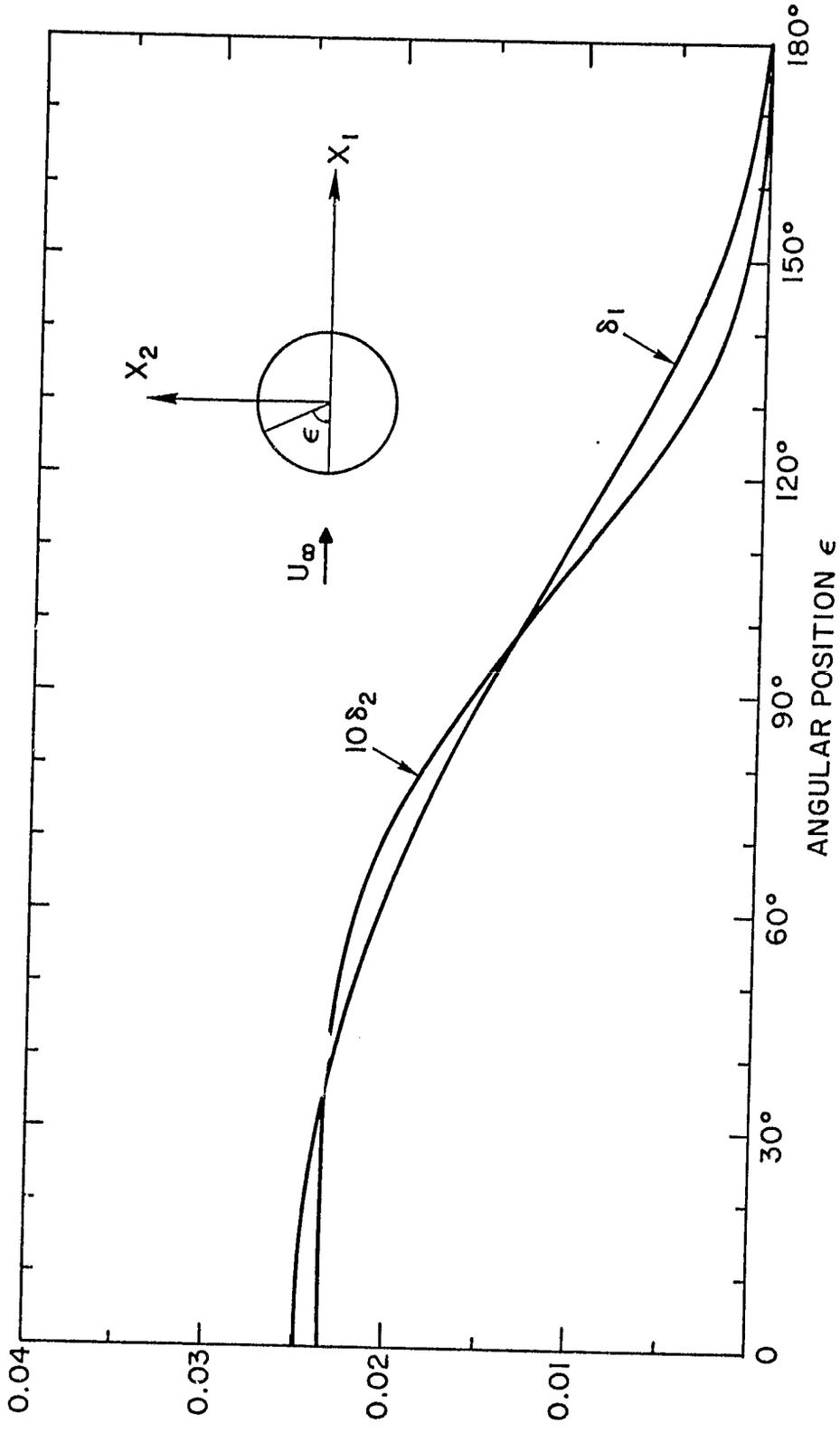
0.04
0.03
0.02
0.01
0
30°
60°
90°
120°
150°
180°
ANGULAR POSITION ϵ
δ_1
$10\delta_2$
X_1
X_2
ϵ
U_∞

Figure 2.

Effecting the integration yields:

$$L(t) \simeq 0.0186 \frac{\rho U_\infty^2 d}{2} \cos \omega t \quad , \tag{3.21}$$

$$D(t) \simeq 0.0007 \frac{\rho U_\infty^2 d}{d} \cos 2\omega t \quad , \tag{3.22}$$

the time origin being not the same in both expressions. From (3.21) and (3.22) it is seen that the magnitude of the lift fluctuations is about 25 times larger than that of the drag fluctuations.

3.3.4 Estimation of the Error Involved in Integrating Over a Finite Domain.

In this section the error involved in evaluating the right-hand side of (3.19) by integration over the limited domain $2 \leq \frac{X_1}{d} \leq 20$, $0 \leq \frac{X_2}{d} \leq 5$ is examined. The estimation procedure is instructive and elucidates the manner in which the velocity fluctuations in the wake induce the fluctuating surface-pressure field.

Referring back to the expression of p' as given by (3.10) and to the relation (3.2) and (3.3) we note that for a fixed value of X_1 , we have:

$$\frac{\partial^2 G}{\partial X_1^2} \sim \frac{1}{X_2^2} \quad \text{for} \quad |X_2| \to \infty \quad ,$$

$$\frac{\partial^2 G}{\partial X_1 \partial X_2} \sim \frac{1}{X_2^3} \quad \text{for} \quad |X_2| \to \infty \quad ,$$

and similarly for a fixed value of X_2 :

$$\frac{\partial^2 G}{\partial X_1^2} \sim \frac{1}{X_1^2} \quad \text{for} \quad |X_1| \to \infty \quad ,$$

$$\frac{\partial^2 G}{\partial X_1 \partial X_2} \sim \frac{1}{X_1^3} \quad \text{for} \quad |X_1| \to \infty \quad ,$$

but for a fixed ratio of $\frac{X_2}{X_1}$ we have:

$$\frac{\partial^2 G}{\partial X_1^2} \sim \frac{1}{X_1^2} \quad \text{for} \quad |X_1| \, , \, |X_2| \to \infty \quad ,$$

$$\frac{\partial^2 G}{\partial X_1 \partial X_2} \sim \frac{1}{X_1^2} \quad \text{for} \quad |X_1| \, , \, |X_2| \to \infty \quad .$$

This is due to the fact that $\frac{\partial^2 G}{\partial X_1 \partial X_2}$ admits a local extremum whose value is of the order of $\frac{1}{X_1^2}$ and whose X_2-coordinate increases linearly with X_1 . However for a fixed ratio $\frac{X_2}{X_1^{\frac{1}{2}}}$:

$$\frac{\partial^2 G}{\partial X_1^2} \sim \frac{1}{X_1^2} \quad \text{for} \quad |X_1| \, , \, |X_2| \to \infty$$

$$\frac{\partial^2 G}{\partial X_1 \partial X_2} \sim \frac{1}{X_1^{5/2}} \quad \text{for} \quad |X_1| \, , \, |X_2| \to \infty$$

and therefore inside the wake and at large distances or at a fixed X_1 station and for large $|X_2|$, $\frac{\partial^2 G}{\partial X_1 \partial X_2}$ is of smaller order than $\frac{\partial^2 G}{\partial X_1^2}$. Since v_1' and v_2' are of the same order of magnitude, this implies that it is sufficient to examine only the rate of convergence of the integral containing $\frac{\partial^2 G}{\partial X_1^2}$. We denote by I that integral:

$$I = 2\rho \iint_{\Sigma} \frac{\partial^2 G}{\partial X_1^2} \overline{v_1} \, v_1' \, dX_1 \, dX_2 \quad .$$

which can also be written as:

$$I = 2\rho \int_{2d}^{20d} \left\{ \int_{-5d}^{+5d} \frac{\partial^2 G}{\partial X_1^2} \overline{v_1} v_1' \, dX_2 \right\} dX_1 + I_1 + I_2 \quad , \tag{3.23}$$

where:

$$I_1 = 2\rho \int_{20d}^{+\infty} \left\{ \int_{-5d}^{+5d} \frac{\partial^2 G}{\partial X_1^2} \overline{v_1} v_1' \, dX_2 \right\} dX_1 \quad , \tag{3.24}$$

$$I_2 = 2\rho \int_{2d}^{+\infty} \left\{ \int_{5d}^{+\infty} \frac{\partial^2 G}{\partial X_1^2} \overline{v_1} v_1' \, dX_2 \right\} dX_1 + 2\rho \int_{2d}^{+\infty} \left\{ \int_{-\infty}^{-5d} \frac{\partial^2 G}{\partial X_1^2} \overline{v_1} v_1' \, dX_2 \right\} dX_1 \quad , \tag{3.25}$$

and we propose to estimate the values of I_1 and I_2. Introducing the non-dimensional variables as before and letting $\overline{v_1}$, φ_1, φ_2, Y_1, Y_2, X_1, and X_2 denote these new variables we can write:

$$\frac{I_1}{\rho U_\infty^2} = -\frac{2}{\pi} \int_{20}^{+\infty} \left\{ \int_{-5}^{5} \left\{ \frac{(X_2-Y_2)^2-(X_1-Y_1)^2}{[(X_1-Y_1)^2+(X_2-Y_2)^2]^2} - \frac{1}{2} \frac{X_2^2-X_1^2}{(X_1^2+X_2^2)^2} \right\} \overline{v_1} \times \right.$$

$$\left. \left\{ \varphi_1 \cos 2\pi(\theta_1 - ft) + \varphi_2 \cos 4\pi(\theta_2 - ft) \right\} dX_2 \right\} dX_1 \quad ,$$

or since φ_1 is an odd function of X_2, φ_2 and $\overline{v_1}$ are even functions of X_2:

$$\frac{I_1}{\rho U_\infty^2} = -\frac{2}{\pi} \int_{20}^{+\infty} \left\{ \int_{0}^{+5} \left\{ \frac{(X_2-Y_2)^2-(X_1-Y_1)^2}{[(X_1-Y_1)^2+(X_2-Y_2)^2]^2} - \frac{(X_2+Y_2)^2-(X_1-Y_1)^2}{[(X_1-Y_1)^2+(X_2+Y_2)^2]^2} \right\} \overline{v_1} \varphi_1 \cos 2\pi(\theta_1 - ft) \, dX_2 \right\} dX_1$$

$$- \frac{2}{\pi} \int_{20}^{+\infty} \left\{ \int_{-5}^{+5} \left\{ \frac{(X_2-Y_2)^2-(X_1-Y_1)^2}{[(X_1-Y_1)^2+(X_2-Y_2)^2]^2} - \frac{X_2^2-X_1^2}{(X_1^2+X_2^2)^2} \right\} \overline{v_1} \varphi_2 \cos 4\pi(\theta_2 - ft) \, dX_2 \right\} dX_1$$

$$-\frac{2}{\pi}\int_{20}^{+\infty}\left\{\int_{0}^{5}\frac{X_2^2-X_1^2}{(X_1^2+X_2^2)^2}\,\overline{v_1}\,\varphi_2\cos 4\pi(\theta_2-ft)\,dX_2\right\}dX_1 \quad . \tag{3.26}$$

As is clear from (3.26) and from the expression of p' in the form (3.19), the shedding frequency component of the surface-pressure is the result of an incomplete cancellation of the contributions coming from the parts of the wake below and above the X_1-axis. This is best seen by putting $Y_2 = 0$ in the above expression or in (3.19), the resulting contribution then vanishes. This is due to the fact that at a given time t and at fixed X_1 station the shedding frequency component of v_1' for instance, is antisymmetric with respect to the wake axis, and consequently the induced pressure at a point on that axis is the sum of two exactly opposite contributions; if,however, Y_2 is not zero the cancellation is not complete and there is a net contribution. The double frequency component on the other hand results from two additive contributions and is not the result of an incomplete cancellation effect. With this in mind it is clear that contributions from distant points in the wake are small not only because the velocity fluctuations at the shedding frequency there are small but also because the difference in distance between a point on the cylinder and two points symmetric with respect to the X_1-axis becomes small. This however does not apply when the double frequency component is involved. For these reasons, and in order to achieve better estimates, I_1 was (and I_2 will be) written in the above form. We now write:

$$\frac{I_1}{\rho U_\infty^2} = \frac{J_1}{\rho U_\infty^2} + \frac{J_2}{\rho U_\infty^2} + \frac{J_3}{\rho U_\infty^2} \quad , \tag{3.27}$$

where $\frac{J_1}{\rho U_\infty^2}$, $\frac{J_2}{\rho U_\infty^2}$, and $\frac{J_3}{\rho U_\infty^2}$ are respectively the first, second, and third term on the right-hand side of (3.26). An estimate of each of these terms as well as of I_2 is found in Appendix B. The results are as follows:

$$\left|\frac{J_1}{\rho U_\infty^2}\right| \leq 0.0788\times10^{-3} \quad , \tag{3.28}$$

$$\left|\frac{J_2}{\rho U_\infty^2}\right| \leq 0.0190\times10^{-3} \quad , \tag{3.29}$$

$$\left|\frac{J_3}{\rho U_\infty^2}\right| \leq 0.1329\times10^{-3} \quad , \tag{3.30}$$

$$\left|\frac{I_2}{\rho U_\infty^2}\right| \leq 0.6308\times10^{-3} \quad . \tag{3.31}$$

We note that the above estimates constitute only upper bounds to the values of the integrals $\frac{J_1}{\rho U_\infty^2}$, $\frac{J_2}{\rho U_\infty^2}$, $\frac{J_3}{\rho U_\infty^2}$, and $\frac{I_2}{\rho U_\infty^2}$. These upper bounds are sometimes too gross (in view of the limitations of the formal procedure) to yield close estimates to the real values of the integrals. If we consider for instance the component of the pressure at the shedding frequency f , an estimate of the error involved in integrating I (see (3.23)) over the finite domain $2 \leq X_1 \leq 20$, $-5 \leq X_2 \leq 5$ is given by (3.28) and (3.31). By referring to Figure 1 we can see that an upper bound to that error is about 1% (given by (3.28)) plus 10% (given by (3.31)) of the maximum calculated value. The estimate given by (3.31) is too gross as is discussed in Appendix B and we can conclude, after assuming that a similar accuracy is obtained from the second term in (3.10), that to a very good approximation the contribution to the fluctuating surface-pressure at the shedding frequency comes from the near-wake region defined by $2 \leq X_1 \leq 20$,

$-5 \leq X_2 \leq 5$. On the other hand if we consider the component of the pressure at the double frequency $2f$ the estimates (3.29) and (3.30) yield an upper bound for the error involved which is about 20% of the maximum calculated value. This, however, does not give any indication of the accuracy of the results which, we believe, is much better than is revealed by the above figure; and as for the shedding frequency component, we can conclude that the component of the surface-pressure at the double frequency is determined to a large extent by the velocity fluctuations in the near-wake region.

3.3.5 Comparison with Other Results and Discussion.

As we have said in Section 3.2, the only available experimental results on the unsteady loading on the cylinder in the stable Reynolds number range are those of Tanida et al. (1973). They measured directly the fluctuating lift force, but found that the fluctuating drag was too small to be measured accurately. Their data on the magnitude $|\tilde{C}_L|$ of the lift coefficient have been introduced already in Section 3.2. Comparison of our result (3.21) (at $Re = 56$) with these data shows excellent agreement and confirms the rather low level of lift fluctuation inherent to the low Reynolds number regime. By contrast the value for $|\tilde{C}_L|$ obtained by Phillips (1956) at $Re = 56$ is in strong disagreement with the above results. This value ($|\tilde{C}_L| = 0.76$) is about 40 times larger than ours ($|\tilde{C}_L| = 0.0186$) . Phillips used the same data of Kovasznay which have been used in the previous sections, and calculated the fluctuations in lift and drag according to the formulas:

$$L = \rho \frac{d}{dt} \iint_{\Sigma} v_2' \, dX_1 \, dX_2 \quad , \tag{3.32}$$

$$D = \rho \frac{d}{dt} \iint_{\Sigma} v_1' \, dX_1 \, dX_2 \quad . \tag{3.33}$$

However, since behind an infinitely long cylinder the wake remains unsteady (if it is so near the cylinder) at arbitrarily large distances downstream the above formulas are incomplete and an additional non-vanishing term should be added to the right-hand side of each of the relations (3.32) and (3.33). This can be seen by applying the momentum theorem to the fluid inside the control volume, having Σ_R as cross-section and one diameter in depth in the spanwise direction, in the following manner:

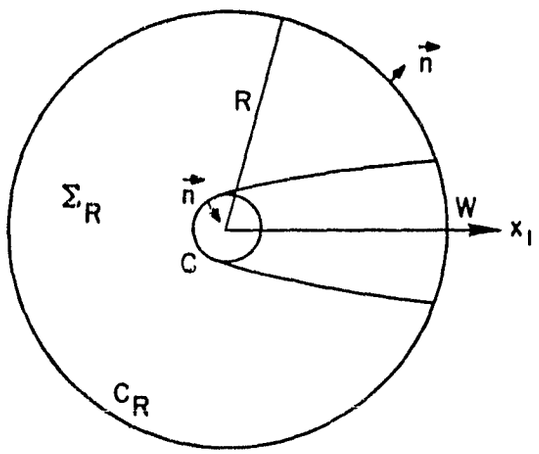

$$\iint_{\Sigma_R} \frac{\partial}{\partial t}(\rho v_i) dX_1 dX_2 = \int_{C+C_R} \{-p\delta_{ij} + \mu(\frac{\partial v_i}{\partial X_j} + \frac{\partial v_j}{\partial X_i}) - \rho v_i v_j\} n_j \, ds$$

or after separation of the mean and fluctuating parts of each variable:

$$\iint_{\Sigma_R} \frac{\partial}{\partial t}(\rho v_i') dX_1 dX_2 = \int_{C+C_R} \{-(\bar{p}+p')\delta_{ij} + \mu(\frac{\partial \bar{v}_i}{\partial X_j} + \frac{\partial \bar{v}_j}{\partial X_i}) + \mu(\frac{\partial v_i'}{\partial X_j} + \frac{\partial v_j'}{\partial X_i})$$

$$- \rho(\bar{v}_i + v_i')(\bar{v}_j + v_j')\} n_j \, ds \quad .$$

Taking the time average of the above relation and subtracting the result from the relation itself we obtain:

$$\iint_{\Sigma_R} \frac{\partial}{\partial t}(\rho v_i')dX_1 dX_2 = \int_{C+C_R} \{-p'\delta_{ij} + \mu(\frac{\partial v_i'}{\partial X_j} + \frac{\partial v_j'}{\partial X_i}) - \rho(\overline{v_i}v_j' - \overline{v_i}v_i')$$

$$- \rho(v_i'v_j' - \overline{v_i'v_j'})\}n_j\, ds \quad .$$

If now we designate by F_i' the ith component of the fluctuating force per unit span on the cylinder the above relation becomes:

$$F_i' = -\iint_{\Sigma_R} \frac{\partial}{\partial t}(\rho v_i')dX_1 dX_2 + \int_{C_R} \{-p'\delta_{ij} + \mu(\frac{\partial v_i'}{\partial X_j} + \frac{\partial v_j'}{\partial X_i}) - \rho(\overline{v_i}v_j' + \overline{v_j}v_i')$$

$$- \rho(v_i'v_j' - \overline{v_i'v_j'})\}n_j\, ds \quad . \tag{3.34}$$

On C_R, R being very large, $|v_i'| \sim \frac{1}{R^2}$ except on the wake portion W where $|v_i'| \sim \frac{1}{R^{\frac{1}{2}}}$, $p' \sim \frac{1}{R}$ but since the flow is only approximately two-dimensional we can assume for the present purpose that it is of smaller order than $\frac{1}{R}$. Since $W \sim R^{\frac{1}{2}}$, upon increasing R indefinitely and assuming that the first term on the right-hand side of (3.34) converges we obtain:

$$F_i' = -\iint_{\Sigma} \frac{\partial}{\partial t}(\rho v_i')dX_1 dX_2 - \int_W \rho(\overline{v_i}v_j' + \overline{v_j}v_i')n_j\, ds \quad . \tag{3.35}$$

On W $n_1 = 1$ and $n_2 = 0$, assuming that $\overline{v_2}$ vanishes in the far-wake and taking i equal to 1 and 2 separately we obtain the following relations:

$$L = -\rho \frac{d}{dt}\iint_{\Sigma} v_2' dX_1 dX_2 - \rho \int_W \overline{v_1}v_2' ds \quad , \tag{3.36}$$

$$D = -\rho \frac{d}{dt} \iint_{\Sigma} v_1' dX_1 dX_2 - 2\rho \int_W \overline{v_1} v_1' ds \qquad (3.37)$$

(3.36) and (3.37) are to be compared with (3.32) and (3.33). In addition, we note that even in the above form it is doubtful whether (3.36) and (3.37) can be used efficiently to evaluate L and D, for the convergence of the first term on the right-hand side of each of these relations is at best too slow and the integration would require an infinite amount of data. In fact, Phillips used the form (3.33) for the drag only, while for the lift he used the fact that:

$$\iint_{\Sigma} v_2' dX_1 dX_2 = -\iint_{\Sigma} \left(\frac{\partial v_2'}{\partial X_1} - \frac{\partial v_1'}{\partial X_2}\right) dX_1 dX_2 \quad .$$

But since only v_1' is known from measurements he was led to differentiate the numerical data several times (for instance, φ_1 was differentiated numerically three times with respect to X_1) to evaluate L. This, as we have mentioned earlier, can destroy the accuracy of the computations and lead to results totally different from the sought ones.

Experimental results on the surface-pressure distribution when Re is in the stable range are not available. Even at higher Reynolds numbers there are few instances where such results have been reported in the literature. Those of Gerrard (1961) and McGregor (1957) are given in terms of intensity of fluctuations at the shedding frequency and its first harmonic, at several values of Re between 10^4 and a value slightly above 10^5. These two components (i.e., the shedding frequency component and its first harmonic) were found to be dominant in the range studied ($4/10^3 \leq Re < 10^5$ in Gerrard's case). We reproduce below the results in

question as they were presented in Figures 8 and 9 of Gerrard's paper which also include the data of McGregor. The main feature of these results is the invariance of the angular distribution with Reynolds number:

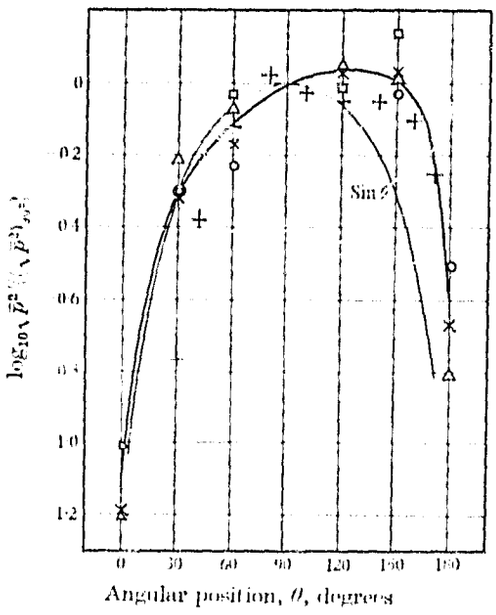

FIGURE 8. Angular distribution of intensity of surface pressure at the fundamental frequency. $\log_{10}R$: □, 4·1; △, 4·3; ×, 4·8; ○, 5·2; +, McGregor 4·64.

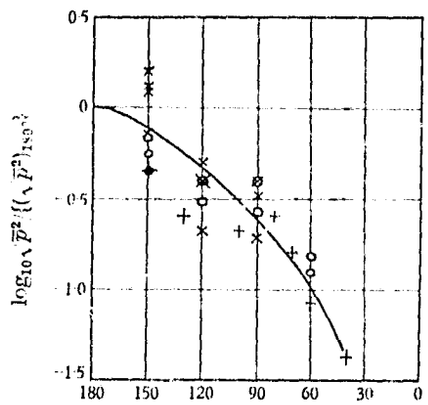

FIGURE 9. Angular distribution of intensity of surface pressure at the second harmonic frequency. ○, 1 in. diam. cylinder; ×, 3 in. diam. cylinder; +, McGregor, 1⅛ in. diam.

the intensity of fluctuations at the shedding frequency is always maximum at about 120° from the front stagnation point and drops substantially at the front and back of the cylinder, while that at the double frequency is maximum at the back of the cylinder. In addition, Gerrard observed that

in the range studied the pressure is essentially in phase over one side (upper or lower) of the cylinder and 180° out of phase with that on the other side. Referring back to Figures 1 and 2 we can see that a remarkable similarity exists between our results at low Reynolds number and the above ones at much higher Reynolds numbers. The question whether the invariance of the angular distribution with Re can be extended to the stable range may tentatively be asked. In order to facilitate the comparison, the results of Figure 1 were plotted again, in the manner followed by Gerrard in Figures 8 and 9, and are shown in Figures 3 and 4. It is readily observed that the two sets of figures are similar to a great degree, the difference being that at high Reynolds numbers, the intensity of fluctuations at the shedding frequency drops more slowly when the front and back stagnation points are approached and the ratio of the intensity of fluctuations at the double frequency on the back of the cylinder to that on the front is greater than it is at low Re . We defer the discussion of these similarities and differences to the next section where a general discussion of the high Reynolds number case is given.

To conclude the present section we examine the effect of varying Re in the range below $Re = 90$. As we have said at the beginning of § 3.3, the nature of the velocity fluctuations in the wake does not change when Re is varied from 40 to some value below 90 : the fluctuations develop always as a result of the instability of the laminar wake and the flow remains two-dimensional. The only change is in the intensity of fluctuations and in the distance from the cylinder at which this intensity reaches its peak value. Upon increasing Re the velocity profiles in the laminar wake become steeper, the concentration of vorticity in the street becomes stronger, and the distance at which the intensity of fluctuations

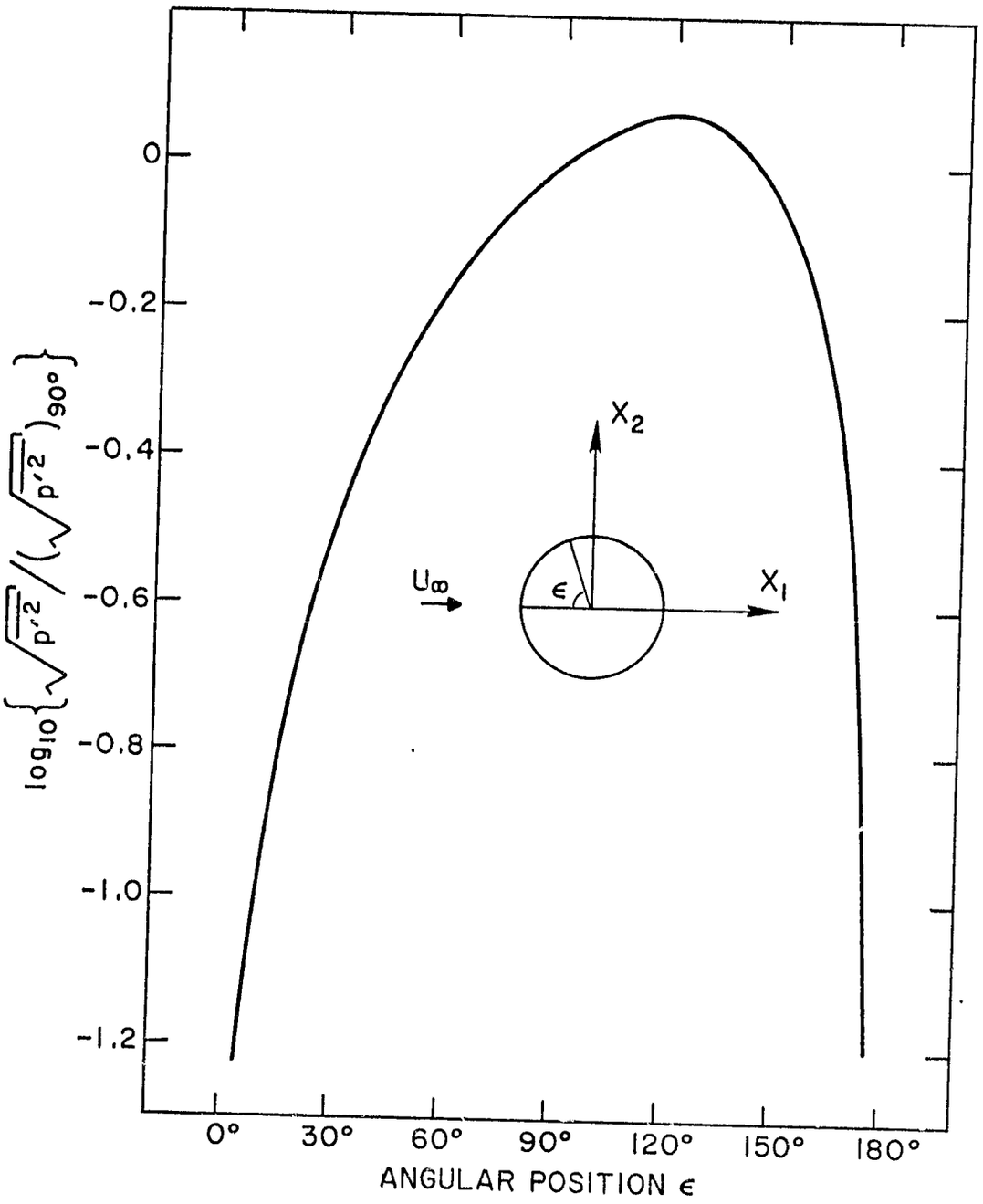
0
-0.2
-0.4
-0.6
-0.8
-1.0
-1.2
$\log_{10}\left\{\sqrt{\overline{p'^2}}/\left(\sqrt{\overline{p'^2}}\right)_{90°}\right\}$
X_2
U_∞
ϵ
X_1
0°
30°
60°
90°
120°
150°
180°
ANGULAR POSITION ϵ

Figure 3.

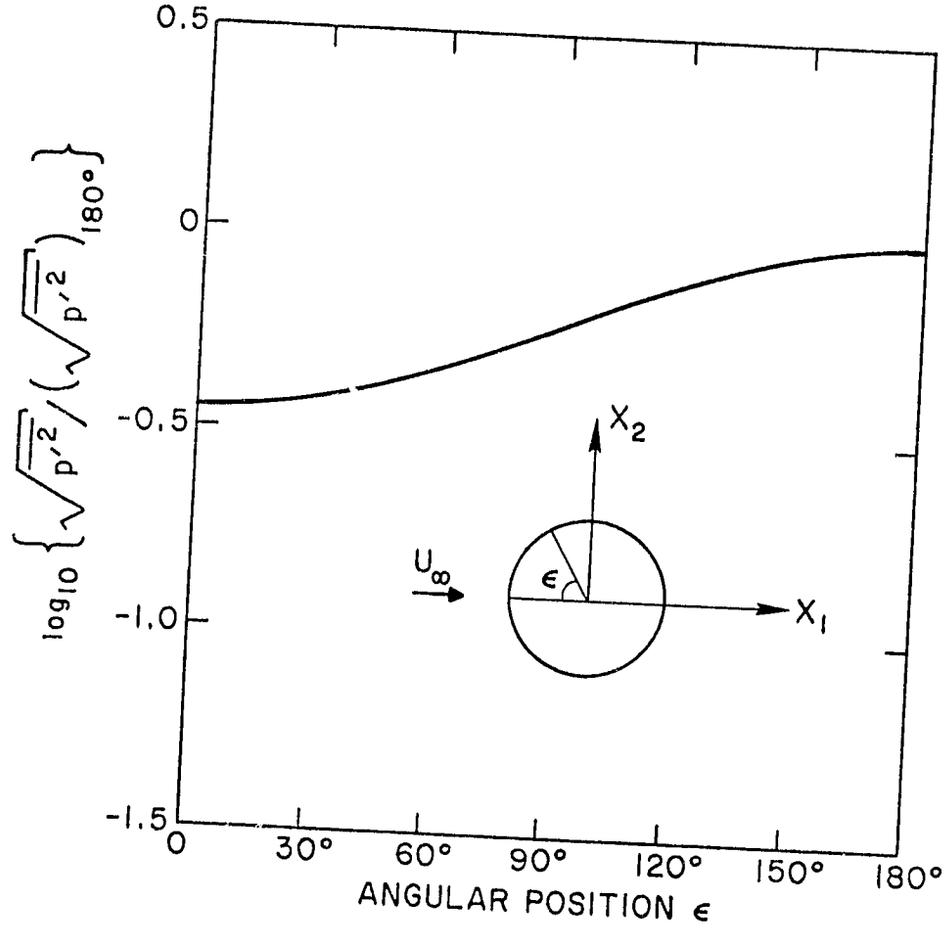
0.5
0
-0.5
-1.0
-1.5
0
30°
60°
90°
120°
150°
180°
ANGULAR POSITION ϵ
$\log_{10}\left\{\sqrt{\overline{p'^2}}/\left(\sqrt{\overline{p'^2}}\right)_{180°}\right\}$
X_2
X_1
U_∞
ϵ

Figure 4.

reaches a maximum value becomes shorter. Consequently, the pressure fluctuations on the cylinder, at the shedding frequency, for instance, continue to be the result of an incomplete cancellation of two contributions coming from the parts of the wake below and above the centerline (see § 3.3.4) and the magnitude of the fluctuating lift can be expected to remain small even though it tends to increase slightly with Re as a result of the increase in the intensity of the velocity fluctuations in the proximity of the cylinder. Similar increase may be expected for the fluctuation in drag for the same reasons.

3.4 General Discussion - Reynolds Number Effect.

When Re exceeds some value near 90 , the flow becomes sensitive to small three-dimensional disturbances or slight non-uniformities in the cylinder or in the flow upstream, and some of the details of the wake pattern become uncertain and dependent upon the nature of these disturbances and non-uniformities, in addition to their dependence on the details of the experimental setup, as has been already discussed in Section 3.2. With this in mind it is clear that it would be impossible to attach a unique value for the magnitude of the fluctuating lift or drag coefficient to each value of the Reynolds number Re . This is true whether we are talking about laboratory experiments or about real life situations as they occur in applications. The theory of the preceeding chapter, on the other hand, allows certain systemization in the study of the fluctuating loads, and this by identifying the role of the cylinder geometry and that of the various components of the wake flow, as they may occur, in bringing about such loads. On the basis of that theory and our experience with the low Reynolds number range treated in the preceding section, we will attempt

below to speculate on, or when it is possible, "predict" the manner in which the unsteady loading on the cylinder would vary with Re under various conditions. At the same time some comments on previous attempts will be made and areas where further research is needed will be indicated.

Using (2.39) and (2.40) the general solution (2.15) given in the preceding chapter can be written in the form:

$$\vec{P}(\vec{Y},k,t) = \rho \iint_{\Sigma} \frac{\partial^2 G(\vec{X}|\vec{Y};k)}{\partial X_i \partial X_j} \{2\overline{v_i} V_j + F[v_i' v_j' - \overline{v_i' v_j'}]\} d\vec{X}$$

$$+ 2i\rho k \iint_{\Sigma} G(\vec{X}|\vec{Y};k)\{(\overline{v}_2\Omega_1 - \overline{v}_1\Omega_2) + F[v_2'\omega_1' - v_1'\omega_2']\} d\vec{X}$$

$$- \rho k^2 \iint_{\Sigma} G(\vec{X}|\vec{Y};k)\{2(\overline{v}_1 V_1 + \overline{v}_2 V_2) + F[v_1'^2 + v_2'^2]\} d\vec{X}$$

$$+ \mu \int_{C} G(\vec{X}|\vec{Y};k)\vec{n}.\nabla^2\vec{V}\, ds \quad . \tag{3.38}$$

From the above relation it is clear that, insofar as the pressure P is concerned the two aspects of the fluctuating wake, namely the two-dimensional one represented in (3.38) by the first, third, and fourth integral and the three-dimensional one represented by the second integral can be examined separately, and both play an important role in the determination of P . Some important features of these two aspects are examined below in detail.

Considering first the two-dimensional aspect, i.e., the wake flow as it appears in the plane (X_1, X_2) and concentrating on the vortex street alone, one can argue that the intensity of the velocity fluctuations V_1 and V_2 and the manner in which it (the intensity) changes with Re

should have an important role in determining the magnitude of P and its variation with Reynolds number. The intensity of the velocity fluctuations on the other hand is closely related to the strength of the vortices in the street. Measuring the strength of these vortices is a difficult process which is usually accomplished by matching a theoretical model of the flow to hot-wire measurements in the wake; this gives only an average value and has been attempted by several investigators. It has always been considered as remarkable that only a part of the rate of vorticity generated in the boundary layers on the cylinder is found in the vortex street (see Berger and Wille 1972). If we define (as in Berger and Wille's review) the rate of discharge of vorticity in one row of the street by:

$$K = \Gamma f = \Lambda U_\infty^2 \quad ,$$

where Γ is the circulation of a vortex, and the initial rate of discharge of vorticity from the boundary layer on one side of the cylinder by:

$$K_s = 0.5 U_s^2 \quad ,$$

where U_s is the velocity at the outer side of the boundary layer near the separation point, the ratio:

$$\frac{K}{K_s} = \frac{2\Lambda}{1-C_{p_s}}$$

where C_{p_s} is the base-pressure coefficient is a measure of the fraction of the vorticity which escapes annihilation during the interaction of the shear layers from both sides of the cylinder. This ratio is found to be about 0.4 in the low Reynolds number range corresponding to Tritton's low-speed mode and to vary between 0.5 and 0.6 or 0.66 at higher Reynolds

numbers (see Berger and Wille 1972). On the other hand a measure of the strength of the individual vortices in the street is Γ. From the above relations it follows that:

$$\frac{\Gamma}{U_\infty d} = \frac{\Lambda}{St} = \frac{1-C_{p_s}}{2St} \frac{K}{K_s} \quad .$$

C_{p_s} varies with Re ; it is about -0.5 when the wake oscillations begin, it decreases to about -0.9 at $Re = 200$, then increases to about -0.7 at $Re = 10^3$, and finally decreases to -1.2 near $Re = 10^5$ before increasing again at the critical Reynolds number (see Roshko and Fiszdon 1967). As for St , it is about 0.12 at the onset of oscillations, it increases to about 0.19 at $Re = 200$, then to about 0.21 at $Re = 10^3$ and remains near this value for all subcritical Reynolds numbers (see Roshko 1954). After some calculations one can easily see that the ratio $(1-C_{p_s})/2St$ varies little in the range considered; it takes the values 6, 5, 4, and 5 at $Re = 50$, 200, 10^3, and 10^5 respectively. In view of the small changes of K/K_s with Re we note here that it is even more remarkable that the strength of the vortices in the street (non-dimensionalized) varies little over the whole range of Re below the critical value. With this in mind, if we look at the results of Tanida et al. (1973) and those shown in Figure 15 of Morkovin (1964) (both introduced in Section 3.2) concerning the magnitude of the fluctuating lift coefficient we see that this coefficient increases from very low values in the range below $Re = 100$ to high values near $Re = 10^5$ and this despite the increasing three-dimensionality of the vortex filaments in the street with Re . Therefore, neglecting for the moment whatever contribution to P the flow-wise vorticity term (the second on the right-hand side of (3.38))

has, the absolute strength of the individual vortices in the street and the closely related intensity of velocity fluctuations there are not of prime importance in determining the magnitude of P. What is important rather is the net strength of the total vorticity (mean and fluctuating part) in the wake, which does not vanish at all times as in the case of an idealized Kármán street,* and upon which the intensity of velocity fluctuations in the vicinity of the cylinder depends to a large extent. This can be seen in the following way. Let us consider a cylinder started from rest in an infinite fluid equally at rest. As a result of the no-slip condition, vorticity is generated at the coundary and is mainly swept to the back of the cylinder (at sufficient high Re) to form the wake. By applying Kelvin's theorem as in airfoil theory it is seen that an equal amount of vorticity must be placed inside the cylinder so that the circulation on a contour surrounding the cylinder and the part of the fluid which has already received some vorticity is zero. Before the onset of instability the vorticity generated at the boundary is antisymmetrically distributed with respect to the wake centerline, therefore the net vorticity in the wake vanishes and so does the bound vorticity inside the cylinder. This implies that no circulation exists on a circuit closely surrounding the cylinder and consequently the cylinder does not experience any lift force. On the other hand, when the high shear region in the wake becomes unstable to small disturbances, antisymmetric (with respect to the wake centerline) in the longitudinal velocity, modes of disturbance vorticity, symmetric with respect to the wake centerline, grow and travel downstream in a wavelike pattern (see Mattingly and Criminale 1972). This

*An idealized Kármán street, if left alone in an infinite fluid, does not move in a transversal direction.

additional vorticity is simply superposed on the original mean velocity distribution in the early stage of its growth while further downstream it interacts with the mean vorticity, modifies it, gets modified itself and begins to diffuse in the fluid. However, at all times the mean vorticity remains antiysmmetric with respect to the wake centerline and the disturbance vorticity at the fundamental frequency remains symmetric. Therefore the net vorticity in the wake does not vanish and alternates (at the fundamental frequency) between positive and negative values. In addition, by the nature of the process of generation of the disturbance vorticity, this net strength is small: if for instance at a given time, and at each downstream station we sum the vorticity in the transversal direction and plot the obtained values as a function of the downstream coordinate X_1 we obtain a curve of the form shown in the figure, the net strength in question is nothing but the algebraic area under this curve, this is of the order of the area under the curve AB and therefore is small. This implies that the bound vorcicity is small and so is the lift force. As for the velocity fluctuations in the wake, they are due to the field of the unsteady vorticity both in the wake and in the cylinder. Near the cylinder the field of the bound vorticity is dominant, and since in this case the latter is small, the velocity fluctuations there are small.

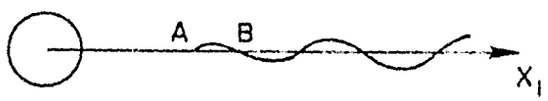

What we have described above is the state of affairs corresponding to the low-speed mode of vortex shedding. This is to be contrasted to the case when the vortex shedding results from the direct interaction of the

two shear layers emanating from the surface of the cylinder (correponding to the high-speed mode of Tritton) the way it was described by Gerrard (1966b) and observed by Mattingly (1962), and to which the fundamental study on the non-linear interaction of two infinite vortex sheets of Abernathy and Kronauer (1962) applies.

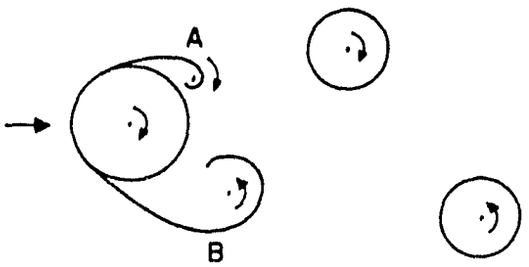

Without entering into details (reference is made to the mentioned papers) and referring to the figure, the net vorticity in the wake (assuming that all the vorticity is concentrated in the street) is dominated by the difference in strength between vortex B and vortex A. At certain moments which occur periodically this difference is large; the induced bound vorticity is then large and the lift has a maximum amplitude. In addition, the velocity fluctuations in the vicinity of the cylinder, which are due mainly to the field of vortex B and the bound vortex, reach high values and are in phase in a direction parallel to the X_1-axis.*

The three-dimensional nature of the flow in the wake, when Re is above 90, is far less clear and much more difficult to describe. The pieces of information available are scattered in the literature and are often reported in a rather crude manner. For instance, spanwise correlation lengths determined using two hot-wires separated in the x_3-direction,

*This is the reason that calculated convection speeds, of the street vortices, based on phase measurements increase without limit in the vicinity of the cylinder (see Bloor and Gerrard 1966, and Simmons 1974). Simmons recognized the existence of the bound vortex, but assumed that the vortices in the wake are equivalent to a distribution of vortex doublets, while in fact it is the total vorticity including the bound vortex which is so.

are usually given without specifying whether the signals from the hot-wires were filtered at the shedding frequency or not. Similarly it is not clear sometimes whether the periodicity in the spanwise direction, observed at certain values of Re , is associated with slantwise shedding or simply with waviness in the vortex filaments. Even the more specialized studies of Gerrard (1966a) and Gaster (1969, 1971) on the effect of spanwise non-uniformities (in the cylinder or in the free-stream) leave some important issues unanswered. In addition, Gerrard (1966a) attributed the existence of low frequency modulations, in the transition range, to the simultansous existence in a direction along the span of laminar and turbulent vortices, which also resulted in the continuation of the vortex filaments into the direction of the free-stream. He also noted that in the irregular range, when all the vortices are turbulent, this effect is less pronounced. However, he later showed (Gerrard 1967b) that suppressing the vortex street with a splitter plate did not alter the low frequency component in the vicinity of the cylinder, thus proving that this component is unrelated to the vortices in the street.

Leaving aside such factors as the spanwise non-uniformity and the details of the experimental setup, one thing we can be sure about is that the presence of three-dimensional disturbances in the free-stream will ultimately render the flow in the near wake three-dimensional. In Section 2.6 we have suggested that such a phenomenon takes place in the individual shear layers, and gave as evidence the observations of Humphrey (1960) at the critical Reynolds number. Other pieces of evidence can be given to support further this point: for instance, the observation of Hama (1957) that "the transverse waviness of the vortex lines appears almost immediately,

further develops apparently in the shear layer." In addition, we can argue that a free shear layer is more likely to be vulnerable to small disturbances than a rolling or rolled up vortex. It is also tempting to conclude, as we did in Section 2.6, that as a result of the growth of these disturbances, flow-wise vorticity is generated, which either takes the form of waviness in the vortex filaments, or causes the slantwise shedding of vortices,* or even leads to the low frequency irregularities. If we accept this sequence of cause and effect, the various observations mentioned above become less puzzling. Another item of observation seems to fit the above picture: by oscillating the cylinder at the shedding frequency, Berger (see Wille 1966) has shown that laminar vortex streets with parallel (as opposed to slantwise) shedding could be upheld until $Re = 350$. It is possible that upon oscillating the cylinder the separated shear layers become more stable against both small and large scale three-dimensional distrubances, thereby delaying the transition to turbulence and preventing the formation of flow-wise vorticity which would otherwise lead to slantwise shedding. Let us emphasize that the preceding discussion is merely speculative and is not intended to be definitive. Nevertheless, as is clear from the general solution (3.38), the knowledge of the three-dimensional nature of the flow in the near-wake or the form under which it manifests itself under various conditions is essential for a successful prediction of the unsteady loading on the cylinder. This, we believe, can be achieved only by conducting experiments under controlled conditions.

We now proceed to the discussion of the changes in the magnitude of

*Slantwise shedding is equivalent, from a kinematical point of view, to a vortical component in the direction of the mean flow plus a certain periodicity in the spanwise direction.

7-2

the unsteady loading with Reynolds number. The first question one is faced with, when Re exceeds 90 , is which of the two modes of vortex shedding discussed above is likely to occur. Is it the low-speed mode or is it the high-speed mode. We know that the low-speed mode is caused by the instability of the laminar wake and is triggered by the presence of linearizably small disturbances. On the other hand, the high-speed mode can only be triggered by finite disturbances (Abernathy and Krouanaer 1962). If we increase Re gradually from values below 90 where the low-speed mode is prevailing, the velocity fluctuations induced in the vicinity of the cylinder, which are antisymmetric in the longitudinal component and therefore constitute a potentially triggering agent for the high-speed mode, increase but remain very small at low Re and therefore are not able to cause the non-linear interaction of the two separted shear layers. If on the other hand the level of disturbances in the free-stream is high enough, and Re is increased beyond 90 the absence of the two standing eddies (i.e., the fact that the two shear layers spring freely from the sides of the cylinder) will lead to this type of interaction. We don't know the background turbulence level in Tritton's experiment of 1959, however in the 1971 paper Tritton mentions that this level was high. Kovasznay (1949) who had a background turbulence level of 0.06% did not observe the transition of Tritton and in his words, "the vortices develop some distance downstream within the Reynolds number range 40 to 160 , and are not shed directly from the cylinder, consequently the phenomenon can properly be considered as an instability of the laminar wake, that develops to an amplitude limit but dies out before becoming turbulent." Therefore, we can conclude that with low free-stream turbulence level the wake remains in the low-speed mode even after Re = 90 is exceeded; the

increase in the lift and drag fluctuations with Re is then moderate and is quickly counteracted by the increasing effect of three-dimensionality with Re^* (a typical value of the spanwise correlation length for $90 < Re < 150 - 200$ is 17d , see Phillips 1956). Referring back to the data of Tanida et al. (1973) in the stable range, which were taken in an oil tank where presumably the level of disturbances is very low, it is very likely that the measured values of $|\tilde{C}_L|$ correspond to the low-speed mode of vortex shedding. On the other hand the relatively high value ($|\tilde{C}_L| = 0.27$) obtained by Jordan and Fromm (1972) at $Re = 100$ might have resulted from prematurely triggering the high-speed mode of vortex shedding, by twisting the cylinder back and forth in order to perturb the numerical solution.

When Re is increased beyond the stable range, the increasing effect of three-dimensionality corresponding to the second term in (3.38) becomes more difficult to assess (a typical value of the spanwise correlation length in the transition range is 10d given by Roshko (1954) at $Re = 220$). However, we expect that, like the Strouhal number, the lift and drag fluctuations are not well-defined in the transition range, in particular when Re is close to 400 (see Section 3.2). For this and other reasons it is doubtful that the value $|\tilde{C}_L| = 0.75$ obtained by Jordan and Fromm at $Re = 400$ can be considered as typical of the range in question.

---

*For a given two-dimensional distribution of velocity fluctuations in the wake, the difference in magnitude of the pressure fluctuations corresponding to an infinite or a finite spanwise length scale $2\pi/k$ is the same as the difference in temperature distribution in a medium corresponding respectively to a zero or a finite coefficient of absorption k^2 (see Section 2.2).

The possibility of a coupling between the transition waves of Bloor (1964) and the shedding frequency mode extends to $Re = 1.3\times10^3$. To our knowledge no measurements of unsteady forces have ever been reported in this range, and one may well wonder whether this is due to measurement difficulties of the type encountered in the transition range. Above $Re = 1.3\times10^3$ the transition waves and the shedding frequency component are decoupled, and therefore the lift and drag fluctuations at the sheeding frequency and its first harmonic respectively can be expected to be well defined as in the stable range. However, the question concerning the mode of vortex shedding arises again. In addition, the wake becomes highly three-dimensional; typical values of the spanwise correlation length are three to five or six diameters up to $Re = 10^5$, and we expect the contribution from the flow-wise vortical component to become important. Consequently the changes in the magnitude of the unsteady loading with Re in this range are the result of the simultaneous change in both the two-dimensional and the three-dimensional characteristics of the flow in the near-wake. Since very little is known about the three-dimensional characteristics, it is very difficult at this stage to speculate on their possible effect. On the other hand the two-dimensional characteristics and their effect on the magnitude of the fluctuating lift were the subject of a series of three papers by Gerrard (1965, 1966b, 1967a). Since then two relevant papers appeared in the literature and we feel that some comments here are in order to further emphasize some uncertain issues.

On the basis of a potential flow model Gerrard (1967a) suggested the possibility that, when the turbulence level in the free-stream is very low, the wake remains in the low-speed mode up to values of Re of the order of a few thousands. However he later questioned that possibility, because

of the three-dimensional nature of the flow at such high Reynolds numbers and the invariance of the Strouhal number, which normally can be expected (the Strouhal number) to depend on the mode of shedding. In their photographic study, made in a mercury tank, Papailliou and Kykoudis (1974) observed a wake in the low-speed mode at $Re = 3.4 \times 10^3$ and a formation region whose length is in agreement with the value measured by Bloor (1964). This could have provided a confirmation of Gerrard's suggestion if it was not for the fact that the only picture showing a symmetrical formation region was taken with a cylinder whose span to diameter ratio is only 2.5 . This we know can impose the two-dimensionality on the flow, at least in the near-wake region. In addition, the recent data of Tanida et al (1973) in the range $2 \times 10^3 < Re < 10^4$, which (the data) correspond to a low free-stream turbulence level, do not agree with those of Gerrard. They do not agree with those of Keefe (1961) either, but Keefe had a background turbulence level of 0.3% . On the other hand, the similarity of the data of Gerrard and those of Keefe with the clearance holes open, suggests that perhaps the results of Gerrard suffer from end effects. If this is true, then the reason for the unrealistically large formation region generated by Gerrard's (1967a) numerical model, when forced to yield the very small fluctuating lift he measured, becomes clear. Gerrard (1967a) argued that with a hot-wire in the flow it may be impossible to obtain a symmetrical formation region, hence the discrepancy with Bloor (1964) is natural. But Papailliou and Lykoudis did not have a hot-wire in the flow and yet the length of the symmetrical formation region they observed is in agreementwith Bloor's measured value. Another factor, which might have contributed to the large formation region in Gerrard's model, is the fact that this model is purely two-dimensional.

To conclude, we consider again the question (noted in Section 3.3.5) of the invariance with Reynolds number of the angular distribution of the surface-pressure fluctuations at the shedding frequency and its first harmonic. The similarities in this respect, between the stable range and the subcritical range, can be attributed to the fact that whenever a definite vortex shedding occurs at high Reynolds number, as is the case for instance in the subcritical range, the two-dimensional characteristics of the velocity fluctuations at the shedding frequency and its first harmonic are similar to those in the stable range. For instance, the components v'_{11} and v'_{22} are antisymmetric with respect to the wake centerline, and the components v'_{12} and v'_{21} are symmetric. From this and the continuity equation one can easily deduce that ω'_{11} and ω'_{22} (the second subscript being used as for v'_1 and v'_2) are symmetric with respect to the wake centerline, and ω'_{12} and ω'_{21} are antisymmetric. Referring to (3.38) and noting that $G(\vec{X}|\vec{Y};k)$ is simply a geometrical function which depends only on the spanwise length scale and, like $G(\vec{X}|\vec{Y})$, on $|\vec{X}-\vec{Y}|$, we can see upon inspecting the different integrals (concentrating only on the linear terms) that, as in the two-dimensional case, the component of P at the shedding frequency is the result of an incomplete cancellation of two contributions coming from the regions below and above the wake centerline, while the component at the double frequency is the sum of two such contributions. This implies that the angular distributions of the surface-pressure at these two frequencies should have roughly the same form as at low Reynolds number. The difference between the two cases, on the other hand, lies in the fact that, when Y_2 is put equal to zero (corresponding to the front and back stagnation points), the cancellation is not complete for the component of P at the shedding frequency, as it is at low Re .

This is due to the fact that at high Reynolds numbers the wake 'physical' centerline does not coincide at all times with the wake 'geometrical' centerline (i.e., the X_1-axis). This phenomenon is often referred to as the wobbling of the wake axis and is manifested by a non-vanishing signal, at the shedding frequency, from a hot-wire placed on the X_1-axis (see Bloor and Gerrard 1966). As for the double frequency component, the fact that k is finite at high Reynolds numbers implies that the velocity fluctuations at the double frequency in the immediate vicinity of the cylinder supply a more dominant contribution to the surface-pressure than they do at low Re. This follows from the asymptotic behavior of G at large values of the argument (see Chapter 2) and the effect is more pronounced the larger k is. Hence, the ratio of the distance between the back stagnation point and the region supplying the dominant contribution at that point to the distance between the front stagnation point and the corresponding region which supplies the dominant contribution there is smaller at high Reynolds number than it is at low Reynolds number. This may be the source of dissimilarity between our Figure 4 (at low Re) and Gerrard's (1961) Figure 9 (at high Re).

APPENDIX A

The Role of the Nonlinear Terms in the Source Distribution Function

The source distribution function in its original form, i.e., as given by (2.5) and (2.6), can be written as:

$$q(\vec{x},t) = 2\rho \frac{\partial \overline{v_i}}{\partial x_j} \frac{\partial v_j'}{\partial x_i} + \rho \frac{\partial v_i'}{\partial x_j} \frac{\partial v_j'}{\partial x_i} - \rho \overline{\frac{\partial v_i'}{\partial x_j} \frac{\partial v_j'}{\partial x_i}} \quad . \tag{A.1}$$

The first term on the right-hand side of (A.1) represents the amplifying effect of the mean shear on the velocity fluctuations, while the remaining two represent the effect of these fluctuations on themselves. In all the previous studies which considered the pressure fluctuations on a plane surface supporting a turbulent boundary layer (Kraichnan 1956b, Lilley and Hodgson 1960, and Lilley 1963), the latter effect was neglected. The reason being that due to the large mean shear in the boundary layer, the contribution from the quadratic terms is only a fraction (4 to 6%) of the total contribution. However Corcos (1964) argued that the linear term (the first on the right-hand side of (A.1)) which is large only in a region very near the wall supplies a dominant contribution only at high frequencies, while at low frequencies the remaining terms have contributions at least comparable with that of the former and their scales and convective speed are more typical of those of the observed wall pressure. Nonetheless Panton and Lineberger (1974) in their recent study retained only the turbulence-mean shear term and found that their results were in good agreement with observations for wavenumbers k_1 (in the streamwise direction) as low as $\frac{0.5}{\delta}$, where δ is the boundary layer thickness.

In the wake behind a bluff cylinder the situation is different. The shear layers which spring freely from the sides of the cylinder increase

in width with the downstream distance and at a faster rate the higher the Reynolds number is. Although the velocity fluctuations do not peak very near the boundary where the mean shear is highest, they do peak, at each downstream station x_1, at the center of the shear layers. This is true not only for the high frequency components which result

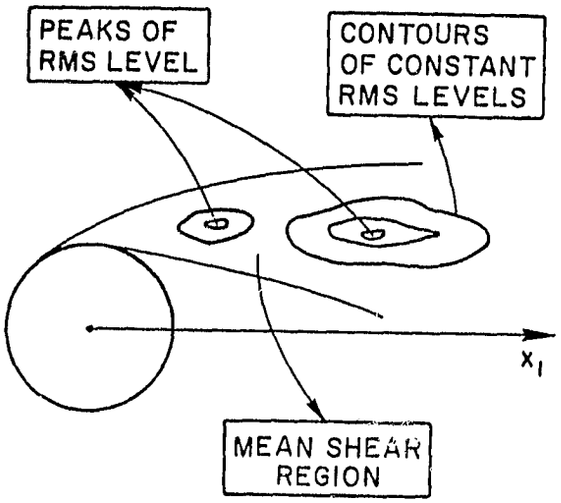

from instability of the individual shear layers themselves but also true for the shedding frequency component (see Gerrard 1967b). Across each layer the change in the mean velocity is of the order of the free-stream velocity U_∞ while the change in the level of velocity fluctuations is about one order of magnitude smaller (see Figs. 2 and 3 of Hanson and Richardson 1968, where contours of constant mean velocity and r.m.s. values of velocity fluctuations in the near-wake are shown at two different values of Re : 10600 and 53000). With this in mind, the first term on the right-hand side of (A.1) can be expected to yield a contribution about one order of magnitude larger than that of the remaining terms. Note however that at values of the wavenumber k (in the spanwise direction) or the frequency ω (in time) for which the velocity fluctuations in the wake are not particularly significant. The linear term in q is not dominant and the main contribution to the fluctuating pressure at these wavenumbers and frequencies comes from the quadratic terms.

For the particular case of Reynolds number equal to 56 which is treated in detail in Chapter 3, the same argument given above is still valid. Inspection of the mean velocity profiles and those of the velocity fluctuations shows that at each downstream station the peak of the fluctuations occurs in the high shear region and that the gradient of these fluctuations in the transversal direction is at least one order of magnitude smaller than that of the mean velocity. Therefore the contribution from the nonlinear terms in q can be expected not to exceed 10% of the total contribution. On the other hand, and as was noted above, the components of the pressure fluctuations at the frequencies $3f$ and $4f$ can be accounted for only by considering the nonlinear terms. But these components are negligibly small and practically non-measurable at this low Reynolds number.

APPENDIX B

Estimation of Some Integrals

Estimation of $J_1/\rho U_\infty^2$. We first consider J_1. We have:

$$\frac{J_1}{\rho U_\infty^2} = -\frac{2}{\pi}\int_{20}^{+\infty}\left\{\int_0^{+5}\frac{\partial^2}{\partial X_2^2}\left\{\log\left[(X_2+Y_2)^2+(X_1-Y_1)^2\right]^{\frac{1}{2}}-\log\left[(X_2-Y_2)^2+(X_1-Y_1)^2\right]^{\frac{1}{2}}\right\}\times\right.$$

$$\left.\overline{v_1}\,\varphi_1\cos 2\pi(\theta_1-ft)dX_2\right\}dX_1$$

$$= -\frac{1}{\pi}\int_{20}^{+\infty}\left\{\int_0^{5}\frac{\partial^2}{\partial X_2^2}\left\{\log\left[1+\frac{2X_2Y_2+Y_2^2}{(X_1-Y_1)^2+X_2^2}\right]-\log\left[1+\frac{-2X_2Y_2+Y_2^2}{(X_1-Y_1)^2+X_2^2}\right]\right\}\times\right.$$

$$\left.\overline{v_1}\,\varphi_1\cos 2\pi(\theta_1-ft)dX_2\right\}dX_1 \quad .$$

Since $-\frac{1}{2}\leq Y_1, Y_2\leq\frac{1}{2}$ we have in the domain of integration:

$$\pm 2X_2Y_2+Y_2^2 \ll (X_1-Y_1)^2+X_2^2 \quad .$$

By expanding the logarithms and retaining only the first term in each expansion, we obtain:

$$\frac{J_1}{\rho U_\infty^2} = -\frac{1}{\pi}\int_{20}^{+\infty}\left\{\int_0^{5}\frac{\partial^2}{\partial X_2^2}\left[\frac{4X_2Y_2}{(X_1-Y_1)^2+X_2^2}\right]\overline{v_1}\,\varphi_1\cos 2\pi(\theta_1-ft)dX_2\right\}dX_1$$

$$= \frac{4Y_2}{\pi}\int_{20}^{+\infty}\left\{\int_0^{5}\frac{\partial^2}{\partial X_2^2}\left[\frac{-X_2}{(X_1-Y_1)^2+X_2^2}\right]\overline{v_1}\,\varphi_1\cos 2\pi(\theta_1-ft)dX_2\right\}dX_1$$

or,

$$\frac{J_1}{\rho U_\infty^2} = \frac{4Y_2}{\pi}\int_{20}^{+\infty}K_1(X_1)\cos 2\pi(\theta_1-ft)dX_1 \quad , \qquad (B.1)$$

where:

$$K_1(X_1) = \int_0^5 \frac{\partial^2}{\partial X_2^2}\left[\frac{-X_2}{(X_1-Y_1)^2+X_2^2}\right] \overline{v_1}\, v_1\, dX_2 \quad ,$$

in which $\overline{v_1}$, v_1 , and $\frac{\partial^2}{\partial X_2^2}\left[\frac{-X_2}{(X_1-Y_1)^2+X_2^2}\right]$ are all positive functions of X_2 for $X_1 > 20$. Therefore, $K_1(X_1)$ is a positive function of X_1 for $X_1 \geq 20$. In addition, $K_1(X_1)$ is a monotonically decreasing function of X_1 for $X_1 > 20$, because v_1 and $\frac{\partial^2}{\partial X_2^2}\left[\frac{-X_2}{(X_1-Y_1)^2+X_2^2}\right]$ are, while $\overline{v_1}$ is a slightly increasing function of X_1 . An upper bound can be found for K_1 in the interval $20 < X_1 < 100$. By examining the data on the velocity fluctuations we can see that:

$$v_1 < \frac{2}{X_1} \quad , \text{ for } \quad 20 < X_1 < 100 \quad ,$$

and since $\overline{v_1} < 1$, we have (for $20 < X_1 < 100$):

$$K_1(X_1) < \frac{2}{X_1} \int_0^5 \frac{\partial^2}{\partial X_2^2}\left[\frac{-X_2}{(X_1-Y_1)^2+X_2^2}\right] dX_2$$

or:

$$K_1(X_1) < \frac{2}{X_1}\left\{\frac{25-(X_1-Y_1)^2}{[(X_1-Y_1)^2+25]^2} + \frac{1}{(X_1-Y_1)^2}\right\}$$

$$< \frac{2}{X_1}\,\frac{3\times 25(X_1-Y_1)^2+(25)^2}{[(X_1-Y_1)^2+25]^2(X_1-Y_1)^2}$$

$$< \frac{2}{X_1}\,\frac{3\times 25(X_1-Y_1)^2+3\times(25)^2}{[(X_1-Y_1)^2+25]^2(X_1-Y_1)^2}$$

$$< \frac{2}{X_1} \frac{3\times25}{[(X_1-Y_1)^2+25](X_1-Y_1)^2}$$

$$< \frac{2}{X_1} \frac{3\times25}{(X_1-Y_1)^4} \quad ,$$

and therefore:

$$K_1(X_1) < \frac{150}{X_1(X_1-Y_1)^4} \quad , \text{ for } \quad 20 \leq X_1 \leq 100 \quad .$$

In estimating J_1 we will neglect the part of the integral beyond $X_1 = 100$ assuming that it is negligibly small and does not affect the order of magnitude of the retained part.* With this in mind we write instead of (B.1)

$$\frac{J_1}{\rho U_\infty^2} = \frac{4Y_2}{\pi} \int_{20}^{100} K_1(X_1) \cos 2\pi(\theta_1 - ft) dX_1 \quad . \tag{B.2}$$

Since $K_1(X_1)$ is a positive monotonically decreasing function, it follows from the second mean value theorem (see Whittaker and Watson 1963) that:

$$\frac{J_1}{\rho U_\infty^2} = \frac{4Y_2}{\pi} K_1(20) \int_{20}^{\xi_1} \cos 2\pi(\theta_1 - ft) dX_1 \quad ,$$

where ξ_1 is such that $20 < \xi_1 < 100$. Now we know that given a linear function $\alpha(X_1)$ such that:

*In the far-wake φ_1 decays more slowly than $1/X_1$ but it is reasonable to assume that the velocity fluctuations beyond $X_1 = 100$ do not affect the surface-pressure field.

$$\frac{d\alpha}{dX_1} = \beta$$

the following integral:

$$\int_a^b \cos 2\pi\alpha \, dX_1 \quad ,$$

where a and b are arbitrary but finite, is bounded with $\frac{1}{\pi\beta}$ as upper bound. θ_1 is an almost linear function of X_1, for the present purpose it can be assumed linear and inspection of the data shows that:

$$\frac{d\theta_1}{dX_1} \simeq \frac{2}{15} \quad .$$

Therefore we have:

$$\left|\frac{J_1}{\rho U_\infty^2}\right| \leq \frac{2}{\pi} K_1(20) \frac{1}{\pi \times \frac{2}{15}} \quad ,$$

or:

$$\left|\frac{J_1}{\rho U_\infty^2}\right| \leq \frac{1}{\pi^2} \frac{15 \times 150}{20(20-Y_1)^4}$$

$$\leq \frac{1}{\pi^2} \frac{15 \times 150}{20(19.5)^4} \quad ,$$

and finally:

$$\left|\frac{J_1}{\rho U_\infty^2}\right| \leq 0.0788 \times 10^{-3} \quad . \qquad \text{(B.3)}$$

Estimation of $J_2/\rho U_\infty^2$. We have:

$$\frac{J_2}{\rho U_\infty^2} = -\frac{2}{\pi}\int_{20}^{+\infty}\left\{\int_{-5}^{+5}\left\{\frac{(X_2-Y_2)^2-(X_1-Y_1)^2}{[(X_1-Y_1)^2+(X_2-Y_2)^2]^2}-\frac{X_2^2-X_1^2}{(X_1^2+X_2^2)^2}\right\}\overline{v_1}\varphi_2\cos 4\pi(\theta_2-ft)\,dX_2\right\}dX_1$$

$$= -\frac{2}{\pi}\int_{20}^{+\infty}\left\{\int_{-5}^{+5}\frac{\partial^2}{\partial X_2^2}\left\{\log(X_1^2+X_2^2)^{\frac{1}{2}}-\log[(X_1-Y_1)^2+(X_2-Y_2)^2]^{\frac{1}{2}}\right\}\overline{v_1}\varphi_2\cos 4\pi(\theta_2-ft)\,dX_2\right\}dX_1$$

$$= -\frac{2}{\pi}\int_{20}^{+\infty}\left\{\tfrac{1}{2}\int_{-5}^{+5}\frac{\partial^2}{\partial X_2^2}\left\{-\log\left(1+\frac{Y_1^2+Y_2^2-2X_1Y_1-2X_2Y_2}{X_1^2+X_2^2}\right)\right\}\overline{v_1}\varphi_2\cos 4\pi(\theta_2-ft)\,dX_2\right\}dX_1 \quad .$$

Again, since in the domain of integration:

$$Y_1^2+Y_2^2-2X_1Y_1-2X_2Y_2 \ll X_1^2+X_2^2 \quad ,$$

by expanding the logarithm and retaining only the part of the first term which is of lowest order:

$$\frac{J_2}{\rho U_\infty^2} = \frac{2}{\pi}\int_{20}^{+\infty}\left\{\int_{-5}^{+5}\frac{\partial^2}{\partial X_2^2}\left\{-\frac{Y_1X_1+Y_2X_2}{X_1^2+X_2^2}\right\}\overline{v_1}\,\varphi_2\cos 4\pi(\theta_2-ft)\,dX_2\right\}dX_1 \quad ,$$

or since $\overline{v_1}$ is even in X_2, φ_2 is even in X_2, and since φ_2 (by inspection of the data) is different from zero only for $-3 \le X_2 \le +3$ and $X_1 \le 100$:

$$\frac{J_2}{\rho U_\infty^2} = \frac{2Y_1}{\pi}\int_{20}^{100}\left\{\int_{-3}^{+3}\frac{\partial^2}{\partial X_2^2}\left\{\frac{-X_1}{X_1^2+X_2^2}\right\}\overline{v_1}\,\varphi_2\cos 4\pi(\theta_2-ft)\,dX_2\right\}dX_1 \quad .$$

$\frac{J_2}{\rho U_\infty^2}$ can be written as:

$$\frac{J_2}{\rho U_\infty^2} = \frac{2Y_1}{\pi} \int_{20}^{100} K_2(X_1)\cos 4\pi(\theta_2 - ft)dX_1 \quad , \qquad (B.4)$$

where:

$$K_2(X_1) = \int_{-3}^{+3} \frac{\partial^2}{\partial X_2^2}\left\{\frac{-X_1}{X_1^2+X_2^2}\right\} \overline{v_1}\, \varphi_2\, dX_2 \quad .$$

As before, it can be shown that $K_2(X_1)$ is a positive monotonically decreasing function of X_1. In addition, since (by inspection of the data):

$$\varphi_2 \leq \frac{0.7}{X_1} \quad , \text{ for } \quad 20 \leq X_1 \leq 100$$

we have:

$$K_2(X_1) \leq \frac{0.7}{X_1} \int_{-3}^{+3} \frac{\partial^2}{\partial X_2^2}\left\{\frac{-X_1}{X_1^2+X_2^2}\right\} dX_2$$

$$\leq \frac{8.4}{(X_1^2+9)^2} \quad .$$

Now from (B.4) and in view of the second mean value theorem it follows that:

$$\frac{J_2}{\rho U_\infty^2} = \frac{2Y_1}{\pi} K_2(20) \int_{20}^{\xi_1} \cos 4\pi(\theta_2 - ft)dX_1 \quad ,$$

where $20 \leq \xi_1 \leq 100$. Like for θ_1 we have:

$$\frac{d\theta_2}{dX_1} = \frac{2}{15} \quad ,$$

and therefore:

$$\left|\frac{J_2}{\rho U_\infty^2}\right| \leq \frac{1}{\pi} K_2(20) \frac{1}{2\pi \times \frac{2}{15}} \quad ,$$

or:

$$\left|\frac{J_2}{\rho U_\infty^2}\right| \leq \frac{1}{\pi^2}\,\frac{15}{4}\times\frac{8.4}{[(20)^2+9]^2}$$

and finally:

$$\left|\frac{J_2}{\rho U_\infty^2}\right| \leq 0.0190\times10^{-3} \quad . \tag{B.5}$$

Estimation of $J_3/\rho U_\infty^2$.

The cancellation effect mentioned in Section 3.3.4 cannot be exploited to find an upper bound for J_3 . However, in order to improve the estimation we can use the fact that:

$$\varphi_2 \leq \frac{0.7}{X_1}\left(1-\frac{X_2^2}{9}\right) \quad .$$

We write:

$$\frac{J_3}{\rho U_\infty^2} = -\frac{2}{\pi}\int_{20}^{100}\left\{\int_0^3 \frac{X_2^2-X_1^2}{(X_1^2+X_2^2)^2}\,\overline{v_1}\,\varphi_2\cos 4\pi(\theta_2-ft)\,dX_2\right\}dX_1$$

$$= \frac{2}{\pi}\int_{20}^{100}\left\{\int_0^3 \frac{\partial}{\partial X_2}\left\{\frac{X_2}{X_1^2+X_2^2}\right\}\overline{v_1}\,\varphi_2\cos 4\pi(\theta_2-ft)\,dX_2\right\}dX_1 \quad ,$$

or:

$$\frac{J_3}{\rho U_\infty^2} = \frac{2}{\pi}\int_{20}^{100} K_3(X_1)\cos 4\pi(\theta_2-ft)\,dX_1 \quad ,$$

where:

$$K_3(X_1) = \int_0^3 \frac{\partial}{\partial X_2}\left\{\frac{X_2}{X_1^2+X_2^2}\right\}\overline{v_1}\,\varphi_2\,dX_2 \quad .$$

$K_3(X_1)$ is a positive monotonically decreasing function of X_1 and:

$$K_3(X_1) \leq \frac{0.7}{X_1} \int_0^3 \frac{\partial}{\partial X_2} \left\{ \frac{X_2}{X_1^2+X_2^2} \right\} (1-\frac{X_2^2}{9}) dX_2$$

$$\leq \frac{1.4}{9} \left\{ \frac{3}{X_1} - \arctan \frac{3}{X_1} \right\}$$

$$\leq \frac{1.4}{9} \left\{ \frac{3}{X_1} - \frac{3}{X_1} + \frac{1}{3}(\frac{3}{X_1})^3 - \frac{1}{5}(\frac{3}{X_1})^5 + \ldots \right\}$$

$$\leq \frac{1.4}{X_1^3} \quad .$$

Also, we have as before:

$$\left| \frac{J_3}{\rho U_\infty^2} \right| \leq \frac{2}{\pi} K_3(20) \frac{1}{2\pi \times \frac{2}{15}} \quad ,$$

or:

$$\left| \frac{J_3}{\rho U_\infty^2} \right| \leq \frac{1}{\pi^2} \frac{15 \times 0.7}{(20)^3} \quad ,$$

and finally:

$$\left| \frac{J_3}{\rho U_\infty^2} \right| \leq 0.1329 \times 10^{-3} \qquad \text{(B.6)}$$

Estimation of $I_2/\rho U_\infty^2$.

$I_2/\rho U_\infty^2$ accounts for the effect of neglecting the contribution from the velocity fluctuations outside the strip $|X_2| \leq 5$. There, only the fluctuations at the shedding frequency are present and they are very small. Upon examining the data we find that:

$$\varphi_1 = \frac{0.0175}{(X_2/5)^2} \quad \text{for} \quad X_2 \geq 5 \quad ,$$

where again the variables are non-dimensional. From (3.25) it follows that:

$$\frac{I_2}{\rho U_\infty^2} = -\frac{2}{\pi}\int_2^{+\infty}\left\{\int_5^{+\infty}\left\{\frac{(X_2-Y_2)^2-(X_1-Y_1)^2}{[(X_1-Y_1)^2+(X_2-Y_2)^2]^2} - \frac{(X_2+Y_2)^2-(X_1-Y_1)^2}{[(X_1-Y_1)^2+(X_2+Y_2)^2]^2}\right\} \times \overline{v_1}\,\varphi_1 \cos 2\pi(\theta_1 - ft)\,dX_2\right\} dX_1 \quad ,$$

where the fact that φ_1 is an odd function of X_2 has been used to eliminate the part of $\frac{\partial^2 G}{\partial X_1^2}$ which is independent of Y_1 and Y_2. We now write:

$$\frac{I_2}{\rho U_\infty^2} = -\frac{2}{\pi}\int_2^{+\infty}\left\{\int_5^{+\infty}\frac{\partial^2}{\partial X_1^2}\left\{\log\left(1+\frac{-2X_2Y_2+Y_2^2}{(X_1-Y_1)^2+X_2^2}\right)-\log\left(1+\frac{2X_2Y_2+Y_2^2}{(X_1-Y_1)^2+X_2^2}\right)\right\} \times \overline{v_1}\,\varphi_1 \cos 2\pi(\theta_1 - ft)\,dX_2\right\} dX_1 \quad ,$$

or, upon expanding the logarithms and retaining only the first terms in each expansion:

$$\frac{I_2}{\rho U_\infty^2} = \frac{4Y_2}{\pi}\int_2^{+\infty}\left\{\int_5^{+\infty}\frac{\partial^2}{\partial X_1^2}\left\{\frac{X_2}{(X_1-Y_1)^2+X_2^2}\right\}\overline{v_1}\,\varphi_1 \cos 2\pi(\theta_1 - ft)\,dX_2\right\} dX_1 \quad . \tag{B.7}$$

We note that:

$$\frac{\partial^2}{\partial X_1^2}\left\{\frac{X_2}{(X_1-Y_1)^2+X_2^2}\right\} = \frac{2X_2[3(X_1-Y_1)^2-X_2^2]}{[(X_1-Y_1)^2+X_2^2]^3} \quad ,$$

and therefore in the domain of integration (i.e., $2 \leq X_1 \leq +\infty$, $5 \leq X_2 \leq +\infty$) this quantity changes its sign. It follows that the procedure used in the previous estimations cannot be applied here to account for the behavior of the cosine function in (B.7). Nevertheless, we will carry out the estimation below by taking the absolute values of the different terms in (B.7), knowing that only a gross estimate can emerge:

$$\left|\frac{I_2}{\rho U_\infty^2}\right| \leq \frac{2}{\pi}\int_2^{+\infty}\left\{\int_5^{+\infty}\left|\frac{\partial^2}{\partial X_1^2}\left\{\frac{X_2}{(X_1-Y_1)^2+X_2^2}\right\}\right|\frac{0.0175}{(X_2/5)^2}\,dX_2\right\}dX_1$$

$$\leq \frac{0.875}{\pi}\int_5^{+\infty}\left\{\int_2^{+\infty}\left|\frac{\partial^2}{\partial X_1^2}\left\{\frac{1}{(X_1-Y_1)^2+X_2^2}\right\}\right|dX_1\right\}\frac{1}{X_2}\,dX_2 \quad .$$

Now, we have:

$$\int_2^{+\infty}\left|\frac{\partial^2}{\partial X_1^2}\left\{\frac{1}{(X_1-Y_1)^2+X_2^2}\right\}\right|dX_1 = \int_2^{+\infty}\left|\frac{6(X_1-Y_1)^2-2X_2^2}{[(X_1-Y_1)^2+X_2^2]^3}\right|dX_1$$

$$= \int_2^{X_2/\sqrt{3}+Y_1}\frac{2X_2^2-6(X_1-Y_1)^2}{[(X_1-Y_1)^2+X_2^2]^3}\,dX_1 + \int_{X_2/\sqrt{3}+Y_1}^{+\infty}\frac{6(X_1-Y_1)^2-2X_2^2}{[(X_1-Y_1)^2+X_2^2)^3}\,dX_1$$

$$= \frac{9}{4\sqrt{3}}\frac{1}{X_2^3} - \frac{2(2-Y_1)}{[(2-Y_1)^2+X_2^2]^3}$$

and therefore:

$$\left|\frac{I_2}{\rho U_\infty^2}\right| \leq \frac{0.875}{\pi}\int_5^{+\infty}\left\{\frac{9}{4\sqrt{3}}\frac{1}{X_2^4} - \frac{2(2-Y_1)}{X_2[(2-Y_1)^2+X_2^2]^2}\right\}dX_2$$

$$\leq \frac{0.175\times\sqrt{3}}{100\,\pi} + \frac{1.75}{\pi}\left\{\frac{1}{2(2-Y_1)[(2-Y_1)^2+25]} + \frac{1}{(2-Y_1)^3}\log\frac{5}{\sqrt{(2-Y_1)^2+25}}\right\} .$$

The maximum value of the term containing the logarithm on the right-hand side of the above inequality cannot be determined accurately, we therefore evaluate that term at $Y_1 = \frac{1}{4}$ corresponding to the maximum value of P_1 (see Figure 1). The resulting estimate is:

$$\left|\frac{I_2}{\rho U_\infty{}^2}\right| \leq 0.6308 \times 10^{-3} \quad . \tag{B.8}$$

Abernathy, F.H. and Kronauer, R.E. 1962 The formation of vortex streets. J. Fluid Mech. 13, 1.

Abramowitz, M. and Stegun, I.A. eds. 1964 Handbook of Mathematical Functions. NBS Applied Math. Series No. 55, U.S. Govt. Printing Office, Washington, D.C.

Ayoub, A. and Karamcheti, K. 1975 Pressure fluctuations on the surface of a Circular Cylinder in uniform flow. Proceedings of the Third Interagency Symposium on University Research in Transportation Noise, University of Utah, Nov. 1975.

Batchelor, G.K. 1951 Pressure fluctuations in isotropic turbulence. Proc. Cam. Phil. Soc. 47, 2, 359.

Batchelor, G.K. 1967 An Introduction to Fluid Dynamics. Cambridge Univ. Press.

Bearman, P.W. 1969 On vortex shedding from a circular cylinder in the critical Reynolds number regime. J. Fluid Mech. 37, 577.

Berger, E. and Wille, R. 1972 Periodic flow phenomena. Ann. Rev. Fluid Mech. 4, 313.

Bloor, M.S. 1964 The transition to turbulence in the wake of a circular cylinder. J. Fluid Mech. 19, 290.

Bloor, M.S. and Gerrard, J.H. 1966 Measurements on turbulent vortices in a cylinder wake. Proc. Roy. Soc. A, 294, 319.

Campbell, G.S. 1957 Turbulence in the wake of a thin airfoil at low speeds. NACA TM 1427.

Corcos, G.M. 1964 The structure of the turbulent pressure field in boundary-layers flows. J. Fluid Mech. 18, 353.

Curle, N. 1955 The influence of solid boundaries upon aerodynamic sound. Proc. Roy. Soc. A, 231, 412.

Davis, S.S. 1974 Theory of discrete vortex noise. AIAA 12th Aerospace Sciences Meeting, Washington, D.C., paper No. 74-90.

El Baroudi, M.Y. 1960 Measurement of two-point correlations of velocity near a circular cylinder shedding a Kármán vortex street. Univ. Toronto, Inst. Aerophys. TN No. 31.

Ffowcs Williams, J.E. and Hawkings, D.L. 1969 Sound generation by turbulence and surfaces in arbitrary motion. Phil. Trans. Roy. Soc. A 264, 321.

Fung, Y.C. 1960 Fluctuating lift and drag acting on a cylinder in a flow at supercritical Reynolds numbers. J. Aeron. Sci. 27, 801.

Gaster, M. 1969 Vortex shedding from slender cones at low Reynolds numbers, J. Fluid Mech. 38, 565.

Gaster, M. 1971 Vortex shedding from circular cylinders at low Reynolds numbers. J. Fluid Mech. 46, 749.

Gerrard, J.H. 1961 An experimental investigation of the oscillating lift and drag of a circular cylinder shedding turbulent vortices. J. Fluid Mech. 11, 244.

Gerrard, J.H. 1965 A disturbance-sensitive Reynolds number range of the flow past a circular cylinder. J. Fluid Mech. 22, 187.

Gerrard, J.H. 1966a The three-dimensional structure of the wake of a circular cylinder. J. Fluid Mech. 25, 143.

Gerrard, J.H. 1966b The mechanics of the formation region of vortices behind bluff bodies. J. Fluid Mech. 25, 401.

Gerrard, J.H. 1967a Numerical computation of the magnitude and frequency of the lift on a circular cylinder. Phil. Trans. Roy. Soc. A, 261, 137.

Gerrard, J.H. 1967b Experimental investigation of separated boundary layer undergoing transition to turbulence. Physics of Fluids Supplement S98.

Goldman, R.L. 1958 Kármán vortex forces on Vanguard rocket. Shock and Vibration Bulletin, Pt. II, Nav. Res. Lab., Washington, D.C.

Goldstein, S. ed. 1938 Modern Developments in Fluid Dynamics, Vol. 1, Oxford Univ. Press.

Hama, F.R. 1957 Three-dimensional vortex pattern behind a circular cylinder. J. Aerosp. Sci. 24, 156.

Hanson, F.B. and Richardson, P.D. 1968 The near-wake of a circular cylinder in crossflow. J. Basic Eng. 90, 476.

Hunt, J.C.R. 1973a A theory for fluctuating pressures on bluff bodies in turbulent flows. Proc. IUTAM/IAHR Symp. on Flow Induced Vibrations, Karlsruhe, 1972. Springer.

Hunt, J.C.R. 1973b A theory of turbulent flow round two-dimensional bluff bodies. J. Fluid Mech. 61, 625.

Humphreys, J.S. 1960 On a circular cylinder in a steady wind at transition Reynolds numbers. J. Fluid Mech. 9, 603.

Imai, I. 1964 On an explanation of the formation of Kármán vortex streets. IUTAM Conference on Concentrated Vortex Motions (unpublished, but see Discussion in Hanson and Richardson 1968).

Jones, Jr. G.W., Cincotta, J.J. and Walker, R.W. 1969 Aerodynamic forces on a stationary and oscillating circular cylinder at high Reynolds numbers, NASA TR R-300.

Jordan, S.K. and Fromm, J.E. 1972 Oscillatory drag, lift, and torque on a circular cylinder in a uniform flow. Physics of Fluids 15, 371.

Karamcheti, K. and Ayoub, A. 1974 Pressure fluctuations on the surface of a cylinder in a cross flow. Proceedings of the Second Interagency Symposium on University Research in Transportation Noise, North Carolina State University, June 1974.

Keefe, R.T. 1961 An investigation of the fluctuating forces acting on a stationary circular cylinder in a subsonic stream and of the associated sound field. Univ. Toronto Inst. Aerophys. TR No. 76.

Kovasznay, L.S.G. 1949 Hot-wire investigation of the wake behind cylinders at low Reynolds numbers. Proc. Roy. Soc. A 198, 174.

Kraichnan, R.H. 1956a Pressure field within homogeneous anisotropic turbulence. J. Acous. Soc. Amer. 28, 64.

Kraichnan, R.H. 1956b Pressure fluctuations in turbulent flow over a flat plate. J. Acous. Soc. Amer. 28, 378.

Landau, L.D. and Lifshitz, E.M. 1959 Fluid Mechanics. London; Pergamon Press.

Lilley, G.M. and Hodgson, T.H. 1960 on surface pressure fluctuations in turbulent boundary layers. AGARD Rep. No. 276.

Lilley, G.M. 1963 Wall pressure fluctuations under turbulent boundary layers at subsonic and supersonic speeds. College of Aeronautics, Granfield, COA Note 140.

Macovsky, M.S. 1958 Vortex induced vibration studies. David Taylor Model Basin Rep. 1190.

Mattingly, G.E. 1962 An experimental study of the three-dimensionality of the flow around a circular cylinder. Inst. for Fluid Dyn. and Appl. Math., Univ. of Maryland, TN BN-295.

Mattingly, G.E. and Criminale, W.O. 1972 The stability of an incompressible two-dimensional wake. J. Fluid Mech. 51, 233.

McGregor, D.M. 1957 An experimental investigation of the oscillating pressures on a circular cylinder in a fluid stream. Univ. Toronto Inst. Aerophys. TN 14.

Morkovin, M.V. 1964 Flow around circular cylinder · A kaleidoscope of challenging fluid phenomena. ASME Symp. Fully Separated Flows, Philadelphia.

Panton, R.L. and Linebarger, J.H. 1974 Wall pressure spectra calculations for equilibrium boundary layers. J. Fluid Mech. 65, 261.

Papailliou, D.D. and Lykoudis, P.S. 1974 Turbulent vortex streets and the entrainment mechanism of the turbulent wake. J. Fluid Mech. 62, 11.

Phillips, O.M. 1956 The intensity of aeolian tones. J. Fluid Mech. 1, 607.

Prendergast, V. 1958 Measurement of two-point correlations of the surface pressure on a circular cylinder. Univ. Toronto Inst. Aerophys. TN 23.

Roshko, A. 1954 On the development of turbulent wakes from vortex streets. NACA Rep. 1191.

Roshko, A. 1961 Experiments on the flow past a circular cylinder at very high Reynolds numbers. J. Fluid Mech. 10, 345.

Roshko, A. and Fiszdon, W. 1967 On the persistence of transition in the near-wake. Problems of Hydrodynamics and Continuum Mechanics. Soc. Ind. App. Math. Philadelphia, Pa. 1969.

Schmidt, L.V. 1965 Measurements of fluctuating air loads on a circular cylinder. J. Aircraft 2, 49.

Schmidt, L.V. 1966 Fluctuating force measurements upon a circular cylinder at Reynolds numbers up to 5×10^6 . NASA TM-X-57779.

Shaw, R.A. 1949 The solution of the problem of a cylinder shedding a periodic wake. ARC 12, 696.

Simmons, J.E.L. 1974 Phase-angle measurements between hot-wire signals in the turbulent wake of a two-dimensional bluff body. J. Fluid Mech. 64, 599.

Stakgold, I. 1968 Boundary Value Problems of Mathematical Physics. Vol. II, MacMillan, New York.

Taneda, S. 1952 Studies on wake vortices. Rep. Res. Inst. Appl. Mech., Kyushu Univ. 1, 131.

Taneda, S. 1956 Experimental investigation of wakes behind cylinders and plates at low Reynolds numbers. J. Phys. Soc. Japan, 11, 302.

Tanida, Y., Okajima, A. and Watanabe, Y. 1973 Stability of a circular cylinder oscillating in uniform flow or in a wake. J. Fluid Mech. 61, 769.

Tritton, D.J. 1959 Experiments on the flow past a circular cylinder at low Reynolds numbers. J. Fluid Mech. 6, 547.

Tritton, D.J. 1971 A note on vortex streets behind circular cylinders at low Reynolds number. J. Fluid Mech. 45, 203.

Wille, R. 1966 On unsteady flows and transient motions. Progress in Aeronautical Sciences, Vol. 7, Pergamon Press, Oxford.

Whittaker, E.T. and Watson, G.N. 1963 A Course of Modern Analysis. Cambridge Univ. Press.